



저작자표시-비영리-변경금지 2.0 대한민국

이용자는 아래의 조건을 따르는 경우에 한하여 자유롭게

- 이 저작물을 복제, 배포, 전송, 전시, 공연 및 방송할 수 있습니다.

다음과 같은 조건을 따라야 합니다:



저작자표시. 귀하는 원저작자를 표시하여야 합니다.



비영리. 귀하는 이 저작물을 영리 목적으로 이용할 수 없습니다.



변경금지. 귀하는 이 저작물을 개작, 변형 또는 가공할 수 없습니다.

- 귀하는, 이 저작물의 재이용이나 배포의 경우, 이 저작물에 적용된 이용허락조건을 명확하게 나타내어야 합니다.
- 저작권자로부터 별도의 허가를 받으면 이러한 조건들은 적용되지 않습니다.

저작권법에 따른 이용자의 권리는 위의 내용에 의하여 영향을 받지 않습니다.

이것은 [이용허락규약\(Legal Code\)](#)을 이해하기 쉽게 요약한 것입니다.

[Disclaimer](#)

**A THESIS  
FOR THE DEGREE OF DOCTOR OF PHILOSOPHY**

**Dieckol and Diphlorethohydroxycarmalol  
isolated from *Ecklonia cava* and *Ishige okamurae*  
promote vasodilation in the co-culture system  
and zebrafish model**

**Yu An Lu**

**DEPARTMENT OF MARINE LIFE SCIENCES  
GRADUATE SCHOOL  
JEJU NATIONAL UNIVERSITY**

**August, 2021**

**Dieckol and Diphlorethohydroxycarmalol isolated from  
*Ecklonia cava* and *Ishige okamurae* promote vasodilation  
in the co-culture system and zebrafish model**

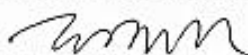
**Yu An Lu**

**(Supervised by Professor You-Jin Jeon)**

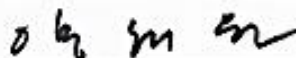
A thesis submitted in partial fulfillment of the requirement for the degree of  
**DOCTOR OF PHILOSOPHY**

**August, 2021**

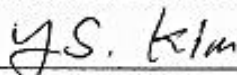
This thesis has been examined and approved by



Thesis director, BoMi Ryu (PhD), Research Professor of Marine Life Science, Jeju National University



Hye-Won Yang (PhD), Research Professor of Marine Life Science, Jeju National University



Young-Sang Kim (PhD), Research Professor of Marine Science, Jeju National University



Sang-Hoon Lee (PhD), Senior Researcher, Korea Food Research Institute



You-Jin Jeon (PhD), Professor of Marine Life Science, Jeju National University

Data: August, 2021

**DEPARTMENT OF MARINE LIFE SCIENCES**

**GRADUATE SCHOOL**

**JEJU NATIONAL UNIVERSITY**



## Contents

<b>Summary</b> .....	<b>vi</b>
<b>List of figures</b> .....	<b>x</b>
<b>Part I</b> .....	<b>1</b>
<b>Bioactive compounds isolated from <i>Ecklonia cava</i> and <i>Ishige okamurae</i> promote vasodilation in endothelial via calcium signalling and PI3K/Akt/eNOS pathway</b>	<b>1</b>
<b>1.1. Introduction</b> .....	<b>2</b>
<b>1.2. Material and methods</b> .....	<b>4</b>
1.2.1. Chemicals and reagents .....	4
1.2.2. Extraction and isolation of DK .....	4
1.2.3. Extraction and isolation of DPHC .....	5
1.2.4. EA.hy926 cells culture and cytotoxicity analysis .....	5
1.2.5. Evaluation of the intracellular NO production .....	6
1.2.6. Measurement of the intracellular H <sub>2</sub> S levels .....	6
1.2.7. Quantification of the cytosolic calcium levels.....	6
1.2.8. Western blot analysis .....	7
1.2.9. Statistical analysis.....	8
<b>1.3. Results</b> .....	<b>9</b>
1.3.1. Evaluation of cytotoxicity and intracellular NO concentrations under the ECE, DK, IOE, and DPHC treatments .....	9
1.3.2. Intracellular H <sub>2</sub> S levels induced by DK and DPHC treatments.....	14

1.3.3.	ECE, DK, IOE, DPHC promoted phosphorylation of the PI3K/Akt/eNOS pathway in E.A.hy926 cells .....	16
1.3.4.	Regulatory effects of ECE, IOE, DK, and DPHC on the $[Ca^{2+}]_{cytol}$ levels	19
1.3.5.	Computational prediction of the AchR/VEGFR2 and docking stimulation with DK/DPHC .....	22
1.3.6.	DK and DPHC modulated $[Ca^{2+}]_{cytol}$ levels by activating AchR, VEGFR2, and VDCC .....	26
<b>1.4.</b>	<b>Discussion.....</b>	<b>30</b>
<b>1.5.</b>	<b>Conclusion.....</b>	<b>33</b>
<b>Part II</b>	<b>.....</b>	<b>34</b>
	<b>Bioactive compounds isolated from <i>Ecklonia cava</i> and <i>Ishige okamurae</i> promote vasodilation in endothelial-smooth muscle cell co-culture system via down-regulation of CaM and p-MLC expression .....</b>	<b>34</b>
<b>2.1.</b>	<b>Introduction .....</b>	<b>35</b>
<b>2.2.</b>	<b>Material and methods .....</b>	<b>37</b>
2.2.1.	Chemicals and reagents .....	37
2.2.2.	Human coronary artery endothelial cells (HCAECs) monoculture .....	37
2.2.3.	Measurement of cytotoxicity and NO production in HCAEC.....	37
2.2.4.	Evaluation of intracellular H <sub>2</sub> S levels.....	38
2.2.5.	Quantitative of cytosolic calcium levels in HCAEC .....	39
2.2.6.	Human coronary artery smooth muscle cells (HCASMCs) monoculture	40
2.2.7.	Measurement of cytotoxicity and intracellular NO production in HCASMC	40

2.2.8.	The protocol for conditional medium preparation .....	40
2.2.9.	The protocol of conditional medium transferred from HCAEC to HCASMC .....	42
2.2.10.	Western blotting analysis.....	43
2.2.11.	The methodology of the HCAEC-HCASMC co-culture model.....	44
2.2.12.	Quantitative of CaM and p-MLC expression in HCASMC by immunofluorescence.....	45
2.2.13.	Statistical analysis.....	46
<b>2.3.</b>	<b>Results .....</b>	<b>47</b>
2.3.1.	Measurement of cell viability and intracellular NO production in HCAEC 47	
2.3.2.	The levels of intracellular H <sub>2</sub> S induced by DK and DPHC in HCAEC ...	50
2.3.3.	Evaluation of [Ca <sup>2+</sup> ] <sub>cytol</sub> under the IOE. DPHC, ECE, and DK treatments in HCAEC	52
2.3.4.	Measurement of cytotoxicity under the IOE, DPHC, ECE, and DK treatments in HCASMC .....	54
2.3.5.	Measurement of cell viability and NO production of HCASMC exposed under conditional medium .....	56
2.3.6.	DK and DPHC suppressed the contractile effect by down-regulating the CaM and p-MLC expression in HCASMC .....	59
2.3.7.	Detection of CaM and p-MLC expression by immunofluorescence staining in the co-culture system.....	62

2.3.8. DK and DPHC down-regulated the expression of CaM and p-MLC in the co-culture system.....	67
<b>2.4. Discussion.....</b>	<b>70</b>
<b>2.5. Conclusions .....</b>	<b>73</b>
<b>Part III .....</b>	<b>74</b>
<b>Bioactive compounds isolated from <i>Ecklonia cava</i> and <i>Ishige okamurae</i> promote vasodilation in the zebrafish model .....</b>	<b>74</b>
<b>3.1. Introduction .....</b>	<b>75</b>
<b>3.2. Material and methods .....</b>	<b>77</b>
3.2.1. Zebrafish husbandry and fish strains .....	77
3.2.2. Toxicity of DK and DPHC in zebrafish embryos.....	77
3.2.3. Toxicity of vasoconstriction drug - phenylephrine in zebrafish embryos	78
3.2.4. The vasoconstrictive zebrafish model set up .....	79
3.2.5. Assessment of whole-body fluorescence intensity in the Tg(flk: EGFP) transgenic zebrafish .....	79
3.2.6. Evaluation of associated cardiovascular parameters in the zebrafish model	80
3.2.7. Statistical analysis.....	81
<b>3.3. Results .....</b>	<b>82</b>
3.3.1. Toxicity of DK and DPHC in zebrafish embryos.....	82
3.3.2. The vasoconstrictive zebrafish model set up by using vasoconstrictor ..	84
3.3.3. Assessment of whole-body fluorescence intensity in the Tg(flk: EGFP) transgenic zebrafish .....	86

3.3.4. Evaluation of associated cardiovascular parameters in the zebrafish model 88

<b>3.4. Discussion.....</b>	<b>94</b>
<b>3.5. Conclusions.....</b>	<b>96</b>
<b>Acknowledgements.....</b>	<b>97</b>
<b>References.....</b>	<b>98</b>

## Summary

It is well known that the imbalance between vasoconstriction and vasodilation is deeply related to cardiovascular diseases, especially hypertension (HTN)[1, 2]. Vascular endothelial cells (EC) and vascular smooth muscle cells (VSMC) are the essential components of a typical vessel wall. These two types of cells would cooperate to managing the contraction and relaxation to balance the vascular tone under different physiological conditions. [3-5]. It has been reported that the main problems of HTN are associated with vascular changes characterized by endothelial dysfunction and increased vascular contraction [6, 7]. Based on these viewpoints, the main concepts to reduce blood pressure (BP) could be considered to generate vasodilating factors in EC and decrease the contraction effect in VSMC. Further, resulting in enlarging the vessel diameter and increasing the blood flow rate.

*Ecklonia cava* (E. cava) and *Ishige okamurae* (IO) are famous for the different biological activities, including antioxidant, anti-inflammatory, attenuation of endothelial cell dysfunction, and anti-hypertension, in numerous studies [8-11]. *Son et al.* have indicated that E. cava ethanol extract (ECE) significantly alleviates BP in a mouse model of HTN. Furthermore, dieckol (DK), a polyphenolic compound present in ECE, has been suggested as one of the bioactive components responsible for the potential ACE inhibitory activity [12, 13]. Notably, IO ethanol extract (IOE) and its bioactive substances, diphlorethohydroxycarmalol (DPHC), have shown the remarkable ability to regulate endothelial-dependent vasodilation [14]. However, the molecular signaling pathways were rarely mentioned. Therefore, in the present study, we aim to investigate the vasodilative effect of ECE, DK, IOE, and DPHC and also its molecular signaling pathway *in vitro* and *in vivo*.

The endothelial-dependent vasodilation mechanisms are indicated closely related to nitric oxide (NO), a principal regulator of endothelial vasodilator produced from *L*-arginine by endothelial nitric oxide synthase (eNOS) in the presence of oxygen and the cofactors calcium ( $[Ca^{2+}]$ ) and calmodulin (CaM) [15]. A previous study has indicated that genetically deficient eNOS mice are hypertensive, with lower circulating NO levels, thus indicating the critical role of eNOS and NO in Cardiovascular disease [16, 17]. Furthermore, the  $[Ca^{2+}]$  in the endoplasmic reticulum (ER) ( $[Ca^{2+}]_{ER}$ ) has long been proposed as a critical factor in regulating eNOS activity, resulting in vasodilation [17].  $[Ca^{2+}]$  homeostasis is affected by acetylcholine (Ach) or vascular endothelial growth factor (VEGF), which plays a major role in regulating vasodilation by increasing the  $[Ca^{2+}]$  levels presented in the cytosol ( $[Ca^{2+}]_{cytol}$ ) via calcium influx, further promoting the expression of downstream proteins such as eNOS [18, 19]. Additionally, the increased expression of phosphoinositide 3-kinase (PI3K)/protein kinase B (Akt) pathway directly phosphorylates eNOS, thereby increasing its binding to intracellular CaM, activating eNOS, and promoting NO release [18, 20]. Hence, the increase in NO production effectively dilates the vascular tone to enhance vasodilation. Thus, in the first part, we investigated the endothelial vasodilation effect of ECE, DK, IOE, and DPHC. We observed that all the samples could successfully be generated NO by increasing  $[Ca^{2+}]_{ER}$  and  $[Ca^{2+}]_{cytol}$  levels and the PI3K/Akt/eNOS expression. Thus, we suggested that ECE, DK, IOE, and DPHC, these natural marine resources, can efficiently enhance endothelial-dependent vasodilation.

VSMCs contractile mechanism and  $[Ca^{2+}]$  handling are another major controlling point to achieve vasodilation. An increase in free intracellular  $[Ca^{2+}]$  can result from either increased influx of  $[Ca^{2+}]$  from the extracellular space or the increased  $[Ca^{2+}]$  release from sarcoplasmic reticulum (SR) stores ( $[Ca^{2+}]_{SR}$ ) in VSMC. Moreover, the free

[Ca<sup>2+</sup>] binds to a special protein, calmodulin (CaM), and the [Ca<sup>2+</sup>]-CaM complex would further activate the phosphorylation of myosin light chains kinase (MLCK), a kinase enable to interact with myosin light chain (MLC) and actin then lead to contraction [21]. Therefore, the VSMC relaxation occurs only when there is reduced phosphorylation of MLC. In the second part of the study, we aim to verify the relaxation effect of ECE, DK, IOE, and DPHC in VSMC; we have used the EC-VSMC coculture system to mimic the composition of the human vessel and studied its interaction. Based on our results, we found that the NO stimulated by samples in EC would reduce the [Ca<sup>2+</sup>]<sub>cytol</sub> and also the decreased expressions of CaM and *p*-MLC/MLC ratio in VSMC. In particular, the results demonstrated that DK has a high potential to be the vasodilator.

After knowing that DK and DPHC effectively promote the vasodilator NO in EC then further resulting in vasorelaxation in VSMC *in vivo* experiments. In the third part, we targeted to confirm the vasodilation property *in vitro* model. The zebrafish model has previously revealed several essential insights into vascular structure development and helped verify underlying molecular mechanisms [22]. In order to confirm all the results of *in vivo*, the wild-type zebrafish (*Danio rerio*) and *Tg(flk: EGFP)* transgenic zebrafish were employed for further experiments. The previous study has shown that contractile marker would increase the expression within the period between 4 dpf and 6 dpf [23]. Therefore, we made up a vasoconstriction model by exposing the zebrafish to the classic vasoconstricting agent, Phenylephrine hydrochloride (PE), to determine the vasoactivity at 5 dpf. Further, to evaluate the vasodilation effect of DK and DPHC by measuring the associated cardiovascular parameters such as blood flow (nL/s), linear velocity (μM/s), vessel diameter (μM), and arterial pulse (beats per min). As expected, DK and DPHC treatments effectively promoted vasodilation by increasing the diameter of the dorsal aorta, further regulating blood flow velocity and arterial pulse in the zebrafish model.

In summary, we suggested that the DK and DPHC, which were isolated from *Ecklonia cava* and *Ishige okamurae*, exerted vasodilatory property by regulating the calcium signaling and activating the PI3K/Akt/eNOS in EC and further relaxing the VSMC by decreasing the CaM and *p*-MLC expressions. The vasodilative results were performed in the zebrafish model by showing the increased dorsal aorta diameter, further regulating blood flow velocity and arterial pulse. Based on the present study results, DK and DPHC have a high potential to be developed into a vasodilator for further HTN treatment.

**Keywords:** *Ecklonia cava*; *Ishige okamurae*; diphlorethohydroxycarmalol; dieckol; endothelial-dependent NO production, hydrogen sulfate; calcium; calmodulin; smooth muscle cell; myosin light chain; zebrafish; vasodilation

## List of figures

- Figure 1- 1 Extraction and fractionation of *E.Cava*. (A) The *E.Cava* powder was extracted with 50% ethanol and fractionated with Hexan, Chloroform, Ethyl acetate, and n-butanol. (B) and (C) The BUCHI pure chromatography system was used for DK separation. Chromatography was performed on a reverse-phase YMC Pack ODS-A column (250 × 20 mm i.d. and 5µm particle size). DK was obtained from ethyl acetate solvent fraction of 50% ethanol extract of brown seaweed *E.Cava* after though FlashPrep system purification..... 10
- Figure 1- 2 Extraction and fractionation of *I. okamurae*. (A) The *I. okamurae* powder was extracted with 50% ethanol and fractionated with Hexan, Chloroform, Ethyl acetate, and n-butanol. (B) and (C) Liquid chromatography – Mass Spectrometry (LC-MS/MS) analysis of DPHC, DPHC was obtained from ethyl acetate solvent fraction of 50% ethanol extract of brown seaweed *I. okamurae* after though FlashPrep system purification..... 11
- Figure 1- 3 Measurements of cytotoxicity under the sample treatments. Cells were treated with different concentrations of (A) ECE, (B) DK, (C) IOE, and (D) DPHC. Each column and bar represent the mean ± standard deviation (S.D.). \*  $p < 0.05$ , significant difference compared to the control group. DPHC: diphloretohydroxycarmalol; ns: not significant. .... 12
- Figure 1- 4 The levels of intracellular NO. The EA.hy926 cells were treated with different concentrations of (A) ECE, (B) DK, (C) IOE, and (D) DPHC. Experiments were performed in triplicates. Each column and bar represent the mean ± standard deviation (S.D.). \*  $p < 0.05$ , \*\*  $p < 0.01$ . \*\*\*  $p < 0.001$ , significant difference compared to the control group. .... 13

Figure 1- 5 The intracellular H<sub>2</sub>S levels induced by different concentrations of DK and DPHC treatments. (A) different concentration of DK. (B) different concentrations of DPHC. For statistical significance, each time-point was compared to the 0 min of each concerntractions. Experiments were performed in triplicates. \*  $p < 0.05$ , \*\*  $p < 0.01$ , and \*\*\*  $p < 0.001$ . ns: not significant ..... 15

Figure 1- 6 Evaluation of vasodilation-associated proteins expression under ECE and IOE treatments. (A)(E) Representatives Western blot analysis. Quantification of phosphorylated (B) *p*-PI3K (C) *p*-Akt (D) *p*-eNOS (d) in EA.hy926 cells treated with different concentrations of ECE; and the quantification of phosphorylated (F) *p*-PI3K (G) *p*-Akt (H) *p*-eNOS in EA.hy926 cells treated with different concentrations of IOE. The protein bands were ultimately developed and photographed with the FUSION Solo Vilber Lourmat system. Quantitative data were analysed using Image J 1.50i soft-ware (NIH, USA). Results are expressed as the mean ± standard deviation (S.D.) of three independent experiments. \*  $p < 0.05$ , \*\*  $p < 0.01$ . \*\*\*  $p < 0.001$ , significant difference com-pared to the control group. DPHC: diphlorethohydroxycarmalol; PI3K: phosphoinositide 3-kinase; Akt: protein kinase B; eNOS: endothelial nitric oxide synthase. .... 17

Figure 1- 7 Evaluation of vasodilation-associated proteins expression under DK and DPHC treatments. (A)(E) Representatives Western blot analysis. Quantification of phosphorylated (B) *p*-PI3K (C) *p*-Akt (D) *p*-eNOS (d) in EA.hy926 cells treated with different concentrations of DK; and the quantification of phosphorylated (F) *p*-PI3K (G) *p*-Akt (H) *p*-eNOS in EA.hy926 cells treated with different concentrations of DPHC. The protein bands were ultimately developed and photographed with the FUSION Solo Vilber Lourmat system. Quantitative data were analysed using Image J 1.50i soft-ware (NIH, USA). Results are expressed as

the mean  $\pm$  standard deviation (S.D.) of three independent experiments. \*  $p < 0.05$ , \*\*  $p < 0.01$ . \*\*\*  $p < 0.001$ , significant difference compared to the control group.

DPHC: diphloretohydroxycarmalol; PI3K: phosphoinositide 3-kinase; Akt: protein kinase B; eNOS: endothelial nitric oxide synthase. .... 18

Figure 1- 8 Quantification of the  $[Ca^{2+}]_{cytol}$  levels stimulated by different concentrations of ECE and IOE in EA.hy926 cells. The traces (A, C) and box plots (B, D) indicating the levels of  $[Ca^{2+}]_{cytol}$ . For statistical significance, each sample treatment group was compared to the control group. Experiments were performed in triplicates. \*  $p < 0.05$ , \*\*  $p < 0.01$ , and \*\*\*  $p < 0.001$ . ns: not significant; AUC: area under the curve;  $[Ca^{2+}]_{cytol}$ : calcium level in the cytosol; PSS: physiological salt solution. .... 20

Figure 1- 9 Quantification of the  $[Ca^{2+}]_{cytol}$  levels stimulated by different concentrations of DK and DPHC in EA.hy926 cells. The traces (A, C) and box plots (B, D) indicating the levels of  $[Ca^{2+}]_{cytol}$ . For statistical significance, each sample treatment group was compared to the control group. Experiments were performed in triplicates. \*  $p < 0.05$ , \*\*  $p < 0.01$ , and \*\*\*  $p < 0.001$ . ns: not significant; AUC: area under the curve;  $[Ca^{2+}]_{cytol}$ : calcium level in the cytosol; PSS: physiological salt solution. .... 21

Figure 1- 10 Computational prediction of the AchR and docking stimulation with DK/DPHC. (A) Specific interaction between the DK and the ligand. (B) Two-dimensional (2D) diagram of ligand-AchR and DK and DK complex (C) The results of interaction energy and binding energy of DK-AchR complex. (D) Specific interaction between the DPHC and the ligand. (B) Two-dimensional (2D) diagram of ligand-AchR and DPHC complex (C) The results of interaction energy and binding energy of DPHC-AchR complex ..... 24

Figure 1- 11 Computational prediction of the VEGFR2 and docking stimulation with DK/DPHC. (A) Specific interaction between the DK and the ligand. (B) Two-dimensional (2D) diagram of ligand-VEGFR2 and DK (C) the results of interaction energy and binding energy of DK-VEGFR2 complex. (D) Specific interaction between the DPHC and the ligand. (B) Two-dimensional (2D) diagram of ligand- VEGFR2 and DPHC complex (C) The results of interaction energy and binding energy of DPHC- VEGFR2 complex .....25

Figure 1- 12 Influence of specific antagonists on  $[Ca^{2+}]_{cytol}$  levels in EA.hy926 cells treated with DK. (A) Traces (B) and box plots indicating  $[Ca^{2+}]_{cytol}$  levels in response to treatment with DK and antagonists. (C) Effect of DK on NO production in EA.hy926 cells pre-treated with 100  $\mu$ M of atropine, SU5416, and nifedipine. The NO levels were detected by adding 10  $\mu$ M of 4 ami-no-5-methylamino-2', 7'-difluorescein diacetate (DAF-FM DA). (D) Possible mechanisms. Experiments were performed in triplicates. Each column and bar represent the mean  $\pm$  standard deviation (S.D.). \*\*  $p < 0.01$ . \*\*\*  $p < 0.001$ , significant difference compared to the control group. ns: not significant; AUC: area under the curve; DPHC: diphloretrohydroxycarmalol;  $[Ca^{2+}]_{cytol}$ : calcium level in the cytosol. ....28

Figure 1- 13 Influence of specific antagonists on  $[Ca^{2+}]_{cytol}$  levels in EA.hy926 cells treated with DPHC. (A) Traces (B) and box plots indicating  $[Ca^{2+}]_{cytol}$  levels in response to treatment with DPHC and antagonists. (C) Effect of DPHC on NO production in EA.hy926 cells pre-treated with 100  $\mu$ M of atropine, SU5416, and nifedipine. The NO levels were detected by adding 10  $\mu$ M of 4 ami-no-5-methylamino-2', 7'-difluorescein diacetate (DAF-FM DA). (D) Possible mechanisms. Experiments were performed in triplicates. Each column and bar

represent the mean  $\pm$  standard deviation (S.D.). \*\*  $p < 0.01$ . \*\*\*  $p < 0.001$ , significant difference compared to the control group. ns: not significant; AUC: area under the curve; DPHC: diphlorethohydroxycarmalol;  $[Ca^{2+}]_{cytol}$ : calcium level in the cytosol. ....29

Figure 2- 1 The experimental protocol of conditional media transfer experiments. ....41

Figure 2- 2 The experimental graphic of conditional media transfer experiments.....42

Figure 2- 3 The methodology of the HCAEC-HCASM C co-culture model .....44

Figure 2- 4 Evaluation of cell viability treated with different concentrations of (A) IOE, (B) DPHC, (C) ECE, and (D) DK. Experiments were performed in triplicates. Each column and bar represent the mean  $\pm$  standard deviation (S.D.). \*  $p < 0.05$ , \*\*  $p < 0.01$ . \*\*\*  $p < 0.001$ , significant difference compared to the control group. ....48

Figure 2- 5 Evaluation of the level of intracellular NO concentrations induced by (A) IOE, (B) ECE, (C) DPHC, and (D) DK were measured by 10  $\mu$ M of DAF-FM-DA assay in HCEAECs. Experiments were performed in triplicates. Each column and bar represent the mean  $\pm$  standard deviation (S.D.). \*  $p < 0.05$ , \*\*  $p < 0.01$ . \*\*\*  $p < 0.001$ , significant difference compared to the control group. ....49

Figure 2- 6 Evaluation of the level of intracellular H<sub>2</sub>S concentrations induced by different concentrations of DK and DPHC in HCEAECs. Experiments were performed in triplicates. Each column and bar represent the mean  $\pm$  standard deviation (S.D.). \*  $p < 0.05$ , \*\*  $p < 0.01$ . \*\*\*  $p < 0.001$ , significant difference compared to the control group .....51

Figure 2- 7 Quantification of the  $[Ca^{2+}]_{cytol}$  levels stimulated by different samples in HCAECs. (A) The traces (B) box plots the levels of  $[Ca^{2+}]_{cytol}$ . (C) The images represented the expression of fluorescence under the sample treatments. For

statistical significance, each sample treatment group was compared to the control group. Experiments were performed in triplicates. \*\*\*  $p < 0.001$ ; AUC: area under the curve;  $[Ca^{2+}]_{cytol}$ : calcium level in the cytosol. ....53

Figure 2- 8 Evaluation of cell viability treated with different concentrations of (A) IOE (3, 10, 30, and 100  $\mu\text{g/ml}$ ), (B) DPHC (6, 20, 60, and 100  $\mu\text{M}$ ), (C) ECE (3, 10, 30, and 100  $\mu\text{g/ml}$ ), and (D) DK (4, 13, 40, and 134  $\mu\text{M}$ ) in HCASMC. Experiments were performed in triplicates. Each column and bar represent the mean  $\pm$  standard deviation (S.D.). #  $p < 0.05$  significant difference compared to the control group. n.s: non-significant different. ....55

Figure 2- 9 Measurement of cell viability of HCASMC exposed in the conditional medium. (A) 0 h (B) 0.5 h (C) 1 h (D) 3 h (E) 12 h (F) 24 h in HCASMC. Experiments were performed in triplicates. Each column and bar represent the mean  $\pm$  standard deviation (S.D.) n.s: non-significant difference compared to the control group. ....57

Figure 2- 10 Measurement of NO production at different time points when HCASMC exposure under conditional medium. (A) IOE (100  $\mu\text{g/ml}$ ) (B) DPHC (100  $\mu\text{M}$ ) (C) ECE (100  $\mu\text{g/ml}$ ) (D) DK (134  $\mu\text{M}$ ). The intracellular NO concentrations were detected by 10  $\mu\text{M}$  of DAF-FM-DA assay in HCASMC. Experiments were performed in triplicates. Each column and bar represent the mean  $\pm$  standard deviation (S.D.). \*  $p < 0.05$  significant difference compared to the control group. n.s: non-significant different. ....58

Figure 2- 11 Expression of CaM and phosphorylated myosin light chain ( $p$ -MLC) in HCASMC treated under different concentrations of DK. (A) The examples of the western blot (B) The relative level of CaM/ $\alpha$ -SMA (C) The relative level of  $p$ -MLC/ MLC. Experiments were performed in triplicates. Each column and bar

represent the mean  $\pm$  standard deviation (S.D.). \*  $p < 0.05$ , \*\*\*  $p < 0.001$  significant difference compared to the control group. n.s: non-significant different; CaM: Calmodulin.....60

Figure 2- 12 Expression of CaM and phosphorylated myosin light chain (*p*-MLC) in HCASMC treated with different concentrations of DPHC. (A) The examples of the western blot (B) The relative level of CaM/ $\alpha$ -SMA (C) The relative level of *p*-MLC/ MLC. Experiments were performed in triplicates. Each column and bar represent the mean  $\pm$  standard deviation (S.D.). \*  $p < 0.05$ , \*\*\*  $p < 0.01$  , and \*\*\*  $p < 0.001$  significant difference compared to the control group. n.s: non-significant different; CaM: Calmodulin.....61

Figure 2- 13 Immunofluorescence analysis of HCAEC under the DK treatments. (A) The images were represented the CaM expression (B) The analysis of fluorescence intensity under the treatment of different concentrations of DK. Experiments were performed in triplicates. Each column and bar represent the mean  $\pm$  standard deviation (S.D.). \*  $p < 0.05$ , \*\*\*  $p < 0.01$  , and \*\*\*  $p < 0.001$  significant difference compared to the control group. n.s: non-significant different; CaM: Calmodulin. 63

Figure 2- 14 Immunofluorescence analysis of HCAEC under DPHC treatments. (A) The images were represented the CaM expression (B) The analysis of fluorescence intensity under the treatment of different concentrations of DPHC. Experiments were performed in triplicates. Each column and bar represent the mean  $\pm$  standard deviation (S.D.). \*  $p < 0.05$ , \*\*\*  $p < 0.001$  significant difference compared to the control group. n.s: non-significant different; CaM: Calmodulin.....64

Figure 2- 15 Double-label immunofluorescence analysis of HCASMC under the DK treatments. (A) The images were represented the CaM and *p*-MLC expression (B) The analysis of fluorescence intensity under the treatment of different

concentrations of DK. Experiments were performed in triplicates. Each column and bar represent the mean  $\pm$  standard deviation (S.D.). \*  $p < 0.05$ , \*\*\*  $p < 0.001$  significant difference compared to the control group. n.s: non-significant different; CaM: Calmodulin. ....65

Figure 2- 16 Immunofluorescence analysis of HCASMC under the DPHC treatments.

(A) The images were represented the CaM and *p*-MLC expression (B) The analysis of fluorescence intensity under the treatment of different concentrations of DPHC. Experiments were performed in triplicates. Each column and bar represent the mean  $\pm$  standard deviation (S.D.). \*  $p < 0.05$ , \*\*\*  $p < 0.001$  significant difference compared to the control group. n.s: non-significant different; CaM: Calmodulin.....66

Figure 2- 17 Expression of CaM and phosphorylated myosin light chain (*p*-MLC) in

HCASMC treated under different concentrations of DK. (A) The examples of the western blot (B) The relative level of CaM/ $\alpha$ -SMA (C) The relative level of *p*-MLC/ MLC. Experiments were performed in triplicates. Each column and bar represent the mean  $\pm$  standard deviation (S.D.). \*  $p < 0.05$ , \*\*\*  $p < 0.001$  significant difference compared to the control group. n.s: non-significant different; CaM: Calmodulin.....68

Figure 2- 18 Expression of CaM and phosphorylated myosin light chain (*p*-MLC) in

HCASMC treated under different concentrations of DPHC. (A) The examples of the western blot (B) The relative level of CaM/ $\alpha$ -SMA (C) The relative level of *p*-MLC/ MLC. Experiments were performed in triplicates. Each column and bar represent the mean  $\pm$  standard deviation (S.D.). \*  $p < 0.05$ , \*\*\*  $p < 0.001$  significant difference compared to the control group. n.s: non-significant different; CaM: Calmodulin.....69

Figure 3- 1 The graphic represented the protocol of the vasoconstriction model in zebrafish.....79

Figure 3- 2 The protocol of evaluation of associated cardiovascular parameters in the zebrafish model.....81

Figure 3- 3 The survival rate of the zebrafish embryos under-sample treatments. The test was based on the exposure of newly fertilized zebrafish eggs to different DK, DPHC, and PE concentrations for up to 120 h (n=15 per treatment, three replicates). Embryos were observed at each time point under the stereomicroscope (magnification used in the stereomicroscope for observations was 4x). (A) different concentrations of DK treatment (B) different concentrations of DPHC treatment. DK; diekol, DPHC: diphlorethohydroxycarmalol .....83

Figure 3- 4 The toxicity and heartbeat rate of the zebrafish larva under different concentrations of PE treatments. The test was based on the exposure of zebrafish larva to different concentrations of PE for 24 h (n=10 per treatment, three replicates). \*\*\*  $p < 0.001$  compared to the control group. Zebrafish larva was observed under the stereomicroscope (magnification used in the stereomicroscope for observations was 10 x). PE: Phenylephrine hydrochloride.....85

Figure 3- 5 DK and DPHC induce vasodilation in the whole-body vessel in a *Tg(flk: EGFP)* transgenic zebrafish model. (A1) and (B1) Representative images of the *Tg(flk: EGFP)* transgenic zebrafish larva's whole body under the DK and DPHC treatments; all images were captured using a fluorescence microscope (4×). (A2) and (B2) Quantification of the whole-body fluorescence intensity under the DK and DPHC treatments, respectively. Each column and bar represent the mean ± standard deviation (S.D.), n = 8 per group. #  $p < 0.05$ , ##  $p < 0.01$ , ###  $p < 0.001$ ,

significantly different between PE group and control group. \*  $p < 0.05$ , \*\*\*  $p < 0.001$ , significantly different between the PE group and sample treatment groups; ns: not significant; DK; diekol, DPHC: diphlorethohydroxycarmalol. PE: Phenylephrine hydrochloride. ....87

Figure 3- 6 DK and DPHC promote the vasodilation by enlarging the vessel diameter in a *Tg(flk: EGFP)* transgenic zebrafish model. (A1) and (B1) Images of the vessel were captured using a fluorescence microscope (20×). (a–f) were represented the change of diameter under sample treatments. (A2) and (B2) Measurement of the DA diameter. Each column and bar represent the mean  $\pm$  standard deviation (S.D.),  $n = 8$  per group #  $p < 0.05$ , ##  $p < 0.01$ , ###  $p < 0.001$ , significantly different between PE group and control group. \*  $p < 0.05$ , \*\*\*  $p < 0.001$ , significantly different between the PE group and sample treatment groups. DK; diekol, DPHC: diphlorethohydroxycarmalol. PE: Phenylephrine hydrochloride. ....89

Figure 3- 7 The image was demonstrated by the MicoZebraLab software. The MicoZebraLab application from ViewPoint (Version 3. 4. 4, Lyon, France) was used to evaluate and calculate the cardiovascular parameters. ....90

Figure 3- 8 Measurements of arterial pulse under the treatments of different concentrations of DK and DPHC. The change of arterial pulse (bear per min) under DK (A) and DPHC (B) treatments. Each column and bar represent the mean  $\pm$  standard deviation (S.D.),  $n = 8$  per group. \*  $p < 0.05$ , \*\*\*  $p < 0.001$ , significant difference compared to the control group; #  $p < 0.05$ , ##  $p < 0.01$ , ###  $p < 0.001$ , significant different compared to the PE group. DK; diekol, DPHC: diphlorethohydroxycarmalol. PE: Phenylephrine hydrochloride. ....91

Figure 3- 9 Measurements of blood flow and mean blood velocity under the treatments of different concentrations of DK and DPHC. The change of blood flow (nL/min)

under (A) DK and (B) DPHC treatments. The change of mean blood velocity ( $\mu\text{M/s}$ ) under (C) DK and (D) DPHC treatments. Each column and bar represent the mean  $\pm$  standard deviation (S.D.),  $n = 8$  per group. #  $p < 0.05$ , ##  $p < 0.01$ , ###  $p < 0.001$ , significantly different between PE group and control group. \*  $p < 0.05$ , \*\*  $p < 0.001$ , significantly different between the PE group and sample treatment groups. DK; diekol, DPHC: diphlorethohydroxycarmalol. PE: Phenylephrine hydrochloride. ....93

**Part I**

**Bioactive compounds isolated from *Ecklonia cava* and *Ishige okamurae*  
promote vasodilation in endothelial via calcium signalling and  
PI3K/Akt/eNOS pathway**

## 1.1.Introduction

Under physiological conditions, the vascular endothelium plays a critical role in regulating the vascular tone and blood pressure (BP) by generating vasodilating and vasoconstricting factors to suppress cardiovascular diseases (CVD) (e.g., hypertension, acute coronary syndromes) [3-5]. Nitric oxide (NO) is a well-known vessel-relaxing factor produced from L-arginine by endothelial nitric oxide synthase (eNOS) in the presence of oxygen and the cofactors  $\text{Ca}^{2+}$  and calmodulin [15]. A previous study has indicated that genetically deficient eNOS mice are hypertensive, with lower circulating NO levels, thus indicating the critical role of eNOS and NO in CVD [16, 17]. The cytosolic  $[\text{Ca}^{2+}]$  ( $[\text{Ca}^{2+}]_{\text{cytol}}$ ) can either increase due to influx from the cytosol through specific calcium channels expressed on the cell surface or by release from intracellular stores such as the endoplasmic reticulum (ER) [24]. Furthermore, ER  $[\text{Ca}^{2+}]$  has long been proposed as a critical factor in regulating eNOS activity, resulting in vasodilation [17]. Calcium homeostasis is affected by acetylcholine (Ach) or vascular endothelial growth factor (VEGF), which plays a major role in regulating vasodilation by increasing  $[\text{Ca}^{2+}]_{\text{cytol}}$  levels via calcium influx, further promoting the expression of downstream proteins such as eNOS [18, 19]. Furthermore, the increased expression of Akt directly phosphorylates eNOS, thereby increasing its binding to intracellular calmodulin, activating eNOS, and promoting NO release [18, 20]. Thus, the increase in NO production effectively dilates the vascular tone to prevent cardiovascular diseases.

*Ecklonia cava* (E. cava) and *Ishige okamurae* (IO) are famous for the different biological activities, including antioxidant, anti-inflammatory, attenuation of endothelial cell dysfunction, and antihypertension, in numerous studies [8-11]. *Son et al.* have indicated that E. cava ethanol extract (ECE) significantly alleviates BP in a mouse model of HTN. Furthermore, dieckol (DK), a polyphenolic compound present in ECE, has been suggested as one of the bioactive components responsible for the potential ACE inhibitory activity [12, 25]. Notably, IO ethanol

extract (IOE) and its bioactive substances, diphlorethohydroxycarmalol (DPHC), have shown the remarkable ability to regulate endothelial-dependent vasodilation [14]. However, investigations on the antihypertensive effects of ECE, IOE, and their bioactive compounds have primarily focused on ACE inhibition;  $[Ca^{2+}]$  homeostasis in vascular endothelial cells, a crucial feature of vasodilation that could improve vascular health and function, needs to be evaluated. Therefore, in the present study, we investigated the vasodilatory effect of ECE, DK, IOE, and DPHC and also its molecular signalling pathway *in vitro*.

## **1.2. Material and methods**

### **1.2.1. Chemicals and reagents**

Dulbecco's modified Eagle's medium (DMEM) and penicillin/streptomycin solution were purchased from GIBCO (Grand Island, NY, USA). Fetal bovine serum (FBS) was obtained from Merck (Sacramento, CA, USA); dimethyl sulfoxide (DMSO) and 3-(4-(5-dimethyl-2-yl)-2-5-diphenyltetrasolium bromide (MTT) were purchased from Sigma-Aldrich (St. Louis, MO, USA). The intracellular NO production was detected using DAF-FM DA (Thermo Fisher Scientific, Waltham, MA, USA); the total NO production was measured using the Griess assay (Promega Corporation, Madison, WI, USA). Calcium levels were quantified using Fluo-4-AM dye (1-[2-amino-5-(2,7-difluoro-6-hydroxy-3-oxo-9-xanthenyl)phenoxy]-2-(2-amino-5-methylphenoxy) ethane-N, N, N', N'-tetra acetic acid, pentaacetoxymethyl ester) (Thermo Fisher Scientific, Waltham, MA, USA). Atropine, a specific AchR antagonist, was purchased from Sigma Aldrich. SU5416, a VEGFR2 inhibitor, was obtained from Tocris Bioscience (Bristol, UK).

### **1.2.2. Extraction and isolation of DK**

In brief, the method for preparing ECE and DK is as follows: EC was collected in April on Jeju Island, South Korea. First, EC was washed with running water to remove salt, sand, and epiphytes attached to the surface. Then, it was lyophilized and ground to obtain a dry powder. Dried EC powder was extracted with 50% ethanol at room temperature for 24 h. Isolation of DK was performed according to a previously published method [26]. The BUCHI pure chromatography system (BUCHI, Pure C-850 FlashPrep, Switzerland) was used for DK separation. Chromatography was performed on a reverse-phase YMC Pack ODS-A column (250 × 20 mm i.d. and 5µm particle size). The mobile phase consisted of a water-methanol (MeOH) gradient process (0 min, 90:10 v/v; 0-12 min, 90:10 v/v; 12-36 min, 85:15 v/v; 36-68

min, 80:20 v/v; 68-80 min, 0:100 v/v). The gradient elution was performed as follows: the flow rate was 9 mL/min, and the injection volume was 2 mL. Detection was performed at 230 nm.

### ***1.2.3. Extraction and isolation of DPHC***

DPHC isolation was performed as previously described [13]. In brief, IO leaves were collected from Jeju Island, South Korea. IO specimens were washed with running water to remove salt, sand, and epiphytes attached to the surface. Next, IO specimens were lyophilized and ground to obtain a dry powder. Dried IO powder was extracted in 50% ethanol under refluxing conditions. The extract was concentrated and freeze-dried. Centrifugal partition chromatography (CPC) (CPC240, Tokyo, Japan) was performed with a portion of the extract. The CPC solvent system was composed of a mixture of n-hexane, EtOAc, MeOH, and H<sub>2</sub>O. Further purification was performed using an HPLC system (Milford, Massachusetts, USA) equipped with a YMC-Pack ODS-A column (YMC Co., Ltd., Kyoto, Japan). The sample was eluted using an isocratic solvent system.

### ***1.2.4. EA.hy926 cells culture and cytotoxicity analysis***

Human cardiovascular endothelial cell line EA.hy926 was acquired from the American Type Culture Collection (ATCC; Manassas, VA, USA) and cultured in DMEM supplemented with 100 U/mL penicillin, 0.1 mg/mL streptomycin, and 10% FBS. Cells were grown in a humidified incubator at 37 °C, in an atmosphere with 5% (v/v) CO<sub>2</sub>. Cells at 2–5 passages were used for all experiments. An MTT assay assessed EA.hy926 cell viability. A total of  $1 \times 10^5$  cells/well (180  $\mu$ L of cell suspension) were seeded in a 96-well plate and incubated at 37 °C for 24 h. Cells were treated with different concentrations (6, 20, and 60  $\mu$ M) of DPHC for another 24 h. Then, 100  $\mu$ L (concentration: 2 mg/mL) of MTT was added to the wells, and cells were incubated for 2 h. After 2 h, the medium was replaced with 150  $\mu$ L of DMSO. The

supernatant was collected, and the absorbance was measured using a microplate reader at 540 nm (Synergy HT, BioTek Instruments, Winooski, VT, USA).

#### ***1.2.5. Evaluation of the intracellular NO production***

DAF-FM DA is a fluorescent probe used to detect intracellular NO. DAF-FM DA is a cell-permeable deacetylated form of DAF-FM and is hydrolyzed by intracellular esterases to form a cell-impermeable DAF-FM reacts with NO. Therefore, the fluorescence intensity in cells was used to evaluate intracellular NO levels [45]. EA.hy926 cells were pre-incubated with 10  $\mu$ M of DAF-FM DA reagent for 30 min in the dark. The mean fluorescence intensity was then measured using a spectrofluorometer (Synergy HT, BioTek Instruments, Italy).

#### ***1.2.6. Measurement of the intracellular H<sub>2</sub>S levels***

The isolated were incubated in Krebs-HEPES solution (in mM: 119 NaCl, 4.6 KCl, 1.2 CaCl<sub>2</sub>-2H<sub>2</sub>O; 0.4 KH<sub>2</sub>PO<sub>4</sub>, 1 MgSO<sub>4</sub>-7H<sub>2</sub>O, 5 NaHCO<sub>3</sub>, 5.5 glucose, 20 HEPES, and 0.15 NaH<sub>2</sub>PO<sub>4</sub>, pH = 7.4, at 37 °C) containing 50  $\mu$ M Washington State Probe-5 (WSP-5, Cayman Chemical, Ann Arbor, MI, USA), a fluorescence sensor for H<sub>2</sub>S. After a 30-minute incubation, the samples were treated into cells. The fluorescence was quantified by a blinded investigator calculating the integrated density using a spectrofluorometer (Synergy HT, BioTek Instruments, Italy).

#### ***1.2.7. Quantification of the cytosolic calcium levels***

By definition, cytosolic Ca<sup>2+</sup> levels refer to the concentration of calcium ions in the cytosol ([Ca<sup>2+</sup>]<sub>cytol</sub>). Physiological salt solution (PSS) (140 mM NaCl, 5.9 mM KCl, 1.4 mM MgCl<sub>2</sub>·6H<sub>2</sub>O, 10 mM HEPES, 11.5 mM glucose, 1.2 mM NaH<sub>2</sub>PO<sub>4</sub>, 5 mM NaHCO<sub>3</sub>, and 1.8 mM CaCl<sub>2</sub>, at pH 7.4 with NaOH) was used as the basal reagent. To measure [Ca<sup>2+</sup>]<sub>cytol</sub> levels,

the Ca<sup>2+</sup> -sensitive Fluo-4 probe was dissolved in PSS. EA.hy926 cells were seeded in 96-well plates overnight when they reached approximately 80% confluence. Next, 1× Fluo-4 was added, and cells were incubated for 30 min at 37 °C in the dark. The cells were rinsed twice with 1× phosphate-buffered saline (PBS), and 50 µL of 1× PBS was added to the wells. Fluorescence intensity was measured for 10 s at 1-s intervals. The cells were then treated with 1× PSS (Control); ECE (3, 10, 30, and 100 µg/ml); IOE (3, 10, 30, and 100 µg/ml); DK (4, 13, 40, and 134 µM); DPHC (6, 20, 60, and 100 µM). All the samples were dissolved in 0.1% bovine serum albumin (BSA). After the treatment, fluorescence was detected for another 50 s at 1-s intervals.

To investigate the relationship between samples (DK and DPHC) and AchR, VEGFR2, and voltage-dependent calcium channel activation, cells were pre-treated for 30 min with 100 µM of atropine, an AchR antagonist, and 100 µM SU5416, a VEGFR2 antagonist, and 100 µM of nifedipine, the L-type calcium channel blocker. The 1× Fluo-4 fluorescent dye was added, and cells were incubated for another 30 min at 37 °C in the dark. Calcium levels were then measured as described earlier. The box plot data represent the mean value of the AUC calculated from 0 to 60 s. The error bars indicate the maximum and minimum values.

#### **1.2.8. Western blot analysis**

EA.hy926 cells were treated with different concentrations (0, 6, 20, and 60 µM) of DPHC. After 24 h, cells were washed and harvested with ice-cold PBS and lysed with a lysis buffer on ice for 1 h. Lysates were centrifuged at 12,000 rpm for 20 min, and the protein concentration in the supernatant was evaluated with a BSA protein assay kit (Bio-Rad, Hercules, CA, USA). Next, sodium dodecyl sulfate-polyacrylamide gel electrophoresis (SDS-PAGE) was performed with 10% gel. Proteins were transferred onto a nitrocellulose membrane. Membranes were incubated at 4 °C overnight with the following primary antibodies added separately: anti-β-actin (sc-47778, Santa Cruz Bio-technology, CA, USA; 1:1000), anti-p-AKT (sc-377556,

Santa Cruz Biotechnology; 1:1000), anti-*p*-eNOS (#9571S, Cell Signalling Technology, Danvers, Massachusetts, USA; 1:1000), and anti-*p*-PI3K (#17366S, Cell Signalling Technology; 1:1000) dissolved in 5% skim milk. Immunoblots were incubated for another 2 h at room temperature with specific secondary antibodies (1:3000). Protein bands were ultimately developed and photographed using the FUSION SOLO Vilber Lourmat system, Paris, France. The Image J 1.50i software (NIH, USA) was used for quantifying the band intensities.

### ***1.2.9. Statistical analysis***

All experiments were conducted in triplicates, and data are shown as mean  $\pm$  standard deviation. Statistical analysis was performed using the one-way analysis of variance (ANOVA) with Dunnett's post hoc test with the Prism 5.0 software (Graph Pad Software, La Jolla, CA, USA). The following *p*-values were considered statistically significant, and they have been illustrated with asterisks in all figures: \*  $p < 0.05$ , \*\*  $p < 0.01$ , and \*\*\*  $p < 0.001$ .

## 1.3.Results

### 1.3.1. *Evaluation of cytotoxicity and intracellular NO concentrations under the ECE, DK, IOE, and DPHC treatments*

The cytotoxicity was shown in Figure 1-3. We found that there were not toxic when used ECE, IOE, and DK. However, in DPHC treatments, the 100  $\mu$ M was slightly decreased. NO production is dynamically correlated with concentrations of the stimulatory agent and the incubation time. Our previous study used the DPHC (60  $\mu$ M) to investigate the optimal time for NO formation in EA.hy926 cells. The NO production levels were significantly increased starting from 30 min. The peak was observed at 24 h [14]. Therefore, a 24-h incubation period was selected as the optimal incubation time for further experiments. Next, we investigated the levels of dose-dependent NO production in EA.hy926 cells treated with different concentrations of all the samples (ECE, DK, IOE, and DPHC). We observed that 30 and 100  $\mu$ g/ml of ECE and IOE could significantly increase the NO levels (Figure 1-4A and 4C). Compared to the DPHC (Figure 1-4D), the DK demonstrated a higher ability to induce NO levels in EC (Figure 1-4B).

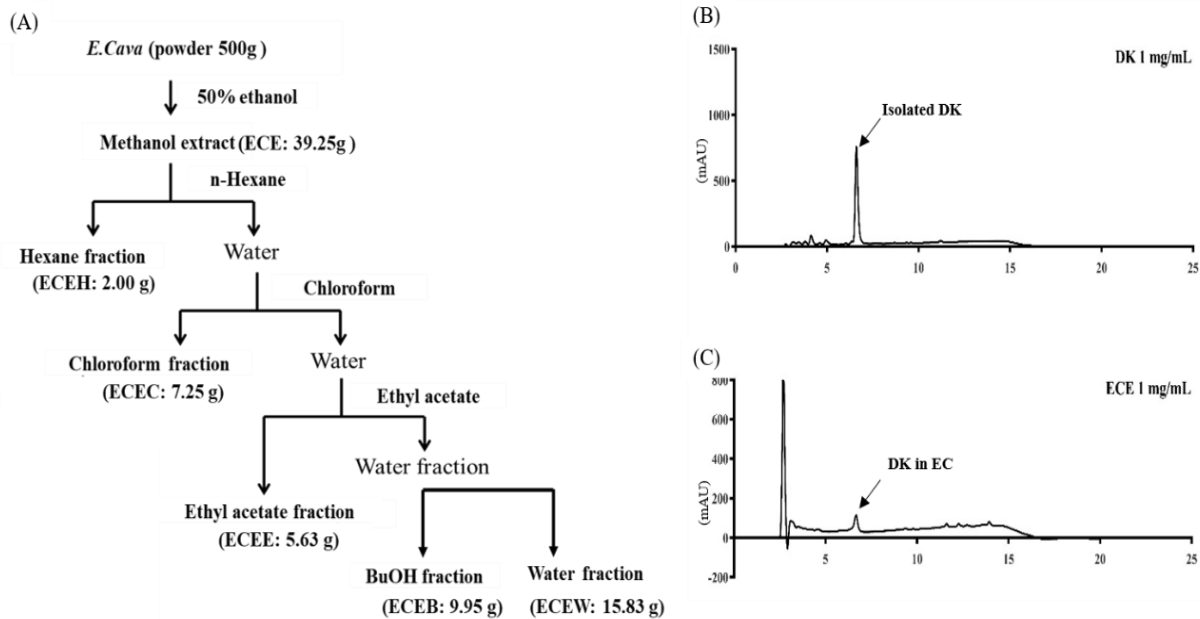


Figure 1- 1 Extraction and fractionation of *E.Cava*. (A) The *E.Cava* powder was extracted with 50% ethanol and fractionated with Hexan, Chloroform, Ethyl acetate, and n-butanol. (B) and (C) The BUCHI pure chromatography system was used for DK separation. Chromatography was performed on a reverse-phase YMC Pack ODS-A column (250 × 20 mm i.d. and 5µm particle size). DK was obtained from ethyl acetate solvent fraction of 50% ethanol extract of brown seaweed *E.Cava* after though FlashPrep system purification.

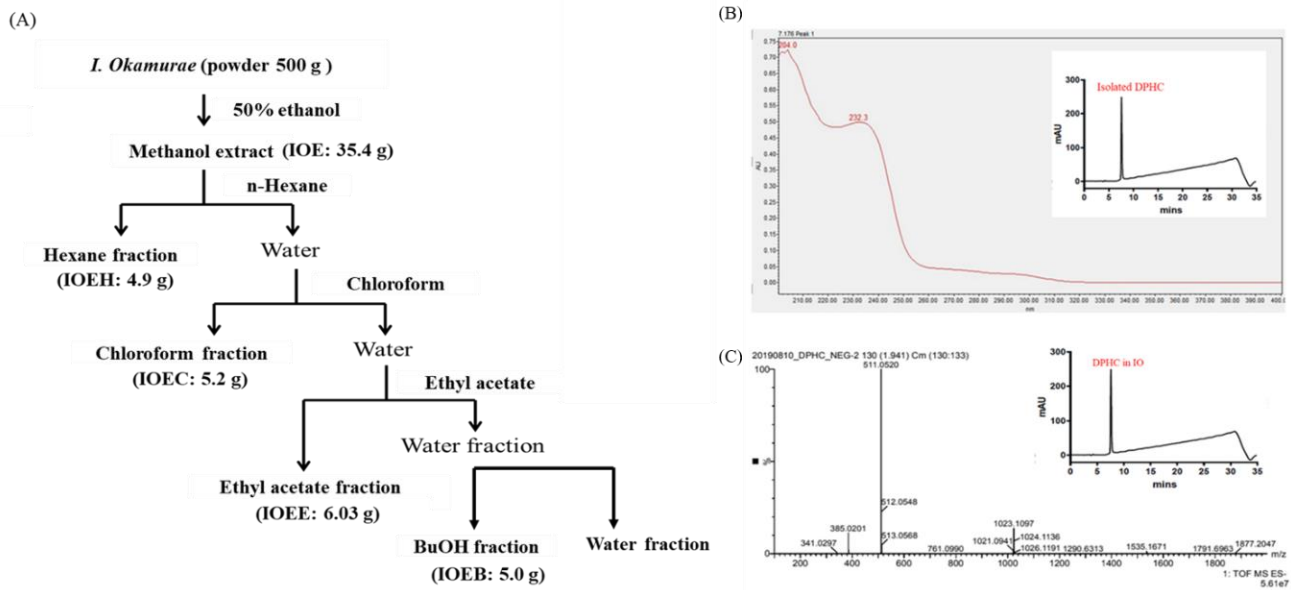


Figure 1- 2 Extraction and fractionation of *I. okamurae*. (A) The *I. okamurae* powder was extracted with 50% ethanol and fractionated with Hexane, Chloroform, Ethyl acetate, and n-butanol. (B) and (C) Liquid chromatography – Mass Spectrometry (LC-MS/MS) analysis of DPHC, DPHC was obtained from ethyl acetate solvent fraction of 50% ethanol extract of brown seaweed *I. okamurae* after though FlashPrep system purification.

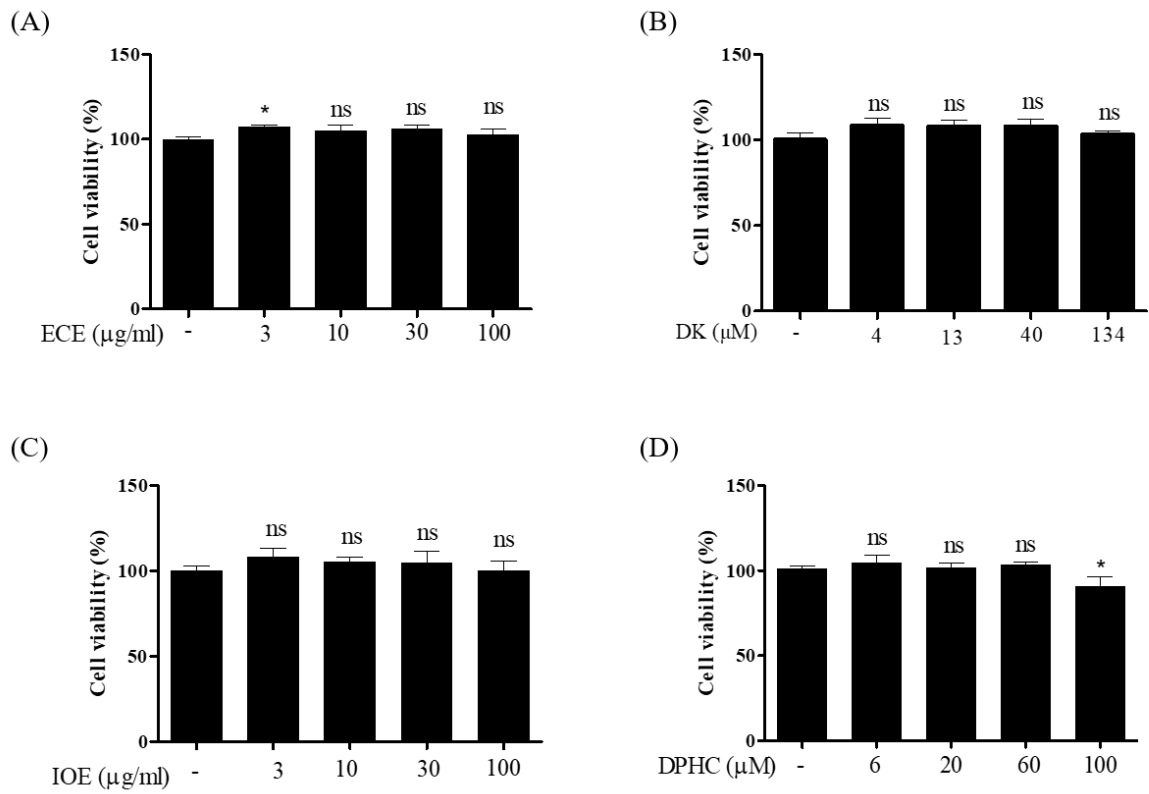


Figure 1- 3 Measurements of cytotoxicity under the sample treatments. Cells were treated with different concentrations of (A) ECE, (B) DK, (C) IOE, and (D) DPHC. Each column and bar represent the mean  $\pm$  standard deviation (S.D.). \*  $p < 0.05$ , significant difference compared to the control group. DPHC: diphlorethohydroxycarmalol; ns: not significant.

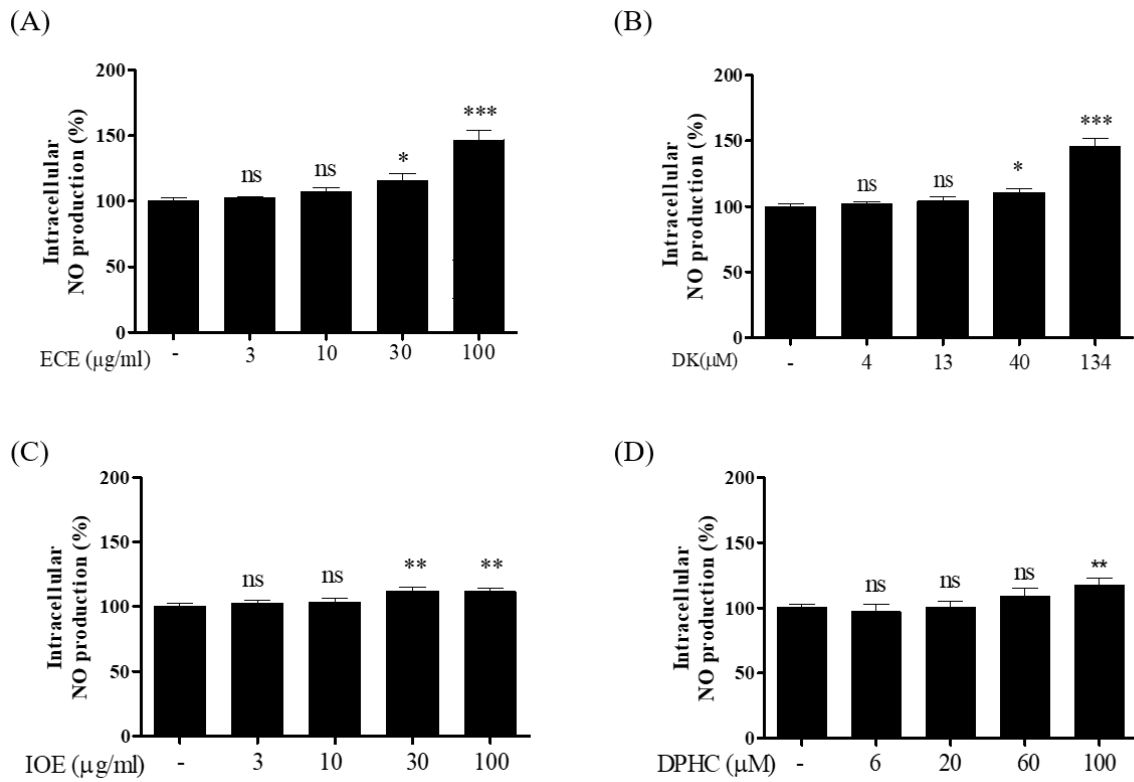


Figure 1- 4 The levels of intracellular NO. The EA.hy926 cells were treated with different concentrations of (A) ECE, (B) DK, (C) IOE, and (D) DPHC. Experiments were performed in triplicates. Each column and bar represent the mean  $\pm$  standard deviation (S.D.). \*  $p < 0.05$ , \*\*  $p < 0.01$ . \*\*\*  $p < 0.001$ , significant difference compared to the control group.

### ***1.3.2. Intracellular H<sub>2</sub>S levels induced by DK and DPHC treatments***

Hydrogen sulfide (H<sub>2</sub>S) is an important endogenous physiological signaling molecule and exerts protective properties in the cardiovascular system, such as vasodilation [27]. We sought to determine whether DK and DPHC improve the intracellular H<sub>2</sub>S levels in EC. Indeed, DK and DPHC treatments promoted the H<sub>2</sub>S levels in time-dependent and dose-dependent trends compared to control. Within 35 min, we observed that a significant difference was detected from 10 min, and DK induced higher concentrations compared to DPHC (Figure 1-5).

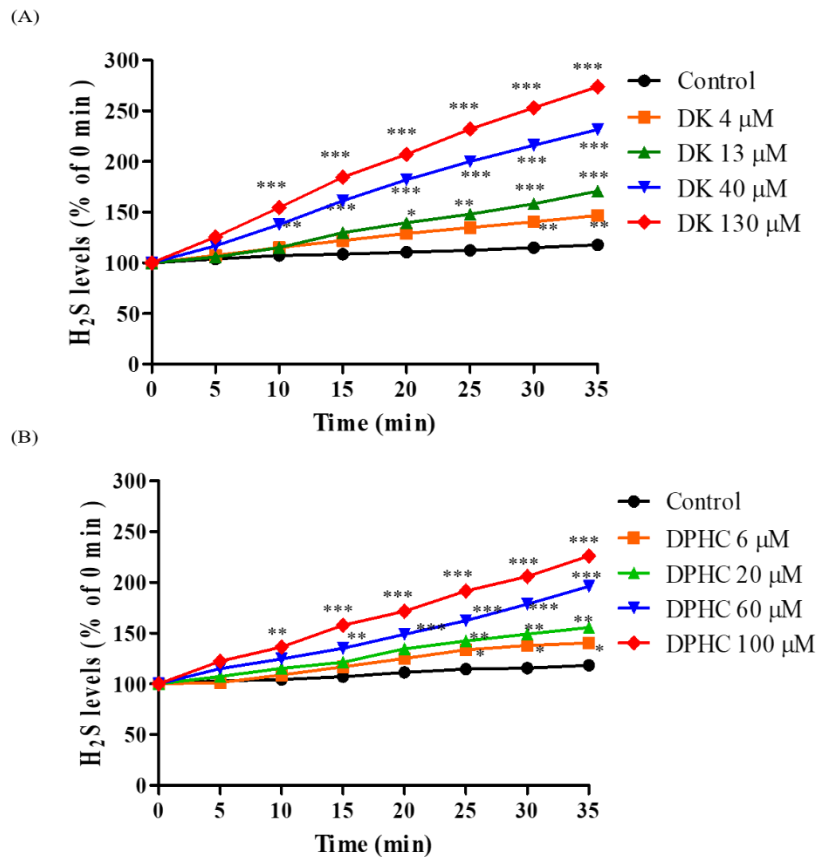


Figure 1- 5 The intracellular H<sub>2</sub>S levels induced by different concentrations of DK and DPHC treatments. (A) different concentration of DK. (B) different concentrations of DPHC. For statistical significance, each time-point was compared to the 0 min of each concentrations. Experiments were performed in triplicates. \*  $p < 0.05$ , \*\*  $p < 0.01$ , and \*\*\*  $p < 0.001$ . ns: not significant

### ***1.3.3. ECE, DK, IOE, DPHC promoted phosphorylation of the PI3K/Akt/eNOS pathway in E.A.hy926 cells***

Since phosphorylation of PI3K and Akt promotes eNOS activity and further enhances NO production [14], we evaluated whether the enhancement of NO production was related to this pathway; protein expression levels of *p*-PI3K, *p*-Akt, and *p*-eNOS were examined by Western blotting of EA.hy926 cells treated with different concentrations of ECE, DK, IOE, and DPHC. The relative levels of *p*-PI3K showed a significant increment only at 100 µg/ml of ECE and IOE (Figure 1-6B and 6F). However, compared to DK (only the group of 134 µM), DPHC showed a significant increase at 20, 60, and 100 µM (Figure 1-6B and 6F). Besides, compared to the control group, the ECE treatments (30 and 100 µg/ml) and IOE (100 µg/ml) enhanced *p*-Akt expression (Figure 1-6C and 6G). Then, the remarkably increments of *p*-Akt were observed at different dosages of DK treatments (Figure 1-7B). However, only 100 µM of DPHC treatment demonstrated a significant increment compared to control (Figure 1-7G). eNOS, the most important protein directly related to NO formation. The expression of *p*-eNOS showed a significant increment at 100 µg/ml of ECE and (30 and 100 µg/ml) of IOE compared to control (Figure 1-7D and 7H). On the other hand, the DK and DPHC could effectively enhance the *p*-eNOS expression in a concentrations-dependent manner in Figures 1-7D and 7H. Based on these results, we knew that all the samples could promote the expressions of PI3K/Akt/eNOS at appropriate dosages. Thus, we hypothesized that DPHC might stimulate the endothelial-dependent NO formation through the PI3K/Akt/eNOS signaling pathway.

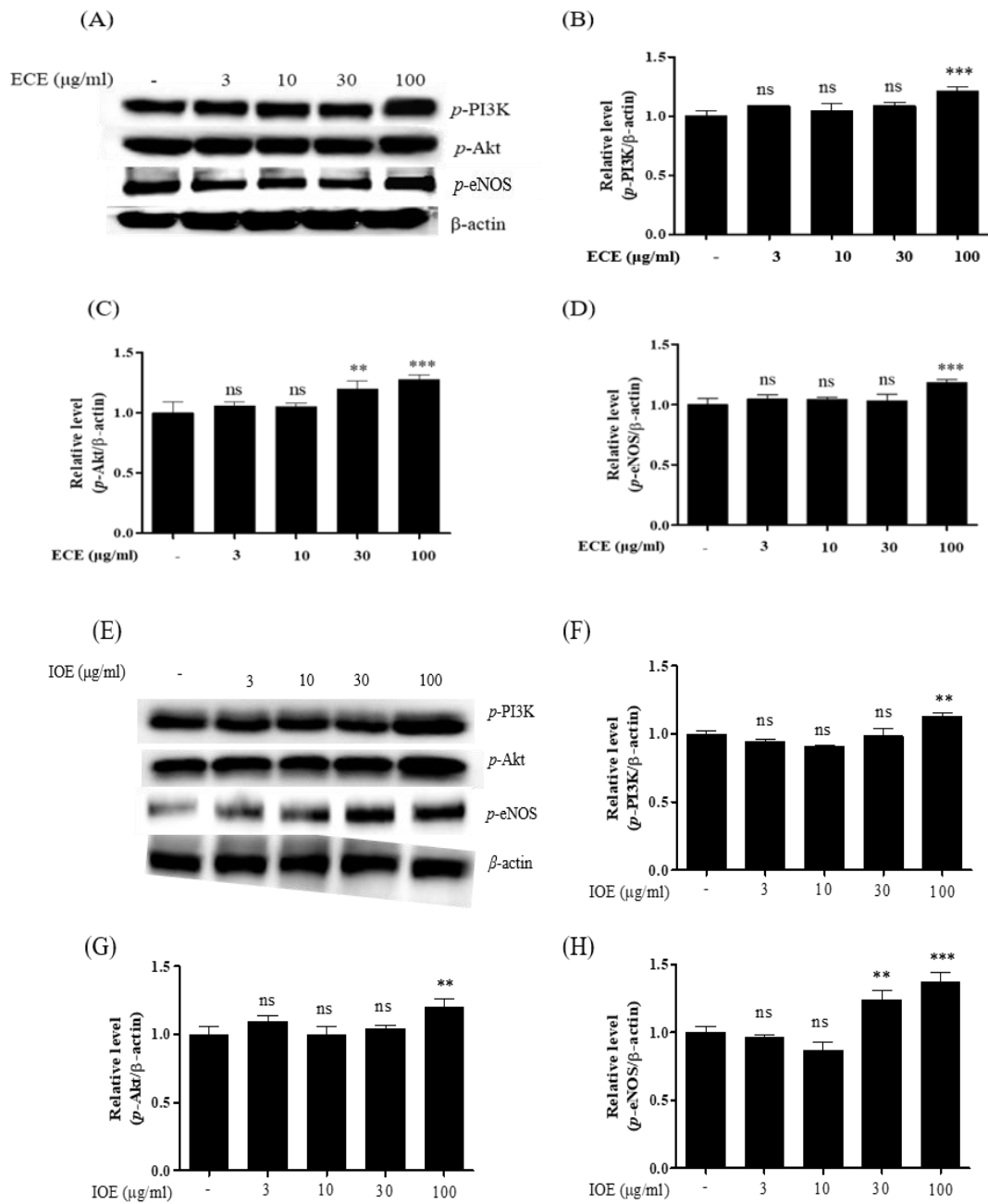


Figure 1- 6 Evaluation of vasodilation-associated proteins expression under ECE and IOE treatments. (A)(E) Representatives Western blot analysis. Quantification of phosphorylated (B) *p*-PI3K (C) *p*-Akt (D) *p*-eNOS (d) in EA.hy926 cells treated with different concentrations of ECE; and the quantification of phosphorylated (F) *p*-PI3K (G) *p*-Akt (H) *p*-eNOS in EA.hy926 cells treated with different concentrations of IOE. The protein bands were ultimately developed and photographed with the FUSION Solo Vilber Lourmat system. Quantitative data were analysed using Image J 1.50i soft-ware (NIH, USA). Results are expressed as the mean  $\pm$  standard deviation (S.D.) of three independent experiments. \*  $p < 0.05$ , \*\*  $p < 0.01$ . \*\*\*  $p < 0.001$ , significant difference compared to the control group. DPHC: diphlorethohydroxycarmalol; PI3K: phosphoinositide 3-kinase; Akt: protein kinase B; eNOS: endothelial nitric oxide synthase.

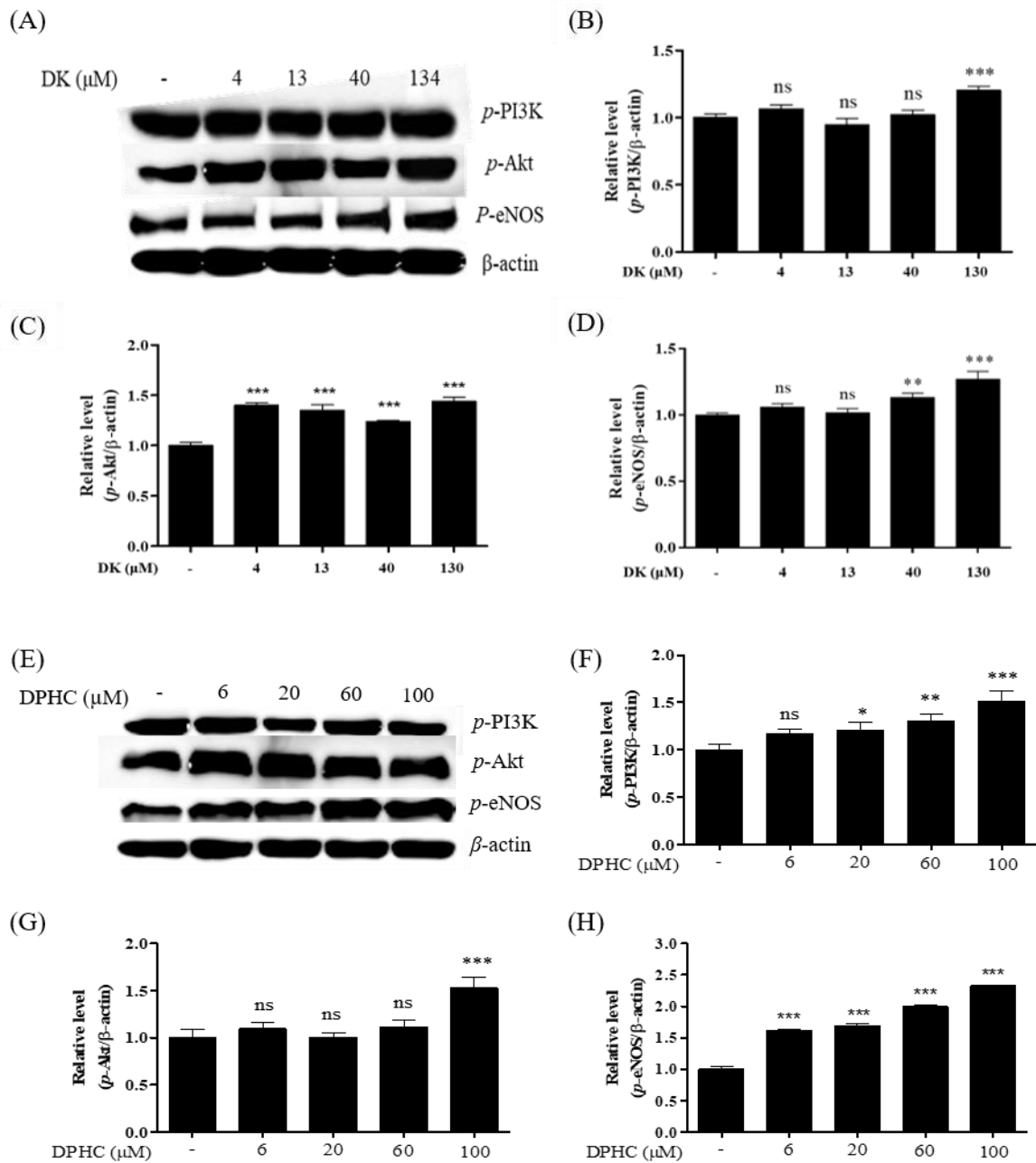


Figure 1- 7 Evaluation of vasodilation-associated proteins expression under DK and DPHC treatments. (A)(E) Representatives Western blot analysis. Quantification of phosphorylated (B) *p*-PI3K (C) *p*-Akt (D) *p*-eNOS (d) in EA.hy926 cells treated with different concentrations of DK; and the quantification of phosphorylated (F) *p*-PI3K (G) *p*-Akt (H) *p*-eNOS in EA.hy926 cells treated with different concentrations of DPHC. The protein bands were ultimately developed and photographed with the FUSION Solo Vilber Lourmat system. Quantitative data were analysed using Image J 1.50i soft-ware (NIH, USA). Results are expressed as the mean ± standard deviation (S.D.) of three independent experiments. \*  $p < 0.05$ , \*\*  $p < 0.01$ . \*\*\*  $p < 0.001$ , significant difference compared to the control group. DPHC: diphloretohydroxycarmalol; PI3K: phosphoinositide 3-kinase; Akt: protein kinase B; eNOS: endothelial nitric oxide synthase.

#### **1.3.4. Regulatory effects of ECE, IOE, DK, and DPHC on the $[Ca^{2+}]_{cytol}$ levels**

In the present study, the  $[Ca^{2+}]_{cytol}$  level represented the calcium levels in the cytosol, which can be influenced by the activation of specific receptors such as vascular endothelial growth factor 2 (VEGFR2) and acetylcholine receptors (AChR). To investigate the calcium prompted effect of ECE, IOE, DK, and DPHC in endothelial cells,  $[Ca^{2+}]_{cytol}$  levels were measured separately. After treating the cells with different concentrations of ECE and IOE at 10 s, the  $[Ca^{2+}]_{cytol}$  levels were elevated after 20 s (Figure 1-8A and 8C). We quantified the increase in  $[Ca^{2+}]_{cytol}$  levels by measuring the area under the curve (AUC). We found that 30 and 100  $\mu$ M of ECE and IOE significantly raised  $[Ca^{2+}]_{cytol}$  levels in EA.hy926 cells (Figure 1-8B and 8D,  $p < 0.001$ ). Moreover,  $[Ca^{2+}]_{cytol}$  levels were dramatically increased starting from 20 s after the treatment, with a gradually decreasing peak detected around 60 s. The results of AUC showed that all the samples strongly stimulated the  $[Ca^{2+}]_{cytol}$  transit by a concentrations-dependent trend compared to the untreated group.

Furthermore, we evaluated the ability of DK and DPHC to detect cytosolic levels. The DK treatment resulted in a significant increase in cytosolic calcium levels, with an AUC value approximately two times higher in calcium level at 134  $\mu$ M DK than control (Figure 1-9B). On the other hand, a similar increasing trend was observed at DPHC treatments. And the effective dosage was found at the 20  $\mu$ M of DPHC, and the optimal concentration was 100  $\mu$ M (Figure 1-9D). However, compared to the AUC of DK and DPHC treatments, we can see that DK showed more high potential to induce calcium transit.

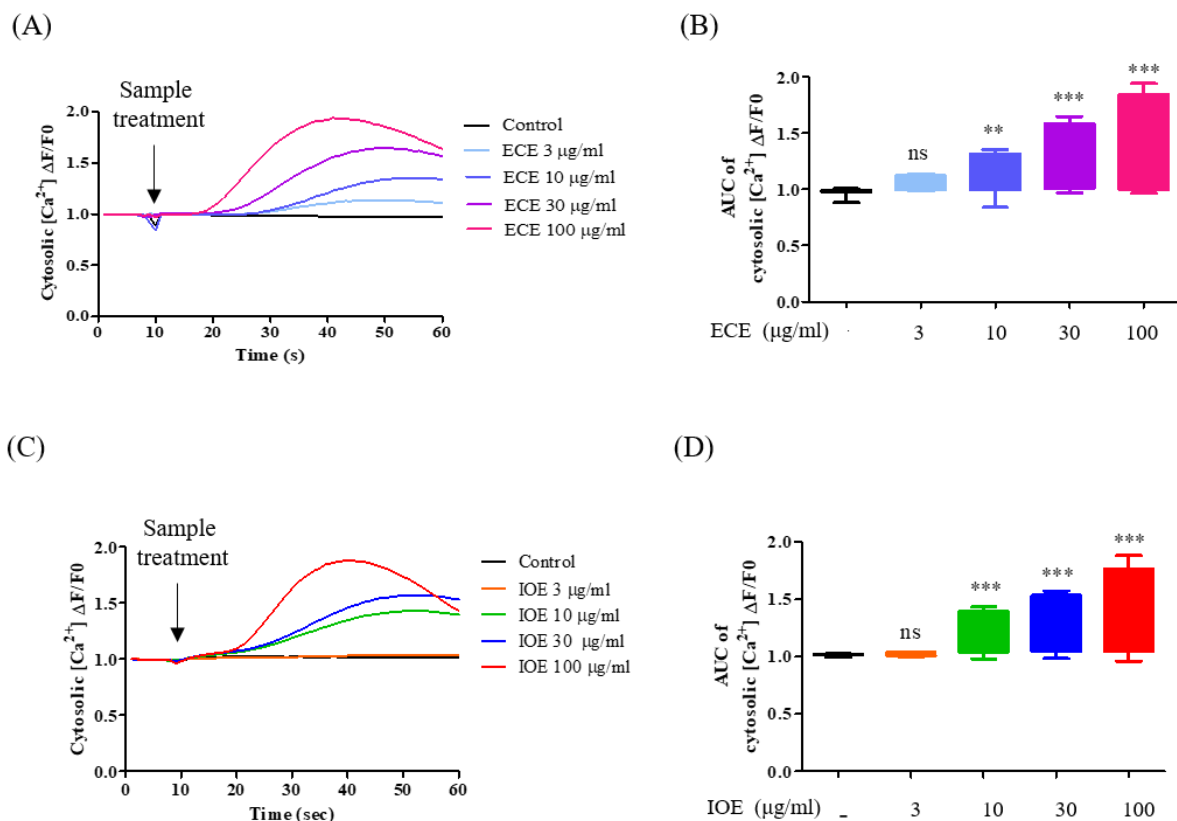


Figure 1- 8 Quantification of the  $[Ca^{2+}]_{\text{cytol}}$  levels stimulated by different concentrations of ECE and IOE in EA.hy926 cells. The traces (A, C) and box plots (B, D) indicating the levels of  $[Ca^{2+}]_{\text{cytol}}$ . For statistical significance, each sample treatment group was compared to the control group. Experiments were performed in triplicates. \*  $p < 0.05$ , \*\*  $p < 0.01$ , and \*\*\*  $p < 0.001$ . ns: not significant; AUC: area under the curve;  $[Ca^{2+}]_{\text{cytol}}$ : calcium level in the cytosol; PSS: physiological salt solution.

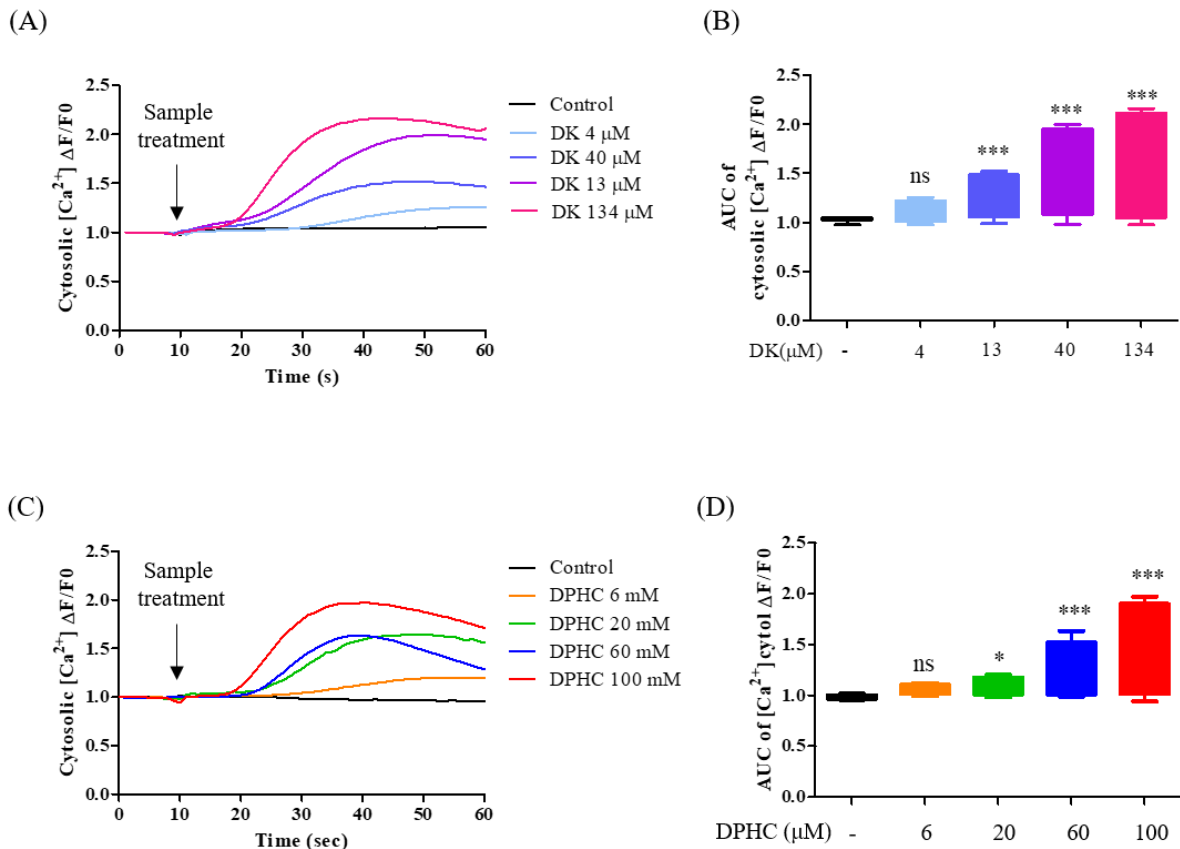


Figure 1- 9 Quantification of the  $[Ca^{2+}]_{cytol}$  levels stimulated by different concentrations of DK and DPHC in EA.hy926 cells. The traces (A, C) and box plots (B, D) indicating the levels of  $[Ca^{2+}]_{cytol}$ . For statistical significance, each sample treatment group was compared to the control group. Experiments were performed in triplicates. \*  $p < 0.05$ , \*\*  $p < 0.01$ , and \*\*\*  $p < 0.001$ . ns: not significant; AUC: area under the curve;  $[Ca^{2+}]_{cytol}$ : calcium level in the cytosol; PSS: physiological salt solution.

### ***1.3.5. Computational prediction of the AchR/VEGFR2 and docking stimulation with DK/DPHC***

After demonstrating that ECE, IOE, DK, and DK markedly increased  $[Ca^{2+}]_{cyto1}$  levels, we further investigated the DK and DPHC structure based on a computational analysis of the role of DK and DPHC in the transit of vasodilatory  $[Ca^{2+}]_{cyto1}$  in EA.hy926 cells. The binding ability was determined via molecular docking studies to confirm the interaction between DK/DPHC and AchR; and DK/DPHC with AchR and VEGFR2. Computational prediction of AchR residues interacting with DK/DPHC and the 3D structure of the complex is shown in Figure 1-10A and 10D, respectively. The 2D diagram of the interaction between DK and the amino acid residues of nearby active sites is shown in Figures 1-10B and 10E. The docking model revealed electrostatic interactions and a network of hydrogen bonds in the complex [25]. DK docking results with AchR generated hydrogen bond interactions with Asp347, Asn A507, and Cys A532. Moreover, van der Waals contacts were observed with Try529, Ser120, ser151, Try533, Ile116, Ala238, Ala235, Trp199, Thr231, Val510, Ile222, Leu144, and Cys220, resulting in unfavorable bump interactions with Tyr506. On the other hand, the strong conventional hydrogen bond was only observed at Ser518 in the DPHC-AchR complex. Additionally, the lower the energy value, the higher the docking score. The CDOCK interaction energy was -104.221 kcal/mol, and the binding energy was -138.507 kcal/mol for DK-AchR (Figure 1-10C); the CDOCK interaction energy was -24.399 kcal/mol, and the binding energy was -99.389 kcal/mol for DPHC-AchR (Figure 1-8F). Compared to the two complexes (DK-AchR and DPHC-AchR), DK showed a more stable binding status compared with DPHC.

Furthermore, the interaction of DK/DPHC with VEGFR2 was performed in Figure 1-11. The computational prediction of VEGFR2 residues interacting with DK/DPHC and the 3D structure of the complex is shown in Figure 1-11A and 11D, respectively. Surprisingly, compared to the AchR, the higher the CDOCK interaction energy and the binding energy were found while the DK/DPHC docked into the VEGFR2 (Figure 1-11C and 11F), and the

interaction bond between DK-VEGFR2 and DPHC-VEGFR2 were shown in Figure 1-11B and 11E. The CDOCKER interaction energy was -97.7618 for the DK-VEGFR2 complex, and the -54.2495 was observed at the DPHC-VEGFR2 complex. Also, the binding energy of DK-VEGFR2 was -356.952 and -419.232 in DPHC-VEGFR2, respectively Figure 1-11C and 11F. Briefly sum up the results, we observed that DK and DPHC could bind more stable with VEGFR2 than AchR. Thus, based on the results, we assumed that DK and DPHC would affect calcium transits by stimulating these two receptors. To prove our hypothesis, the specific antagonists would be employed for further experiments.

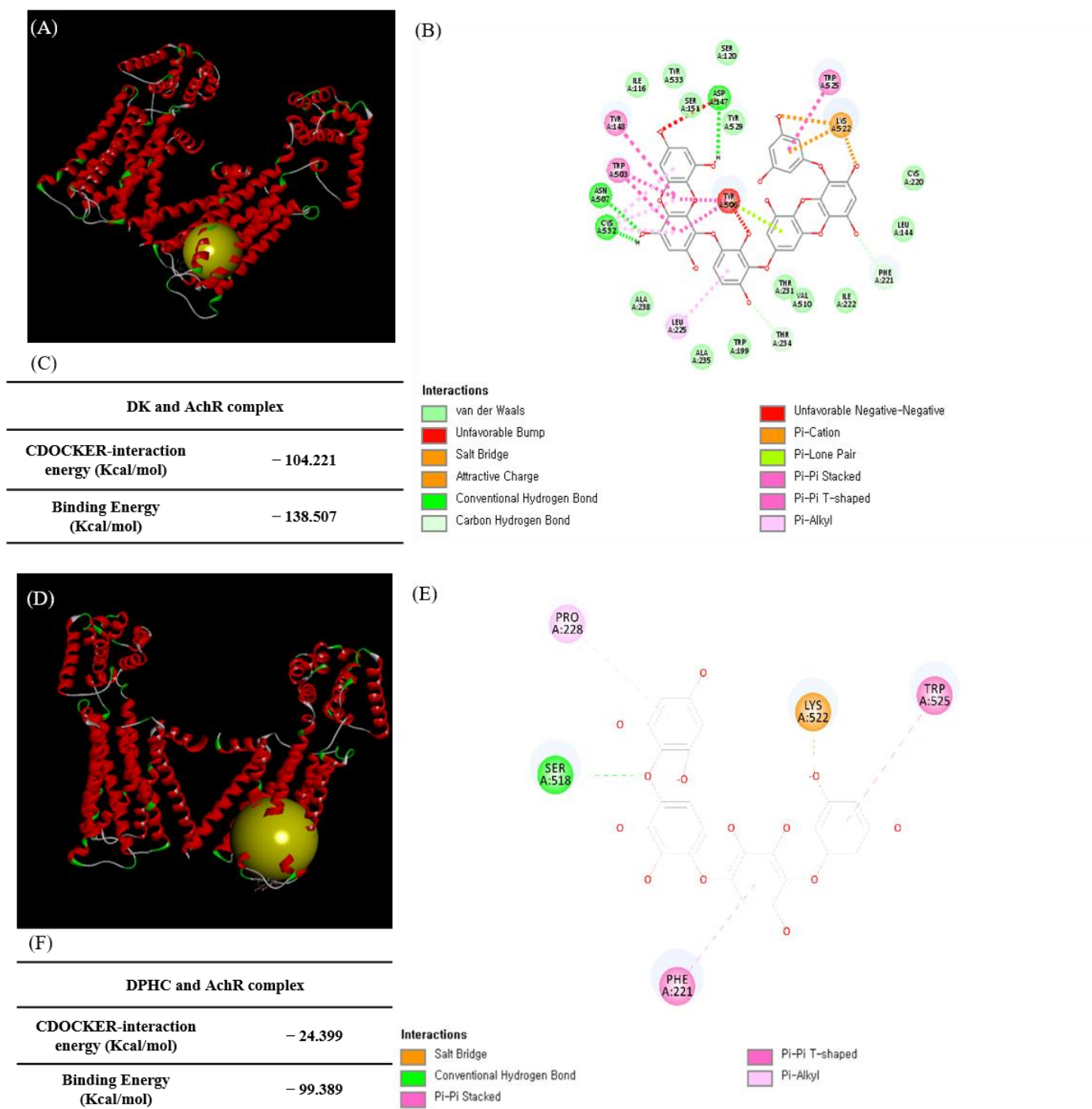


Figure 1- 10 Computational prediction of the AchR and docking stimulation with DK/DPHC. (A) Specific interaction between the DK and the ligand. (B) Two-dimensional (2D) diagram of ligand-AchR and DK and DK complex (C) The results of interaction energy and binding energy of DK-AchR complex. (D) Specific interaction between the DPHC and the ligand. (E) Two-dimensional (2D) diagram of ligand-AchR and DPHC complex (C) The results of interaction energy and binding energy of DPHC-AchR complex

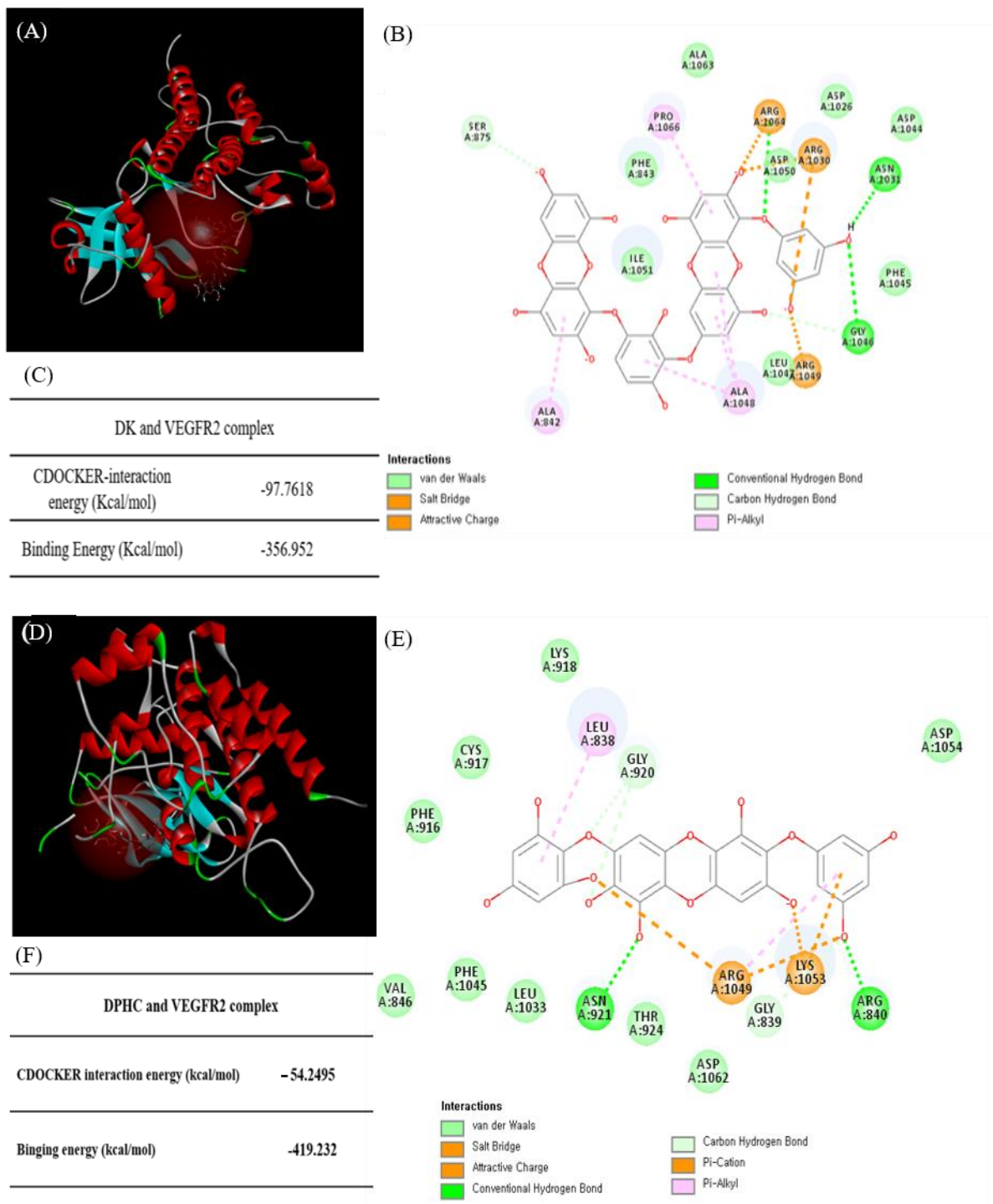


Figure 1- 11 Computational prediction of the VEGFR2 and docking stimulation with DK/DPHC. (A) Specific interaction between the DK and the ligand. (B) Two-dimensional (2D) diagram of ligand-VEGFR2 and DK (C) the results of interaction energy and binding energy of DK-VEGFR2 complex. (D) Specific interaction between the DPHC and the ligand. (E) Two-dimensional (2D) diagram of ligand- VEGFR2 and DPHC complex (F) The results of interaction energy and binding energy of DPHC- VEGFR2 complex

### ***1.3.6. DK and DPHC modulated $[Ca^{2+}]_{cytol}$ levels by activating AchR, VEGFR2, and VDCC***

$[Ca^{2+}]$  levels can be influenced by the activation of VEGFR2 and AchR [15, 16]. Moreover, the voltage-dependent calcium channel (VDCC), another important role in modulating the calcium in endothelial cells. Thus, to investigate whether DK and DPHC-induced NO formation was related to AchR, VEGFR2, VDCC activation, the respective specific antagonists, atropine (AT), SU5416 (SU), and nifedipine (NI) were used. We tested different concentrations of atropine and SU5416 to attain the optimal inhibition conditions. Accordingly, a 2-h incubation with 100  $\mu$ M of AT, 100  $\mu$ M of SU, and 100  $\mu$ M of NI showed the strongest inhibitory activity when administered separately. Therefore, the above concentrations were used in subsequent experiments.

An increase in  $[Ca^{2+}]_{cytol}$  levels was only observed in the DK and DPHC treatment group, with a maximal calcium concentration observed at about 20 s after treatment, followed by a gradual decline (Figure 1-12A and 1-13A). As expected,  $[Ca^{2+}]_{cytol}$  levels were remarkably decreased when cells were treated with AT, SU, and NI compared to cells treated with DK only (Figure 1-12B,  $p < 0.001$ ). Additionally, a similar trend was also observed in DPHC treatments (Figure 1-13B). Thus, these findings indicate that the modulation of  $[Ca^{2+}]_{cytol}$  levels by DK and DPHC were closely related to AchR, VEGFR2, and VDCC activation.

Having found that AchR, VEGFR2, and VDCC activation could regulate  $[Ca^{2+}]_{cytol}$  levels, we further hypothesized that  $[Ca^{2+}]$  levels would deeply influence NO production. To prove our hypothesis, cells were pre-treated with AT, SU, and NI and incubated for 30 h, followed by the addition of 134  $\mu$ M of DK and 100  $\mu$ M of DPHC. After 24 h, intracellular NO concentrations were measured using the DAF-FM DA assay. We observed that both antagonists significantly suppressed NO formation upon DK and DPHC stimulation (Figure 1-12C and Figure 1-13C, respectively). Taken together, our results showed that the modulation

of  $[Ca^{2+}]_{cytol}$  levels by AchR, VEGFR2, and VDCC activation was sufficient and necessary for NO formation in EC.

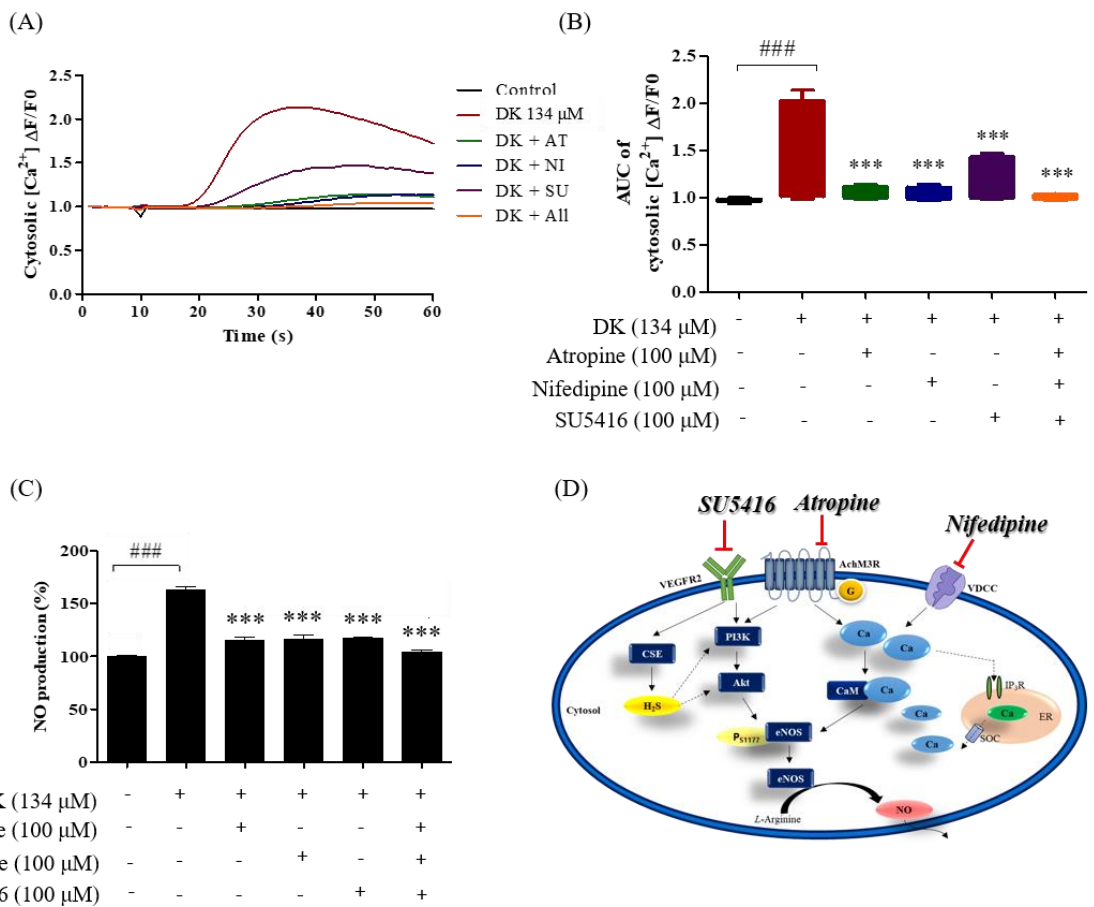


Figure 1- 12 Influence of specific antagonists on  $[Ca^{2+}]_{cytol}$  levels in EA.hy926 cells treated with DK. (A) Traces (B) and box plots indicating  $[Ca^{2+}]_{cytol}$  levels in response to treatment with DK and antagonists. (C) Effect of DK on NO production in EA.hy926 cells pre-treated with 100  $\mu$ M of atropine, SU5416, and nifedipine. The NO levels were detected by adding 10  $\mu$ M of 4 ami-no-5-methylamino-2', 7'-difluorescein diacetate (DAF-FM DA). (D) Possible mechanisms. Experiments were performed in triplicates. Each column and bar represent the mean  $\pm$  standard deviation (S.D.). \*\*  $p < 0.01$ . \*\*\*  $p < 0.001$ , significant difference compared to the control group. ns: not significant; AUC: area under the curve; DPHC: diphloretohydroxycarmalol;  $[Ca^{2+}]_{cytol}$ : calcium level in the cytosol.

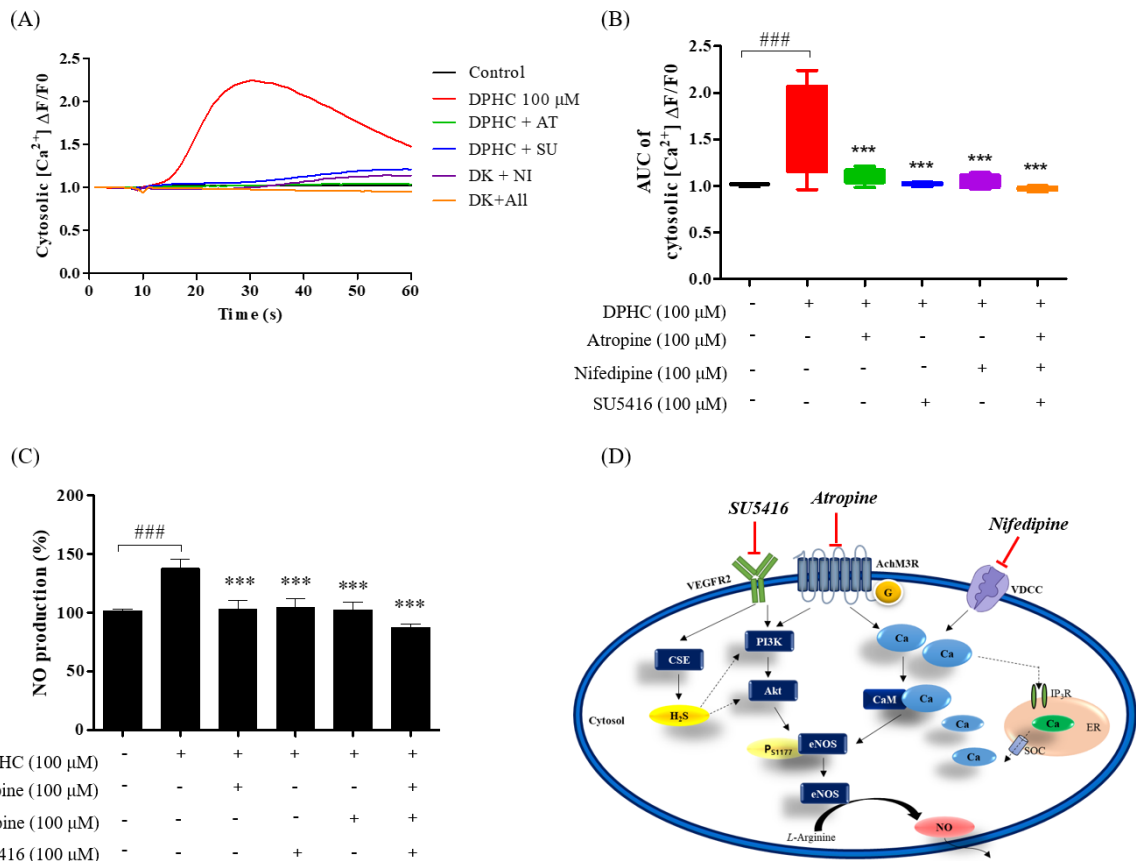


Figure 1- 13 Influence of specific antagonists on  $[Ca^{2+}]_{\text{cytol}}$  levels in EA.hy926 cells treated with DPHC. (A) Traces (B) and box plots indicating  $[Ca^{2+}]_{\text{cytol}}$  levels in response to treatment with DPHC and antagonists. (C) Effect of DPHC on NO production in EA.hy926 cells pre-treated with 100  $\mu\text{M}$  of atropine, SU5416, and nifedipine. The NO levels were detected by adding 10  $\mu\text{M}$  of 4 ami-no-5-methylamino-2', 7'-difluorescein diacetate (DAF-FM DA). (D) Possible mechanisms. Experiments were performed in triplicates. Each column and bar represent the mean  $\pm$  standard deviation (S.D.). \*\*  $p < 0.01$ . \*\*\*  $p < 0.001$ , significant difference compared to the control group. ns: not significant; AUC: area under the curve; DPHC: diphloretohydroxycarmalol;  $[Ca^{2+}]_{\text{cytol}}$ : calcium level in the cytosol.

## 1.4. Discussion

Several polyphenols extracted from terrestrial plants have been reported for their antihypertensive effects caused by increasing NO bioavailability and alleviation of vasoconstriction [28, 29]. Marine algae are also a potentially rich resource of substances with beneficial health effects, but the molecular mechanisms underlying their effect on blood pressure are seldom known. Previous *in vitro* studies have reported that marine polyphenols isolated from increasing the blood flow rate.

*E. cava* and IO are famous for the different biological activities, including antioxidant, anti-inflammatory, attenuation of endothelial cell dysfunction, and anti-hypertension, in numerous studies [8-11]. *Son et al.* have indicated that ECE significantly alleviates BP in a mouse model of HTN. Furthermore, DK, a polyphenolic compound present in ECE, has been suggested as one of the bioactive components responsible for the potential ACE inhibitory activity [12, 13]. Notably, IOE and its bioactive substances, DPHC, have shown the remarkable ability to regulate endothelial-dependent vasodilation [14]. However, the molecular signaling pathways were rarely mentioned.

A concentration-dependent increase in NO production was observed in the DK and DPHC treatment groups. It has been reported that multiple mechanisms control NO production via eNOS activation. First, the PI3K pathway members, including its downstream molecule, Akt, are essential regulators; activated Akt directly phosphorylates ser1177 on eNOS, enhancing the binding activity of  $[Ca^{2+}]$ /calmodulin [30]. Based on these aspects, we systematically examined protein expression in the PI3K/Akt/eNOS axis and measured calcium transit. Indeed, dose-dependent increments in PI3K, Akt, and eNOS were observed under DK and DPHC treatment. Thus, we confirmed that DK and DPHC-induced activation of the PI3K/Akt/eNOS pathway is essential in promoting NO formation in endothelial cells.

Furthermore, activated eNOS promotes the binding of calcium ions to calmodulin, a multifunctional intermediate calcium-binding messenger protein. Once  $[Ca^{2+}]$  is bound to calmodulin, the  $[Ca^{2+}]$  signal transduction pathway is activated [31]. As such, calcium transit is also considered critical in NO generation [32]. Kida et al. indicated that increasing the  $[Ca^{2+}]_{ER}$  level would activate the calmodulin-bound domain of eNOS, resulting in NO production [33]. Additionally, higher  $[Ca^{2+}]_{cytol}$  levels led to NO formation, shown in human umbilical vein endothelial cells [34]. In this study, we investigated the role of  $[Ca^{2+}]$  signaling under DK and DPHC administration. After adding 134  $\mu$ M of DK and 100  $\mu$ M of DPHC, it was possible to detect a remarkable increase in  $[Ca^{2+}]_{cytol}$  levels after 30 s, characterized by a 60 s oscillation peak phase. This increase was completely prevented by different antagonists (AT, SU, and NI). Theoretically, after the peak phase, a stabilization declining phase, also characterized by less intense and less frequent oscillations, would follow [35]. Nevertheless, within 60 s, we did not observe any decreasing trend in  $[Ca^{2+}]_{cytol}$  levels.

When the cells are stimulated, such as during membrane depolarization, extracellular signaling molecules or intracellular messengers enhance  $[Ca^{2+}]_{cytol}$  levels. This increment results from either an influx of  $[Ca^{2+}]$  from the outside of the cell via ion channels on the plasma membrane or the release of  $[Ca^{2+}]$  from internal stores (such as the ER). The increase in  $[Ca^{2+}]_{cytol}$  level is precipitous and is followed by a decline in  $[Ca^{2+}]$  levels, maintained by the homeostatic regulation of  $[Ca^{2+}]$  concentration [36]. Accordingly, having found that DK and DPHC can effectively raise  $[Ca^{2+}]_{cytol}$  levels, we further focused on investigating the possible pathway that DK and DPHC affect calcium regulation via cell membrane receptors (VEGFR2, AchR, and VDCC).

The muscarinic AchR family is divided into 5 subtypes: M1, M2, M3, M4, and M5 [37]. The activation of M3 receptors in vascular endothelial cells induces potent vasodilatation, and this process occurs via the release of an endothelium-derived relaxing factor, such as NO [38].

Ren et al. showed that acetylcholine induces vasodilatation by activating M3 receptors on endothelial and smooth muscle cells [39]. Moreover, AchR activation can induce a downstream pathway involved in the conversion of phosphatidylinositol biphosphate (PIP<sub>2</sub>) into the two secondary messengers, inositol-1, 4,5-trisphosphate (IP<sub>3</sub>) and diacylglycerol (DAG), by phospholipase-C (PLC). IP<sub>3</sub> diffuses into the cytosol and binds to its receptor (IP<sub>3</sub>R) on the ER, triggering the release of Ca<sup>2+</sup> ions [40]. The rise of free Ca<sup>2+</sup> ions mediates activation of NO generation via the phosphorylation of proteins, such as Akt and eNOS [41]. As we expected, the pre-treatment of cells with atropine, a specific antagonist of AchR, completely blocked DK or DPHC-induced rise in [Ca<sup>2+</sup>]<sub>cytol</sub>. Also, we observed that the level of NO was suppressed by atropine. Therefore, we concluded that DK and DPHC-induced rise in [Ca<sup>2+</sup>]<sub>cytol</sub> and NO formation could proceed with AchR activation in EA.hy926 cells.

Another potential regulator of vasodilation is VEGFR2, mainly expressed in the vascular endothelium [42]. When VEGF binds to VEGFR2, the receptor undergoes dimerization and phosphorylation of its tyrosine residues, triggering a downstream phosphorylation cascade targeting pro-angiogenic mediators [43]. Among the activated mediators are the PLCγ1/calcium and PI3K/Akt/eNOS pathways [44]. Both pathways are associated with eNOS activation and NO synthesis. VEGFR2 data demonstrated a similar trend with the AchR results. Treatment with 134 μM of DK and 100 μM of DPHC could not raise [Ca<sup>2+</sup>]<sub>cytol</sub> levels or NO production in EA.hy926 cells pre-treated with SU. Therefore, we hypothesize that DK and DPHC triggered an increase in [Ca<sup>2+</sup>]<sub>cytol</sub> levels by regulating AchR and VEGFR2 activation, resulting in NO production.

## 1.5. Conclusion

Herein, we revealed that ECE, IOE, DK, and DPHC effectively promoted endothelial-dependent NO production by activating the PI3K/Akt/eNOS pathway and  $[Ca^{2+}]_{cytol}$  regulation.  $[Ca^{2+}]_{cytol}$  levels are closely associated with the activation of AchM3R, VEGFR2, and VDCC in EA.hy926 cells. Furthermore, the intracellular H<sub>2</sub>S levels were significantly induced by DK and DPHC treatments. We suggest that the ECE, IOE, DK, and DPHC possess superior vasodilatory effects and can be developed as suitable therapeutic agents.

**Part II**

**Bioactive compounds isolated from *Ecklonia cava* and *Ishige okamurae*  
promote vasodilation in endothelial-smooth muscle cell co-culture system  
via down-regulation of CaM and *p*-MLC expression**

## 2.1.Introduction

Vascular endothelial cells (ECs) and vascular smooth muscle cells (VSMCs) are the essential components of a typical vessel wall. Its functions are contraction and relaxation to modulate the diameter of vessels. ECs secrete many kinds of physiologically active substances such as nitric oxide (NO) and hydrogen sulfate ( $H_2S$ ), which play a well-known, influential factor in promoting vasodilation. There are two mechanisms associated with the NO production in the vascular endothelial cell: i) calcium-independent pathway and ii) calcium-dependent pathway. The previous study has mentioned vascular endothelial growth factor receptor 2 (VEGFR2), one of the main receptors that influenced the NO generation [14]. Once the VEGFR2 is activated by agonists such as VEGF-A or acetylcholine, the downstream proteins phosphoinositide 3-kinase (PI3K)/protein kinase B (Akt) would promote the phosphorylation of eNOS, resulting in the NO generation.

On the other hand, the calcium transit was influenced by the dynamic balance of cytosolic and sarcoplasmic reticulum (SR) [ $Ca^{2+}$ ] levels. Calmodulin (CaM) is a multifunctional intermediate calcium-binding messenger protein. Once bound to the [ $Ca^{2+}$ ], CaM would act as part of a calcium signalling transduction pathway by modifying its interactions with target kinase or phosphatases. Moreover, the interactions between eNOS and CaM have been extensively characterized in endothelial cells [45]. A previous study indicated a high binding affinity of eNOS for CaM, increasing NO synthesis and further promoting vasodilation [46]. Besides regulating vascular tension, NO released from endothelial cells can further inhibit the proliferation of VSMC [47]. Therefore, the [ $Ca^{2+}$ ] levels are the critical connection between EC and VSMC regulating the tone.

VSMC displays a multifunctional and high degree of plasticity. They can switch their phenotype from contractile to a non-contractile or proliferative or synthetic state with considerable change in intracellular calcium signaling [47]. Normally, VSMC expresses genes

and proteins important contraction and dilation, which allows them to control blood flow and blood pressure via regulation of the vascular tone. Calcium homeostasis is the most important point to regulate the cell-cycle initiation/progression of VSMC effectively. When the protein expression involved in influx  $[Ca^{2+}]$  from the extracellular space, and a further increase in the  $[Ca^{2+}]$  release from SR stores ( $[Ca^{2+}]_{SR}$ )[48], the expression of specific protein such as myosin light chains kinase (MLCK) would be stimulated and phosphorylated the myosin light chains (MLC) enabling interaction with actin and thereby contraction [21]. Furthermore, Garland *et al.* indicated that the  $[Ca^{2+}]$  entered VSMCs through voltage-dependent calcium channels, subsequently passed through gap junctions into ECs, and initiated vasodilation mediated by ECs [49].

Based on the viewpoints mentioned above, the present study demonstrated the co-culture model of ECs and VSMCs, mimicking the cellular interactions appearing *in vivo* and focused on the calcium signaling transduction.

## **2.2. Material and methods**

### **2.2.1. Chemicals and reagents**

Dulbecco's modified Eagle's medium (DMEM), penicillin/streptomycin (p/s) were purchased from GIBCO (Grand Island, NY, USA), fetal bovine serum (FBS) was obtained from Merck (Sacramento, CA, USA); Dimethyl sulfoxide (DMSO), 3-(4-(5-dimethyl-2-yl)-2-5-diphenyltetrasolium bromide (MTT) were purchased from Sigma Co. (St. Louis, MO, USA); NO production was measured by Griess assay (Promega Corporation, Madison, WI); The calcium levels were detected by using Fluo-4-AM dye (1-[2-amino-5-(2,7-difluoro-6-hydroxy-3-oxo-9-xanthenyl)phenoxy]-2-(2-amino-5-methylphenoxy) ethane-N, N, N', N'-tetraacetic acid, pentaacetoxymethyl ester) (ThermoFischer®).

### **2.2.2. Human coronary artery endothelial cells (HCAECs) monoculture**

Cryopreserved, second passage, single donor HCAECs were purchased from PromoCell GmbH (Heidelberg, Germany). Cells were routinely grown in the 75T flask contained endothelial cell growth medium MV enriched with Endothelial Cell Growth Supplement Mix (Promocell GmbH, Heidelberg, Germany). Cells were sub-culture using 0.04 % trypsin and 0.03% EDTA (Promocell GmbH, Heidelberg, Germany) and keep an incubator with 37°C and humidified 5% CO<sub>2</sub>. Passage 3-6, were used for experiments.

### **2.2.3. Measurement of cytotoxicity and NO production in HCAEC**

HCAEC were seeded at 1x10<sup>4</sup> cells per well in 96 well plates with 100 µl culture medium. After 24 h, cells were exposed to 6, 20, 60, and 100 µM of DPHC; 4, 13, 40, and 134 µM of DK. Cytotoxicity was assessed by MTT assay. 2mg/ml MTT was added into the 96-well plate and incubated at 37°C in the dark for 3h. Subsequently, removed MTT solution, the DMSO (200µl/well) was added into the well to dissolve formazan crystals. The cytotoxicity was

calculated by reading absorbance at 540 nm via a micro plate reader (BioTech, Winooski, VT, USA).

3-amino, 4-aminomethyl-2', 7'-difluorescein, and diacetate (DAF-FM-DA) assay (Sigma). A fluorescent probe is used to detect intracellular NO. DAF-FM DA is a cell-permeable deacetylated form of DAF-FM and is hydrolyzed by intracellular esterases to form a cell-impermeable DAF-FM reacts with NO. Therefore, the fluorescence intensity in cells was used to evaluate intracellular NO levels. HCAECs were seeded at 96 well culture plate for 24hr at 37°C in the dark. After 24hr, the sample was treated and incubated for another 24hr. Further, the 10µM of DAF-FM-DA solution was treated and incubated with the cell for 30 min at 37°C. The medium contained DAF-FM-DA was removed and washed by PBS three times. Subsequently, 100µl of PBS was added well, then evaluated by a fluorescent micro plate reader (Synergy HT, BioTek Instruments, Italy). The fluorescent intensity was determined at an excitation wavelength of 488 nm and an emission wavelength of 525 nm.

#### ***2.2.4. Evaluation of intracellular H<sub>2</sub>S levels***

The isolated were incubated in Krebs-HEPES solution (in mM: 119 NaCl, 4.6 KCl, 1.2 CaCl<sub>2</sub>-2H<sub>2</sub>O; 0.4 KH<sub>2</sub>PO<sub>4</sub>, 1 MgSO<sub>4</sub>-7H<sub>2</sub>O, 5 NaHCO<sub>3</sub>, 5.5 glucose, 20 HEPES, and 0.15 NaH<sub>2</sub>PO<sub>4</sub>, pH = 7.4, at 37 °C) containing 50 µM Washington State Probe-5 (WSP-5, Cayman Chemical, Ann Arbor, MI, USA), a fluorescence sensor for H<sub>2</sub>S. After a 30-minute incubation, the samples were treated in to cells. The fluorescence was quantified by a blinded investigator calculating the integrated density using a spectrofluorometer (Synergy HT, BioTek Instruments, Italy).

### **2.2.5. Quantitative of cytosolic calcium levels in HCAEC**

By definition, the cytosolic  $[Ca^{2+}]$  levels refer to the concentration of calcium ions in the cytosol ( $[Ca^{2+}]_{cytol}$ ). To detect the  $[Ca^{2+}]_{cytol}$  levels, the sensitive probe Fluo-4 was dissolved in the physiological salt solution (PSS) consisted of 140 mM NaCl, 5.9 mM KCl, 1.4 mM  $MgCl_2 \cdot 6H_2O$ , 10 mM HEPES, 11.5 mM glucose, 1.2 mM  $NaH_2PO_4$ , 5 mM  $NaHCO_3$ , and 1.8 mM  $CaCl_2$ , at pH 7.4 with NaOH. HCAECs were seeded in 96 well plates overnight until cells grow over 80% confluence. Then added 1xFluo-4 and incubated for 30 minutes at 37°C in the dark. Afterward, cells were rinsed twice with 1xPBS two times and added another 1x PBS 50 $\mu$ L in the well. After measuring the intensity of fluorescence for 10 seconds at the interval time of 1 second, cells were directly treated 1xPSS and different concentrations of samples dissolved in 0.1% BSA. After another 50 seconds at interval time 1-second fluorescent detection, the  $[Ca^{2+}]$  levels were reflected in the microscope.

### **2.2.6. Human coronary artery smooth muscle cells (HCASMCs) monoculture**

HCASMCs were purchased from PromoCell GmbH (Heidelberg, Germany). Cells were routinely grown in the 75T flask contained Smooth muscle cell growth medium 2 containing 0.05 ml/ml fetal calf serum supplemented with basic fibroblast growth factor (2 ng/ml), epidermal growth factor (0.5 ng/ml), and insulin (5 µg/ml; all Promocell). Cells were routinely sub-cultured at 70–80% confluency by using 0.04 % trypsin and 0.03% EDTA (Promocell) and keep an incubator with 37°C and humidified 5% CO<sub>2</sub>. Passage 3-6, were used for experiments.

### **2.2.7. Measurement of cytotoxicity and intracellular NO production in HCASMC**

HCASMC were seeded at  $1 \times 10^4$  cells per well in 96 well plates with 190 µl culture medium. After 24 hr, cells were exposed to 10, 20, 100, and 200 µg/ml of ECE and IOE; 4, 13, 40, and 134 µM of DK; 6, 20, 60, and 100 µM of DPHC. Cytotoxicity was assessed by MTT assay. 2mg/ml MTT was added into the 96-well plate and incubated at 37°C in the dark for 3hr. Subsequently, removed MTT solution, the DMSO (200 µl/well) was added into the well to dissolve formazan crystals. The cytotoxicity was calculated by reading absorbance at 540 nm via a microplate reader (BioTech, Winooski, VT, USA).

### **2.2.8. The protocol for conditional medium preparation**

Both HCAECs and HCASMCs were and changed the specific medium every two days. Once the HCAEC reaches 75-80% of confluence, the supplement-Mix free HCAEC medium was replaced and added into the well; simultaneously, the HCASMC medium was replaced by supplement-Mix free HCASMC medium. After 24 h (Day1), samples were treated in the HCAEC and incubated another 24 h. On Day 2, the HCAEC medium was collected and centrifuged at 500xg for 5 min, and the supernatant was termed as the conditioned medium and ready to be applied to HCASMC. The experimental graphic was provided in Figure 2-1.

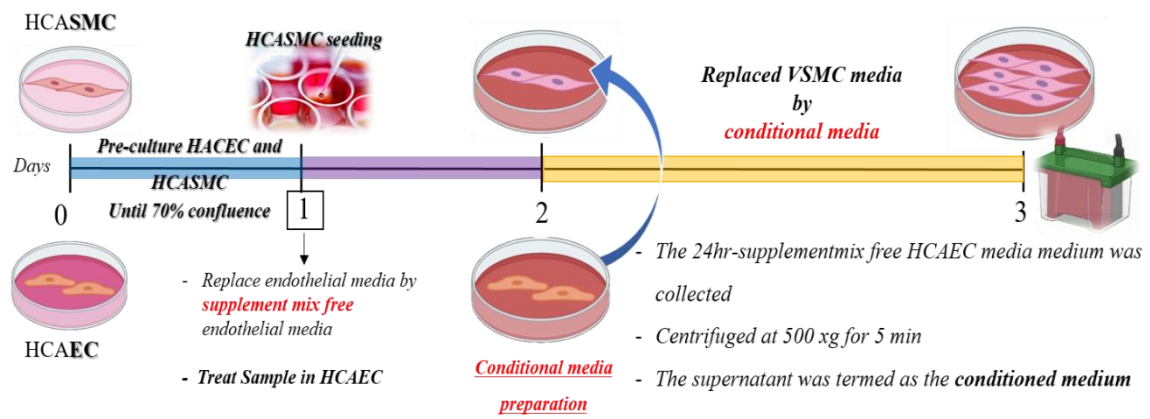


Figure 2- 1 The experimental protocol of conditional media transfer experiments.

### 2.2.9. The protocol of conditional medium transferred from HCAEC to HCASMC

Due to the culture medium of HACEC and HCASMC are different, the cytotoxicity of HCASMC exposed to the HCAEC medium containing NO was checked. Before starting the medium transferred experiments, the HACEC was first treated within 24hr (Day1) after seeding and incubated for another 24hr. The HCASMC culture medium was replaced by the conditional medium (Day 2), transferred from HCAEC. To examined the cytotoxic effect on the time-dependent model, the highest concentrations of samples (Control (PBS only), IOE 100 µg/ml, DPHC 100 µM, ECE 100 µg/ml, and DK 134 µM) were employed in this experiment. The experimental groups were divided into five groups, and six-time points (0min, 30min, 1hr, 3hr, 12hr, and 24hr) were evaluated. All the results were compared with the control group at each time point. The experimental graphic was provided in Figure 2-2.

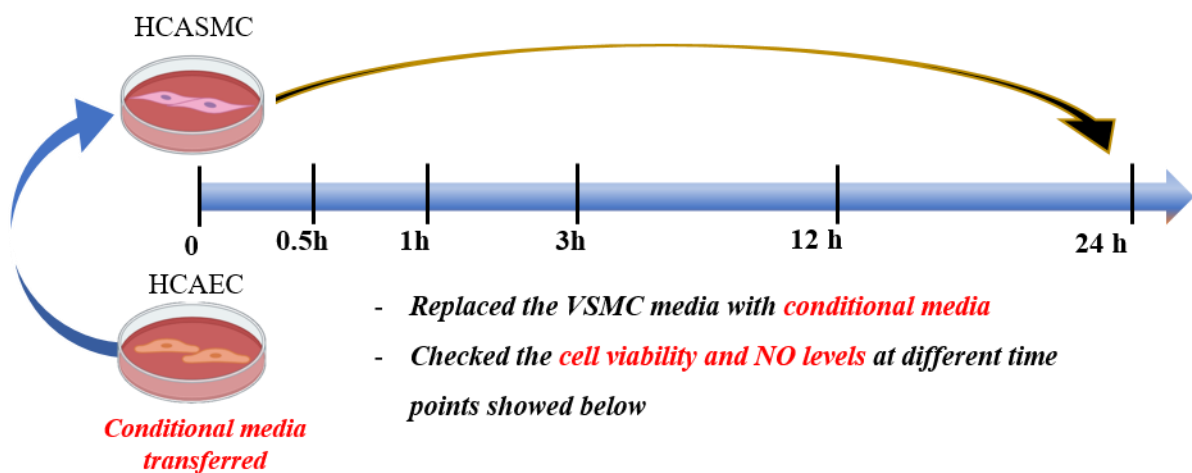


Figure 2- 2 The experimental graphic of conditional media transfer experiments

### **2.2.10. Western blotting analysis**

For western blot examination, the conditional media transfer procedure and sample treatments are the same as section 2.8 (The protocol of conditional medium transferred from HCAEC to HCASMC). Further, the HCASMC were harvested and lysed for western blot analysis. After centrifugation of cells at 12000 rpm for 20 min, the protein content of supernatants was evaluated using a BSA protein assay kit (Bio-Rad, USA). Sodium dodecyl sulfate-polyacrylamide gel electrophoresis (SDS-PAGE) (10 %) and proteins were transferred onto a nitrocellulose membrane. The membranes were incubated overnight at 4°C with the following primary antibodies: anti- $\alpha$ -smooth muscle cell actin ( $\alpha$ -SMA) (sc-53015, Santa Cruz Biotechnology, USA; 1:1000), anti-CaM Antibody (G-3) (sc-137079, Santa Cruz Biotechnology, USA; 1:1000), anti-myosin light chain 2 antibody (#3672, Cell Signalling Technology, USA; 1:1000), anti-phosphorylation -myosin light chain 2 (Thr18/Ser19) (#3674, Cell Signalling Technology, USA; 1:1000), and dissolved in 5% skim milk. The Immunoblots were incubated for another 2 h at room temperature with specific secondary antibodies. The bands were detected using a chemiluminescent substrate (Cyanogen Sri, Bologna, Italy) and visualized on a film using a FUSION SOLO Vilber Lourmat system (FUSION, Paris, France). The band intensity was calculated using Image J software 1.50i software (NIH, USA).

### 2.2.11. The methodology of the HCAEC-HCASMCM co-culture model

For contact co-culture experiments, both cells were cultured on the opposite sides of the insert. The HCASMCM has first seeded  $5 \times 10^4$  cells on the bottom side of the 6-well Trans-well insert comprising translucent membranes with  $0.4 \mu\text{M}$  pore and  $10 \mu\text{m}$  thick translucent polycarbonate membrane (Corning Inc., Corning, NY) coated with fibronectin. After 48 h culturing (Day 0), HCAEC were seeded at the upper side of the inserts with the same density and incubated for another 48 h (Day 2). The samples can be treated until the cell density reached 70-80% confluence (Day 3). The experimental graphic was provided in Figure 2-3.

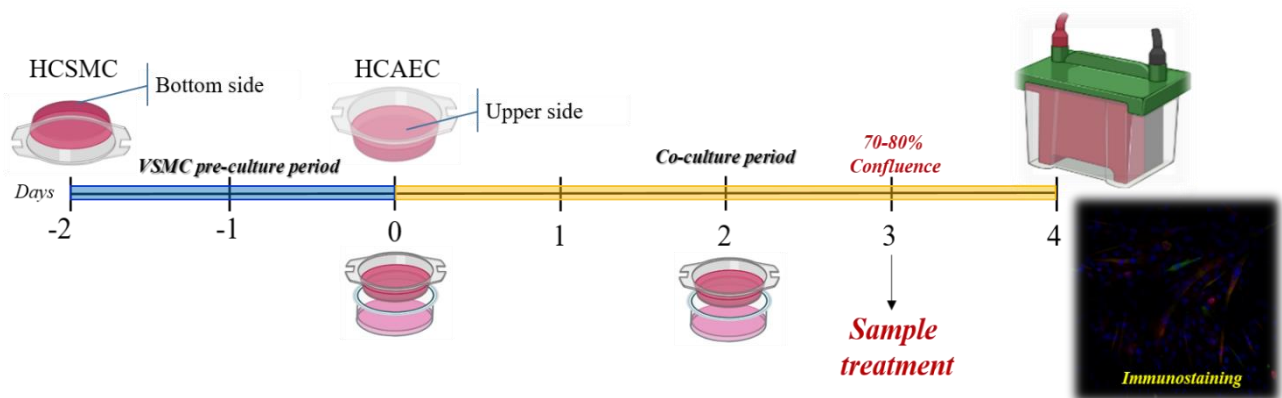


Figure 2- 3 The methodology of the HCAEC-HCASMCM co-culture model

### ***2.2.12. Quantitative of CaM and p-MLC expression in HCASMC by immunofluorescence***

The co-culture insert was washed by ice PBST and fixed in 4% PFA at room temperature for 10 min. The cells were permeabilized with Triton X-100 in PBST for 10min. After washing three times by PBST, the 10% Donkey serum was used for blocking. The specific primary antibodies such as calmodulin (CaM) and phosphorylation of myosin light chain (*p*-MLC) were diluted 1:500 and incubated overnight at 4°C. The cells were conjugated to secondary antibodies Goat Anti-mouse IgG H&L (Alexa Fluor 488) (an150113) purchased from Abcam for 2hr at room temperature.

For immunostaining purposes, the HCAECs and HCASMCs cells were seeded at six well plated with 0.4 µm pore insert. Before immunofluorescence staining started, the cells were washed by ice PBST (PBS + 0.1% Tween20) and fixed in 4% paraformaldehyde (PFA) at room temperature for 10 min. The cells were permeabilized with Triton X-100 in PBST for 10min. After washing three times by PBST, the 10% Donkey serum was used for blocking. The specific primary antibodies such as calmodulin (CaM), phosphorylation of myosin light chain (*p*-MLC) were diluted 1:100 and incubated overnight at 4°C. The cells incubated with CaM would further conjugate to secondary antibody goat anti-mouse IgG H&L (Alexa Fluor 488) (ab150113), and the cells which incubated with *p*-MLC would further conjugate with secondary antibody goat anti-rabbit IgG H&L (Alexa Fluor 647) purchased from Abcam (ab150079) for 2 h at room temperature.

### **2.2.13. Statistical analysis**

All data were carried out in triplicate, and the results were expressed as a mean  $\pm$  standard deviation. Statistical analysis was used one-way ANOVA with Dunnett's post hoc test in Prism 5.0 Graph Pad software (La Jolla, CA, USA) for significant differences from the blank, with \*  $p < 0.05$ , \*\*  $p < 0.01$ , and \*\*\*  $p < 0.001$  were considered as significant.

## **2.3.Results**

### ***2.3.1. Measurement of cell viability and intracellular NO production in HCAEC***

Figures 2-4 and 2-5 exhibit the behavior of HCAEC react under the IOE, DPHC, ECE, and DK stimulated condition. According to the results, all the sample concentrations were non-toxicity and could be used for further experiments (Figure 2-4). To ensure the human coronary endothelial cell could demonstrate the similar effect of endothelial cell-dependent NO generation, we evaluated the intracellular NO production induced IOE, DPHC, ECE, and DK. The comprehension between two types of extract in HCAEC. As the results have shown, under the same concentration, IOE treatment could significantly induce much higher NO production than ECE in Figures 2-4A and C. In the comprehension of DK and DPHC treatments, we observed that DPHC could induce higher levels of intracellular NO compared to DK (Figure 2-4B and D).

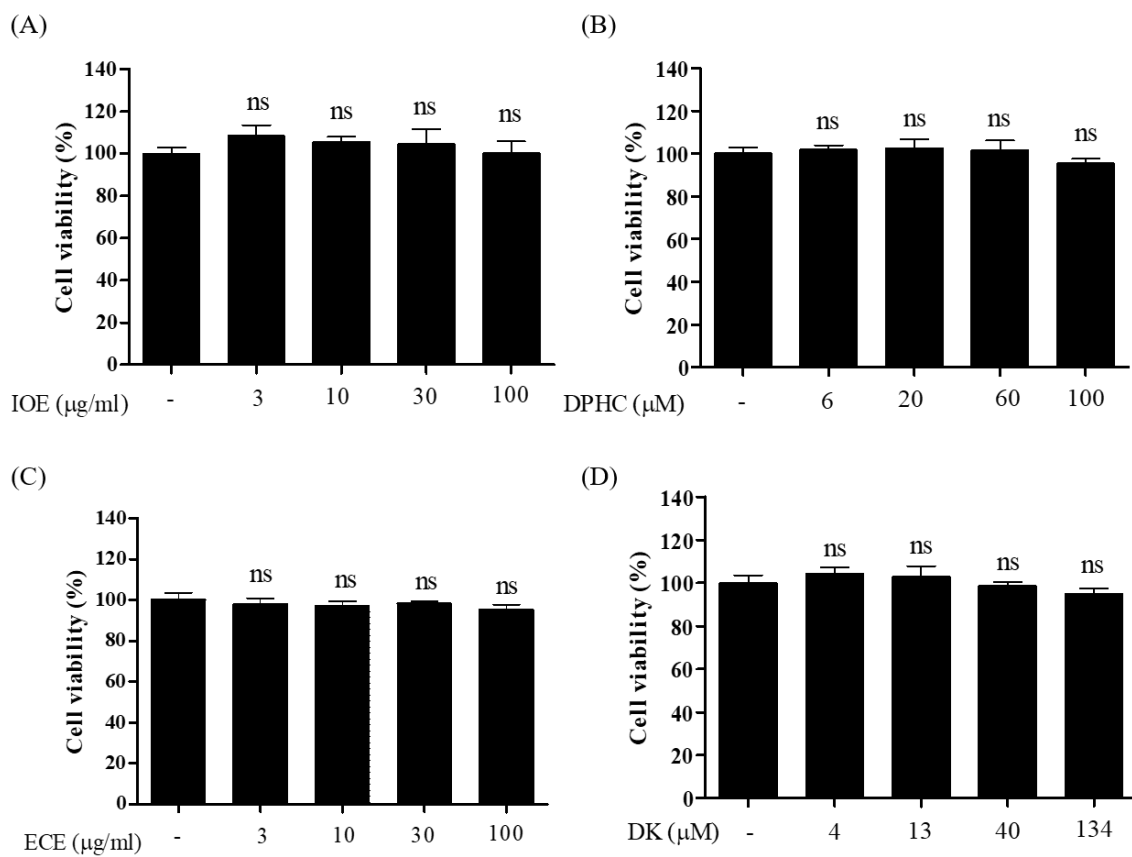


Figure 2- 4 Evaluation of cell viability treated with different concentrations of (A) IOE, (B) DPHC, (C) ECE, and (D) DK. Experiments were performed in triplicates. Each column and bar represent the mean  $\pm$  standard deviation (S.D.). \*  $p < 0.05$ , \*\*  $p < 0.01$ . \*\*\*  $p < 0.001$ , significant difference compared to the control group.

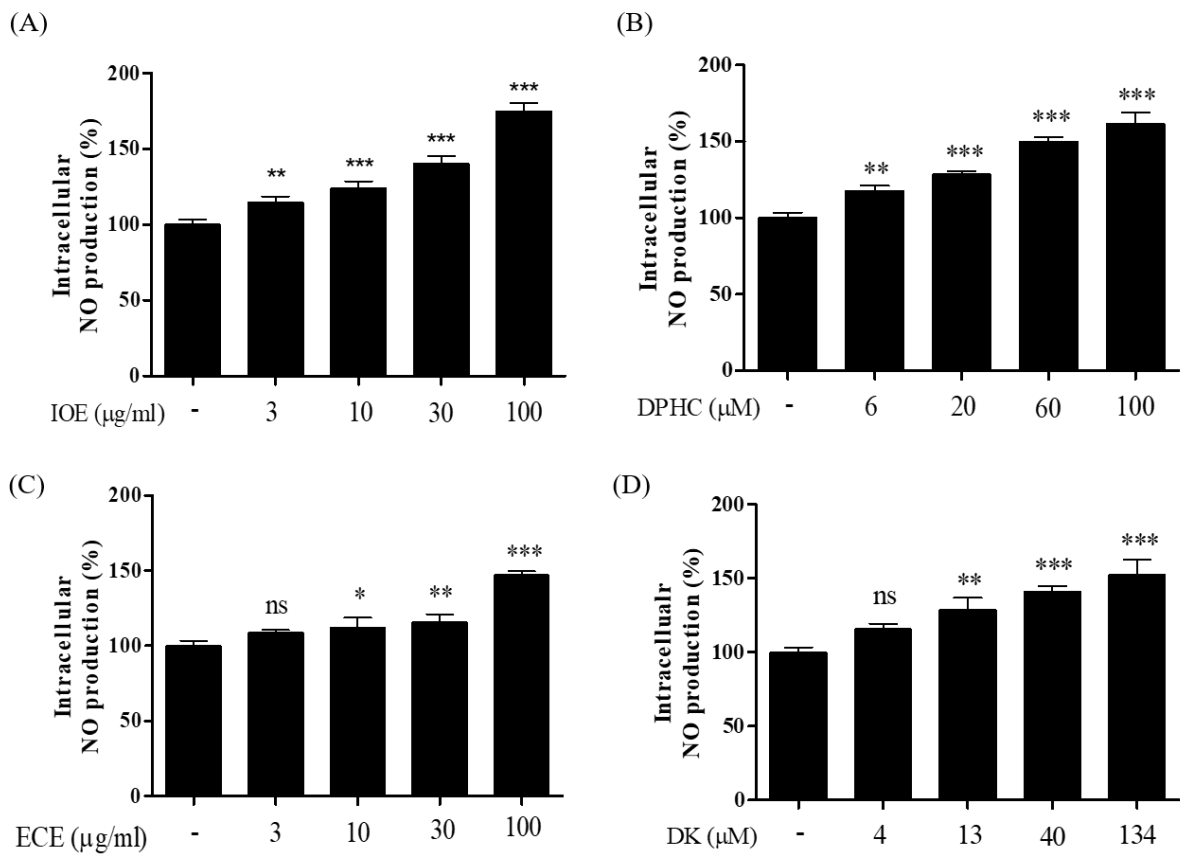


Figure 2- 5 Evaluation of the level of intracellular NO concentrations induced by (A) IOE, (B) ECE, (C) DPHC, and (D) DK were measured by 10  $\mu\text{M}$  of DAF-FM-DA assay in HCEAECs. Experiments were performed in triplicates. Each column and bar represent the mean  $\pm$  standard deviation (S.D.). \*  $p < 0.05$ , \*\*  $p < 0.01$ . \*\*\*  $p < 0.001$ , significant difference compared to the control group.

### ***2.3.2. The levels of intracellular H<sub>2</sub>S induced by DK and DPHC in HCAEC***

Physiologically, endogenous H<sub>2</sub>S exerts a wide variety of biological effects. Regarding the cardiovascular system, H<sub>2</sub>S is known to induce vasodilation [50, 51]. Previously, we have confirmed that DK and DPHC can induce intracellular H<sub>2</sub>S in EA.hy926 cells. Thus, we have to ensure the endothelial-dependent vasodilation effect of DK and DPHC could be repeated in HCAEC. As a result, shown in Figure 2-6, we observed that the H<sub>2</sub>S levels were increased in a dose- and time-dependent manner. The significant difference was first measured under DK (40 and 134 μM) and DPHC (100 μM) treatments at 10 min. Within 35 min, the DK (40 and 134 μM) and DPHC (60 and 100 μM) groups dramatically increased compared to the control group ( $p < 0.001$ ). Hence, we confirm that whether EA.hy926 cells or HCAEC can successfully induce the endogenous H<sub>2</sub>S by DK and DPHC treatments.

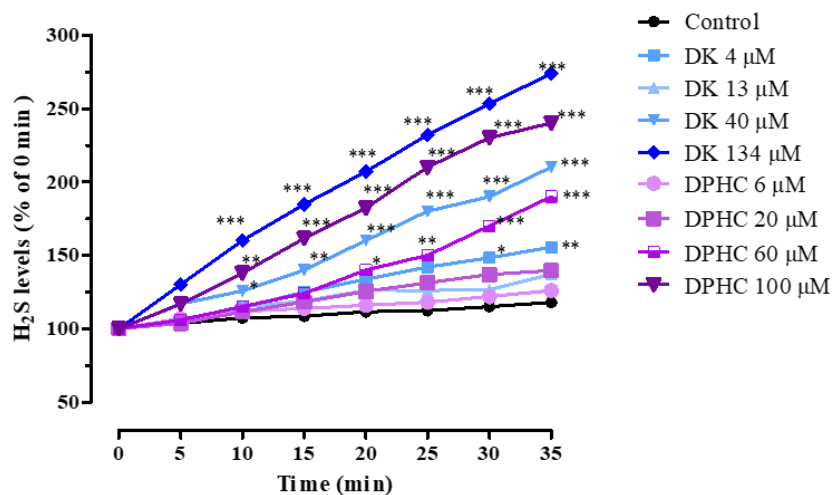


Figure 2- 6 Evaluation of the level of intracellular H<sub>2</sub>S concentrations induced by different concentrations of DK and DPHC in HCEAECs. Experiments were performed in triplicates. Each column and bar represent the mean  $\pm$  standard deviation (S.D.). \*  $p < 0.05$ , \*\*  $p < 0.01$ . \*\*\*  $p < 0.001$ , significant difference compared to the control group

### **2.3.3. Evaluation of $[Ca^{2+}]_{cytol}$ under the IOE, DPHC, ECE, and DK treatments in HCAEC**

Another critical factor we need to confirm is whether the IOE, DPHC, ECE, and DK can promote  $[Ca^{2+}]_{cytol}$  concentration in HCAEC. To do so, we have examined all samples at the highest concentration (100  $\mu$ g/ml of ECE and IOE; 134  $\mu$ M of DK; 100 Mm of DPHC) compared to the positive control - BAY K8644 10  $\mu$ M (a specific agonist of L-type calcium channel). As the results demonstrated in Figure 2-7, the BAY K8644 significantly increased the  $[Ca^{2+}]_{cytol}$  levels compared to control (about 2.4 fold higher than control). Soon after treatments, we have observed that all the samples significantly increased compared to the control (Figure 2-7B). We have noticed that the HCAEC raised the calcium levels much earlier soon after sample treatments than the EA.hy926 cell. It indicated that HCAEC was much sensitive to calcium transit (Figure 2-7A). Also, the DK and DPHC group showed a similar fold compared to BAY K8644. Thus, we knew that DK and DPHC were the powerful calcium promoter in HCAEC. The stimulated cells under the samples treatments were taken the photo at 60s, which showed at Figure 2-7C.

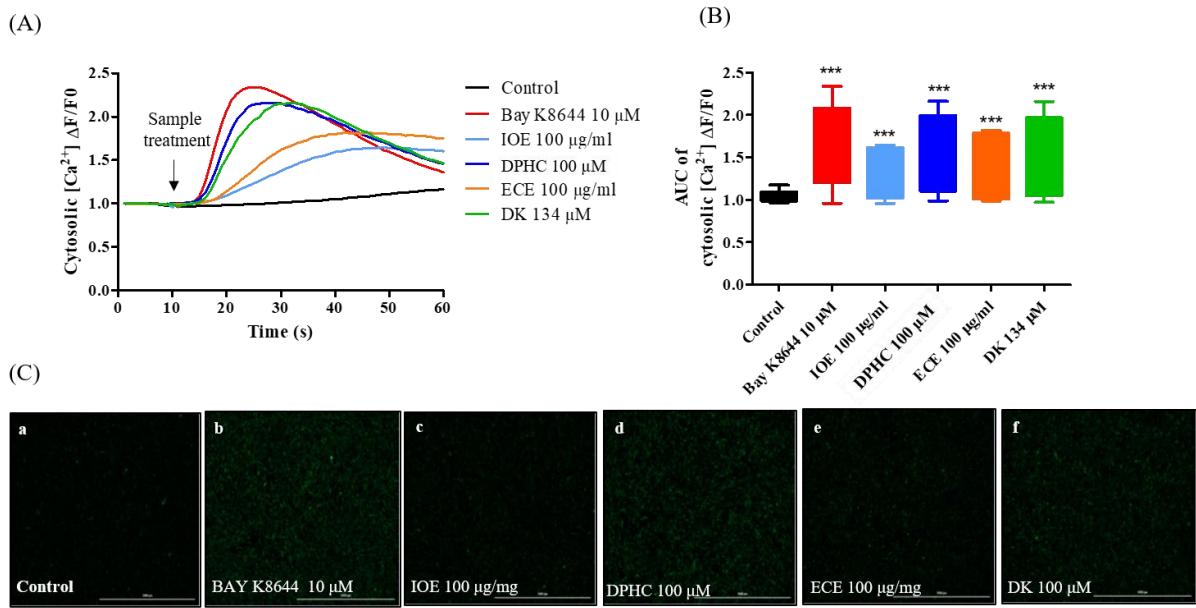


Figure 2- 7 Quantification of the  $[Ca^{2+}]_{cytol}$  levels stimulated by different samples in HCAECs. (A) The traces (B) box plots the levels of  $[Ca^{2+}]_{cytol}$ . (C) The images represented the expression of fluorescence under the sample treatments. For statistical significance, each sample treatment group was compared to the control group. Experiments were performed in triplicates. \*\*\*  $p < 0.001$ ; AUC: area under the curve;  $[Ca^{2+}]_{cytol}$ : calcium level in the cytosol.

#### **2.3.4. Measurement of cytotoxicity under the IOE, DPHC, ECE, and DK treatments in HCASMC**

In order to ensure the cytotoxicity of the samples in HCASMC, the cells were treated with IOE and ECE (3,10, 30, and 100  $\mu\text{g}/\text{ml}$ ), and also DPHC (6, 20, 60, 100  $\mu\text{M}$ ) and DK (4, 13, 40, 134  $\mu\text{M}$ ) for 24 h and cell viability were assessed by using MTT assay. As shown in Figure 2-8, cells treated with IOE, ECE, and DK did not show a significant difference compared to those of the control group. However, a slightly decreasing trend was observed in the DPHC 100  $\mu\text{M}$  group compared with the control (Figure 2-8B).

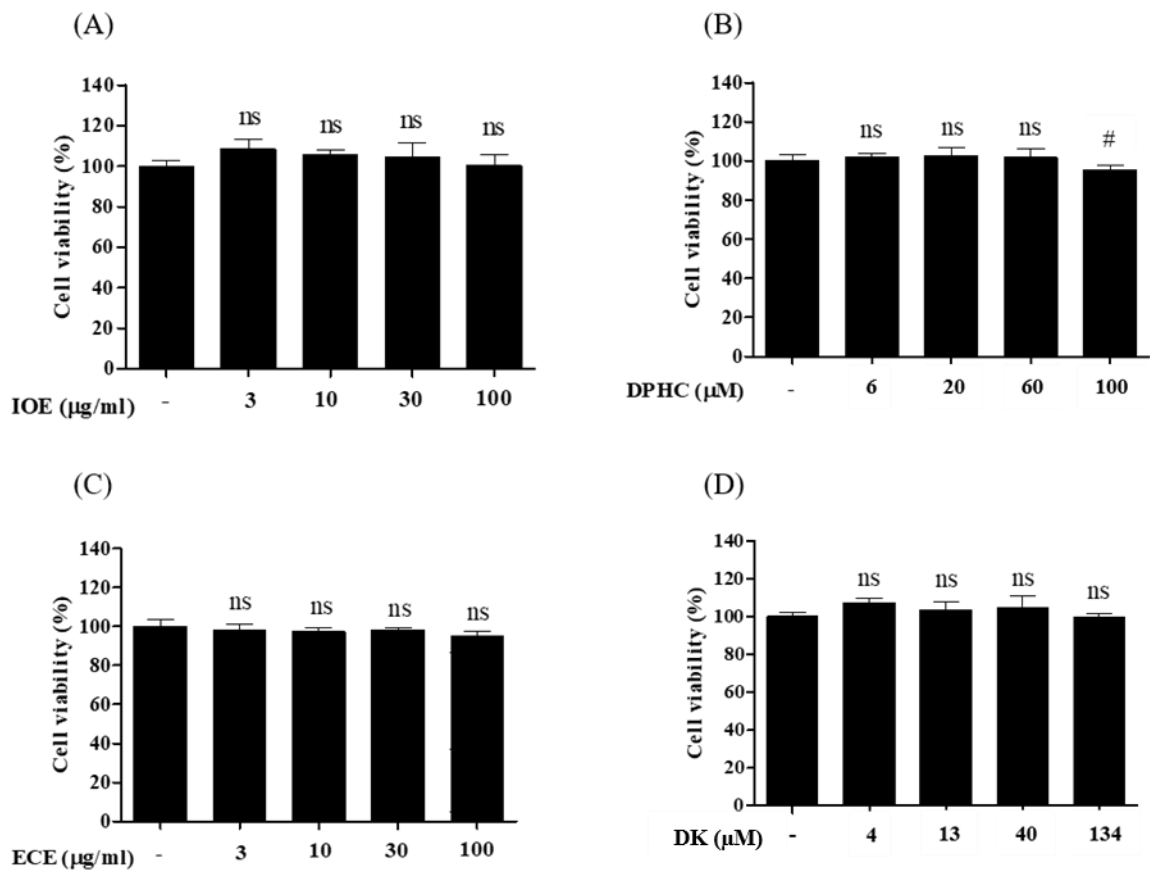


Figure 2- 8 Evaluation of cell viability treated with different concentrations of (A) IOE (3, 10, 30, and 100 μg/ml), (B) DPHC (6, 20, 60, and 100 μM), (C) ECE (3, 10, 30, and 100 μg/ml), and (D) DK (4, 13, 40, and 134 μM) in HCASMC. Experiments were performed in triplicates. Each column and bar represent the mean ± standard deviation (S.D.). #  $p < 0.05$  significant difference compared to the control group. n.s: non-significant different.

### ***2.3.5. Measurement of cell viability and NO production of HCASMC exposed under conditional medium***

Initially, to verify whether the conditional media would cause HCASMC damage, we have evaluated the cell viability of the HCASMC exposed under the conditional media at 0, 0.5, 1, 3, 12, and 24 h time points. The conditional media here implied to the media which contained the highest concentrations of samples (IOE 100  $\mu\text{g/ml}$ , DPHC 100  $\mu\text{M}$ , ECE 100  $\mu\text{g/ml}$ , and DK 134  $\mu\text{M}$ ) in our previous results. Compared to the control group (PBS only) in each time point, no toxicity was observed within 24 h (Figure 2-9).

Interestingly, excepted for the DPHC and DK treatment groups, the IOE and ECE groups did not significantly increment NO production within the experimental period (24h) compared with 0 min. The increasing NO levels were only observed at 24 h time-point under the DPHC and DK treatment (Figure 2-10).

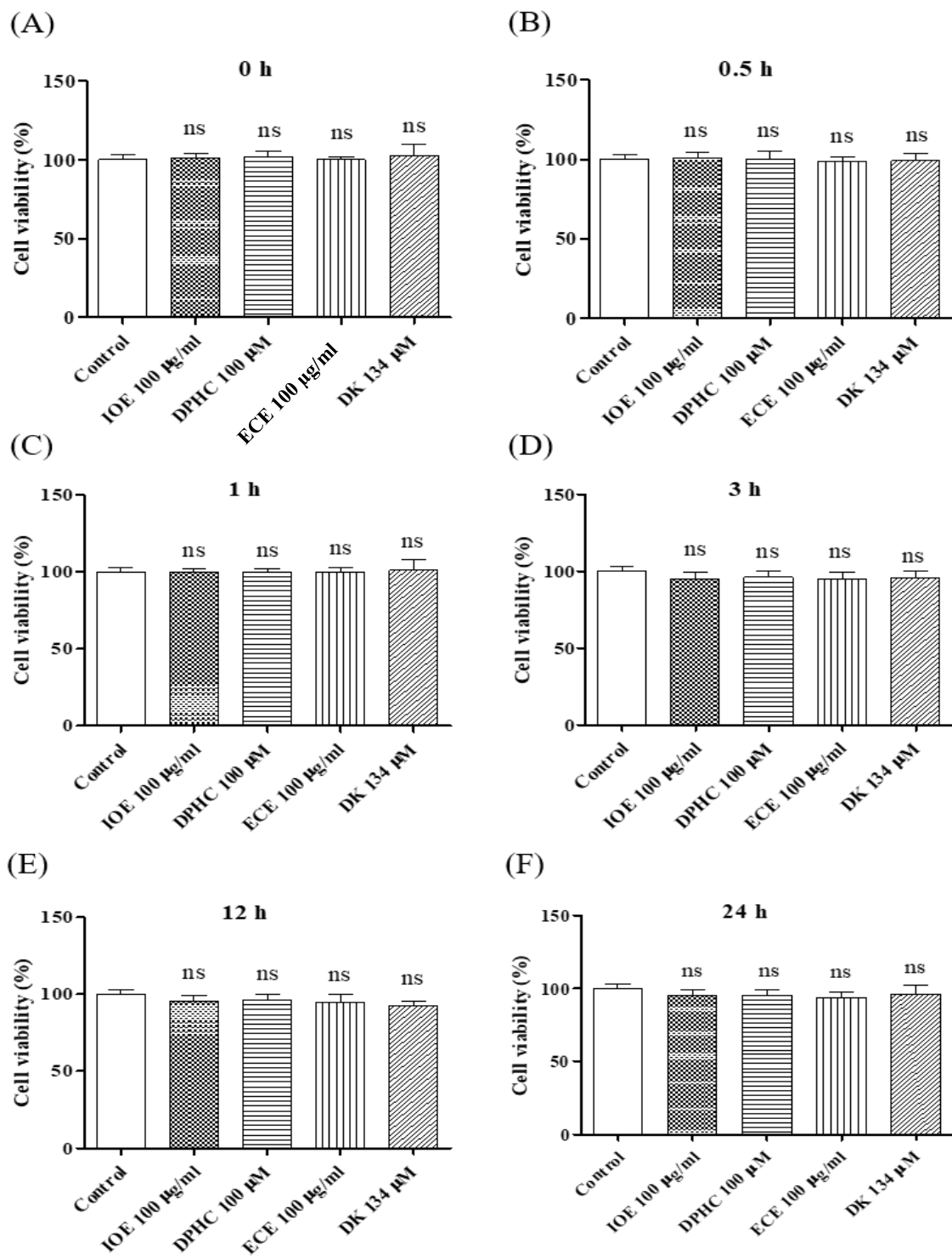


Figure 2- 9 Measurement of cell viability of HCASMC exposed in the conditional medium. (A) 0 h (B) 0.5 h (C) 1 h (D) 3 h (E) 12 h (F) 24 h in HCASMC. Experiments were performed in triplicates. Each column and bar represent the mean  $\pm$  standard deviation (S.D.) n.s: non-significant difference compared to the control group.

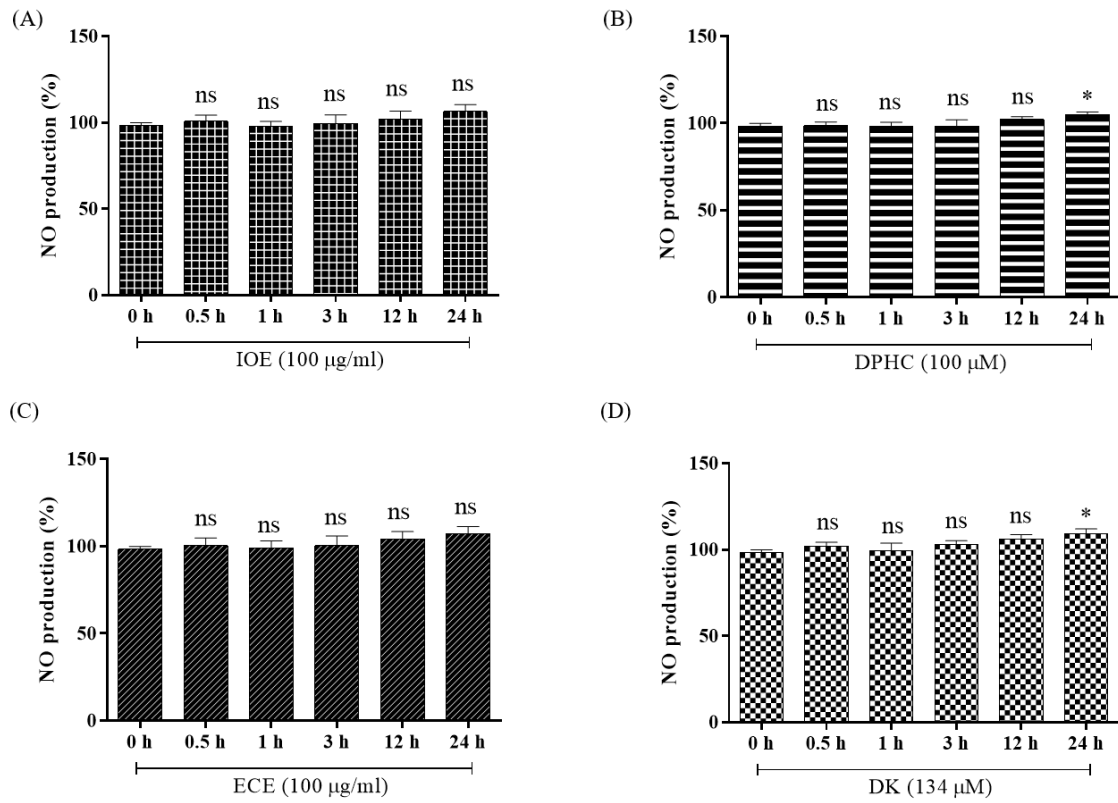


Figure 2- 10 Measurement of NO production at different time points when HCASMC exposure under conditional medium. (A) IOE (100  $\mu\text{g/ml}$ ) (B) DPHC (100  $\mu\text{M}$ ) (C) ECE (100  $\mu\text{g/ml}$ ) (D) DK (134  $\mu\text{M}$ ). The intracellular NO concentrations were detected by 10  $\mu\text{M}$  of DAF-FM-DA assay in HCASMC. Experiments were performed in triplicates. Each column and bar represent the mean  $\pm$  standard deviation (S.D.). \*  $p < 0.05$  significant difference compared to the control group. n.s: non-significant different.

### ***2.3.6. DK and DPHC suppressed the contractile effect by down-regulating the CaM and p-MLC expression in HCASMC***

According to all mechanisms correlated to the endothelial cell that we have done in previous studies [14, 52], we have known that the appropriate concentrations of DK and DPHC can induce endothelial-dependent NO formation and further affected VSMC resulting in vasorelaxations. Our next approach was to examine the expression of vasodilation correlated proteins such as calmodulin (CaM), myosin light chain (MLC), *p*-myosin light chain (*p*-MLC) in the HCASMC which exposure in the conditional media. Earlier, we have demonstrated NO can be effectively induced by the endothelial cell under the appropriate concentrations of DK and DPHC. According to our hypothesis, we assumed that the conditional media which contained NO could effectively suppress the levels of CaM and *p*-MLC resulting in promoting vasodilation. Thus, we first examined the behavior of the CaM and *p*-MLC, the most important protein which major in regulating the contraction of the VSMC. As the results demonstrated in Figure 2-11B and 11C, except the 4  $\mu$ M, other DK concentrations showed the potential to suppress the CaM and *p*-MLC expression.

Moreover, similar dose-dependent down regulation trends were observed under DPHC treatments and Figures 2-12B and 12C. However, compared to the inhibited effect of DK and DPHC, we noticed that DK performed higher potential in regulated the vasodilatory proteins in HCASMC.

Briefly sum up, in the media retransfer experiments, both DK and DPHC showed the vasodilation property via down-regulation the CaM and suppressed the phosphorylation of MLC in the HCASMC.

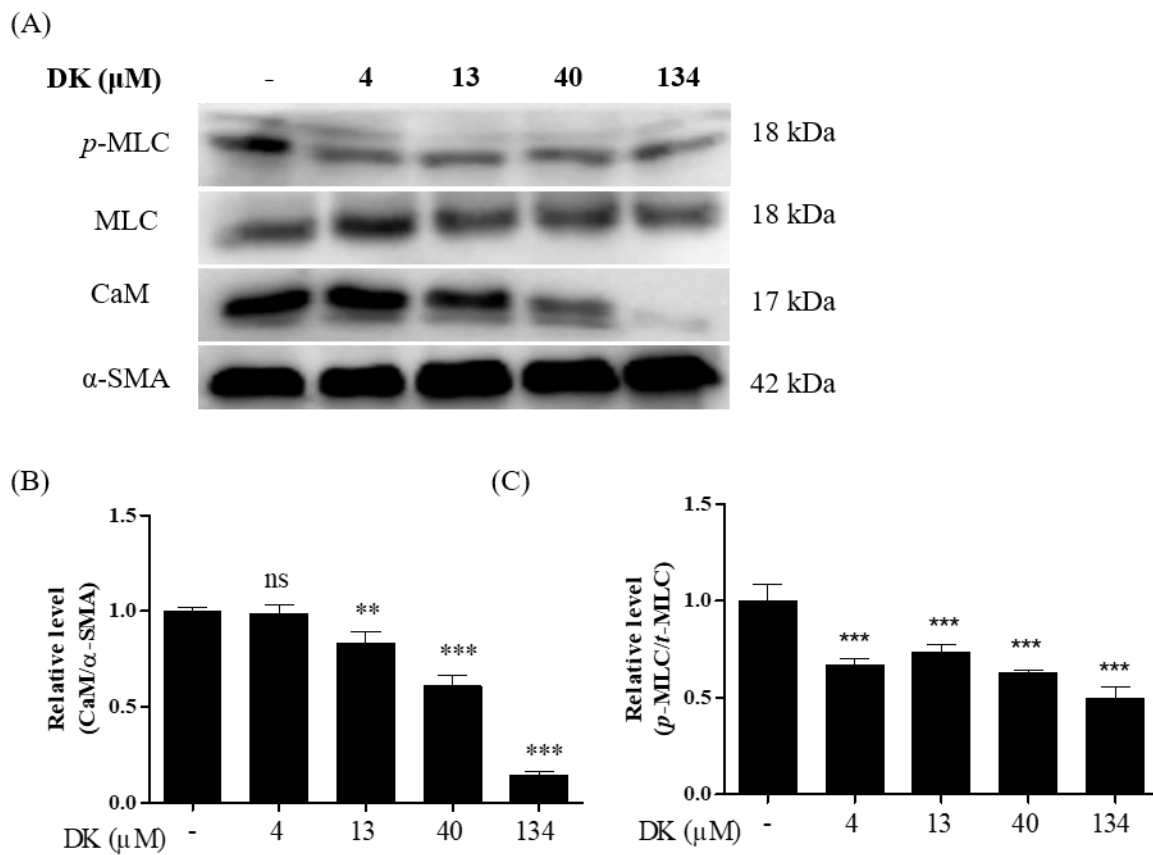
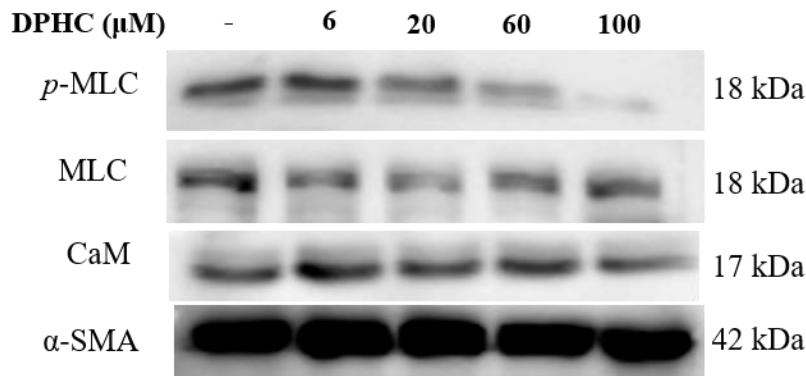
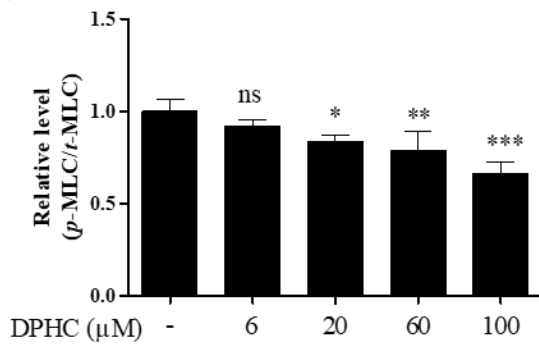


Figure 2- 11 Expression of CaM and phosphorylated myosin light chain (*p*-MLC) in HCASMC treated under different concentrations of DK. (A) The examples of the western blot (B) The relative level of CaM/ $\alpha$ -SMA (C) The relative level of *p*-MLC/ MLC. Experiments were performed in triplicates. Each column and bar represent the mean  $\pm$  standard deviation (S.D.). \*  $p < 0.05$ , \*\*\*  $p < 0.001$  significant difference compared to the control group. n.s: non-significant different; CaM: Calmodulin.

(A)



(B)



(C)

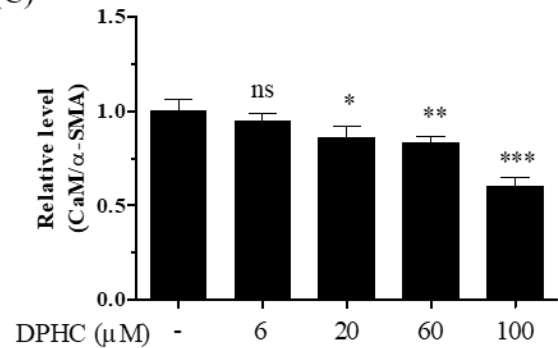


Figure 2- 12 Expression of CaM and phosphorylated myosin light chain (*p*-MLC) in HCASMC treated with different concentrations of DPHC. (A) The examples of the western blot (B) The relative level of CaM/ $\alpha$ -SMA (C) The relative level of *p*-MLC/MLC. Experiments were performed in triplicates. Each column and bar represent the mean  $\pm$  standard deviation (S.D.). \*  $p < 0.05$ , \*\*  $p < 0.01$ , and \*\*\*  $p < 0.001$  significant difference compared to the control group. n.s: non-significant different; CaM: Calmodulin.

### ***2.3.7. Detection of CaM and p-MLC expression by immunofluorescence staining in the co-culture system***

Based on the media transfer experiments, we have known that DK (13, 40, and 134 $\mu$ M) and DPHC (20, 60, 100  $\mu$ M) were the effective dosages to induce endothelium-derived relaxing factor (EDRF) such as NO and H<sub>2</sub>S, and also promote the vasodilatory effect via reduced CaM and suppressed the phosphorylation of MLC. Thereupon, our next goal was to mimic the real environment of the human vessel and study the EC-SMC interaction related to vasorelaxation mechanisms. To do so, we have used the co-culture system to investigate whether DK and DPHC would show similar effects under this EC-VSMC co-culture system.

First of all, we evaluated the levels of CaM in the HCAEC of the co-culture model. As shown in Figure 2-13 and 2-14, except for 20  $\mu$ M of DPHC, the DK and DPHC successfully promoted the CaM expression in HCAEC

On the other hand, the dramatic down-regulation of CaM and *p*-MLC were observed at the DK treatments in HACSMC (Figure 2-15B). Nevertheless, under the DPHC treatment (20  $\mu$ M), the expression of CaM and *p*-MLC was no significantly different than control in HCASMC Figure 2-16B and 16C. While the concentration of DPHC increased to 100  $\mu$ M, the significantly decreasing which observed in Figure 2-16B and 16C. From the co-culture system, we demonstrated that DK and DPHC were successfully decreased the CaM and *p*-MLC protein expression. Compared to DPHC, the DK treatments showed the better potential to suppress the CaM and *p*-MLC protein expression in HCASMC.

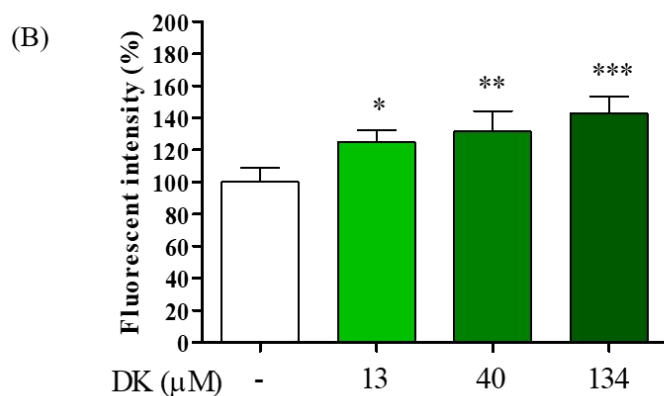
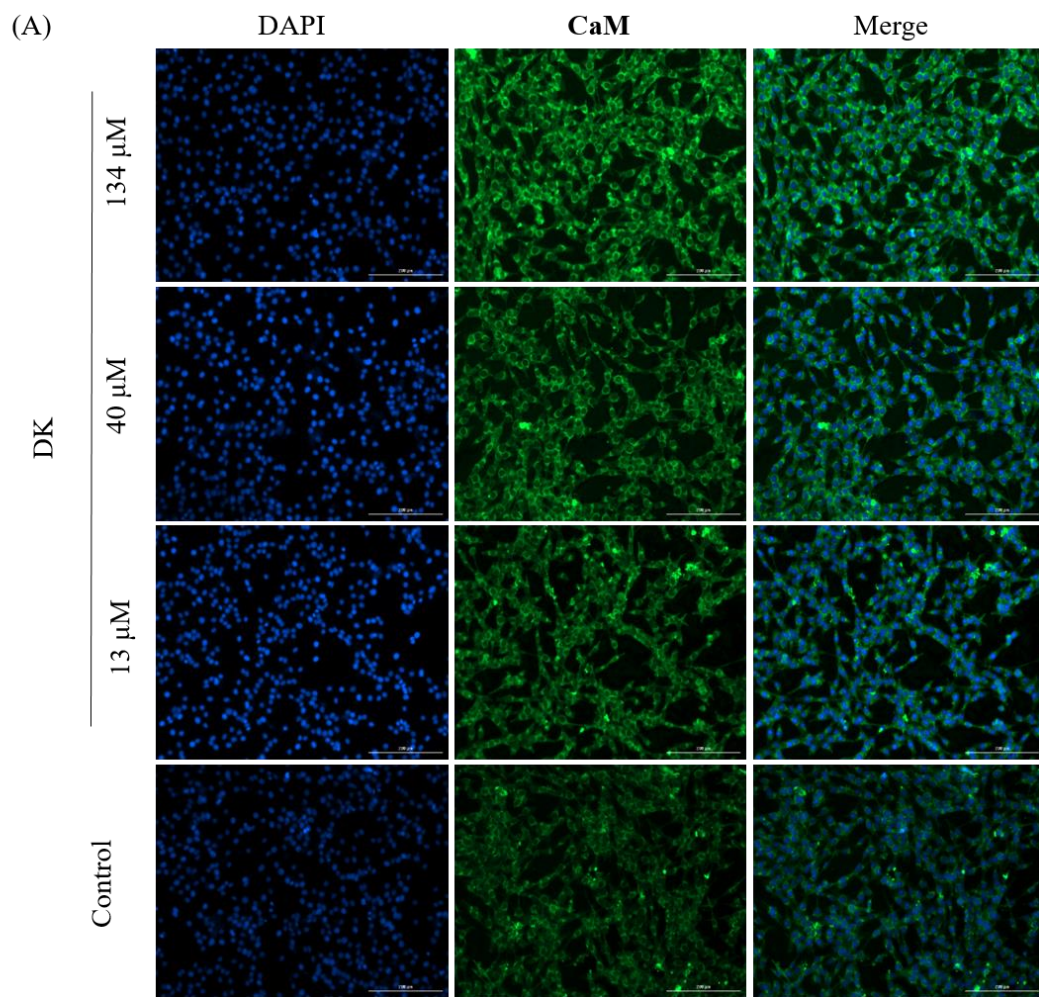


Figure 2- 13 Immunofluorescence analysis of HCAEC under the DK treatments. (A) The images were represented the CaM expression (B) The analysis of fluorescence intensity under the treatment of different concentrations of DK. Experiments were performed in triplicates. Each column and bar represent the mean  $\pm$  standard deviation (S.D.). \*  $p < 0.05$ , \*\*  $p < 0.01$ , and \*\*\*  $p < 0.001$  significant difference compared to the control group. n.s: non-significant different; CaM: Calmodulin.

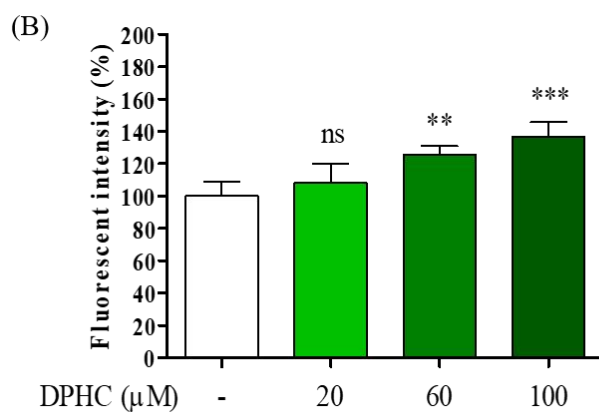
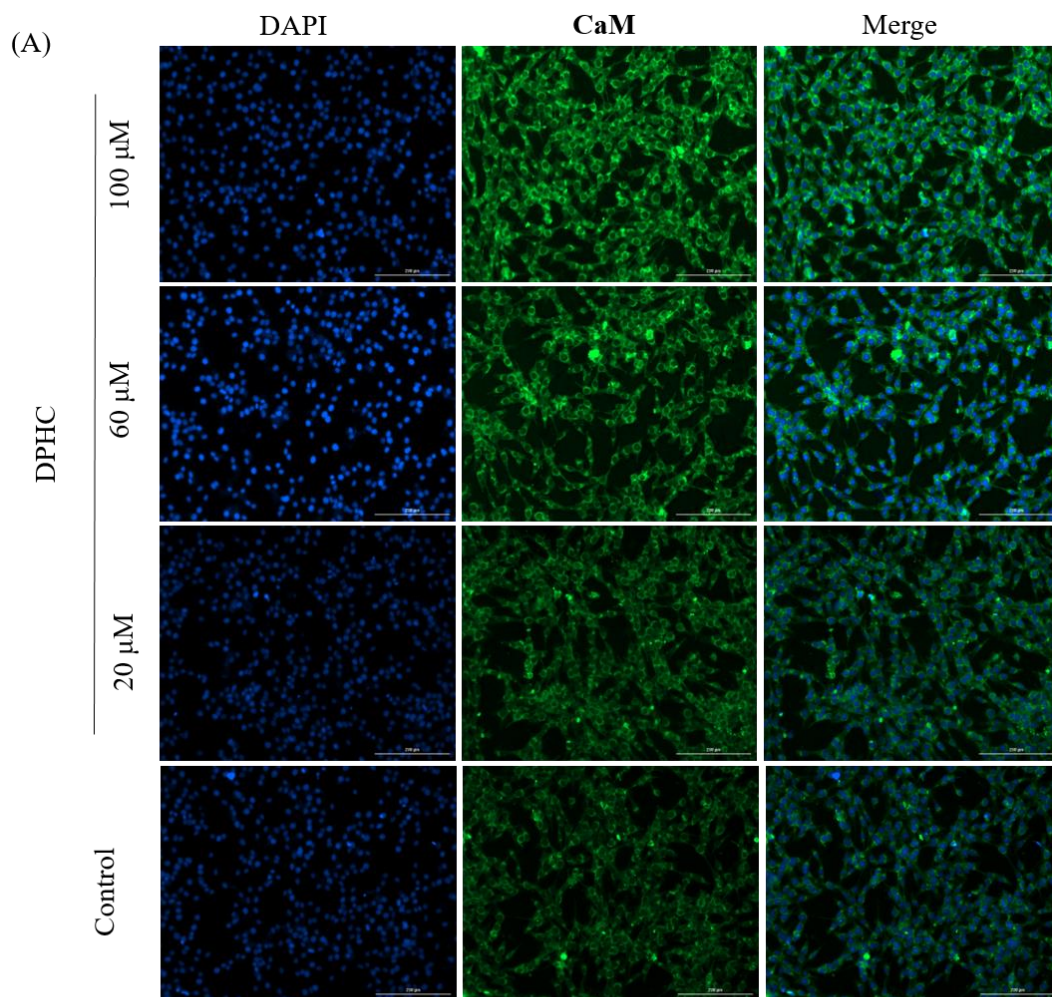


Figure 2- 14 Immunofluorescence analysis of HCAEC under DPHC treatments. (A) The images were represented the CaM expression (B) The analysis of fluorescence intensity under the treatment of different concentrations of DPHC. Experiments were performed in triplicates. Each column and bar represent the mean  $\pm$  standard deviation (S.D.). \*  $p < 0.05$ , \*\*\*  $p < 0.001$  significant difference compared to the control group. n.s: non-significant different; CaM: Calmodulin.

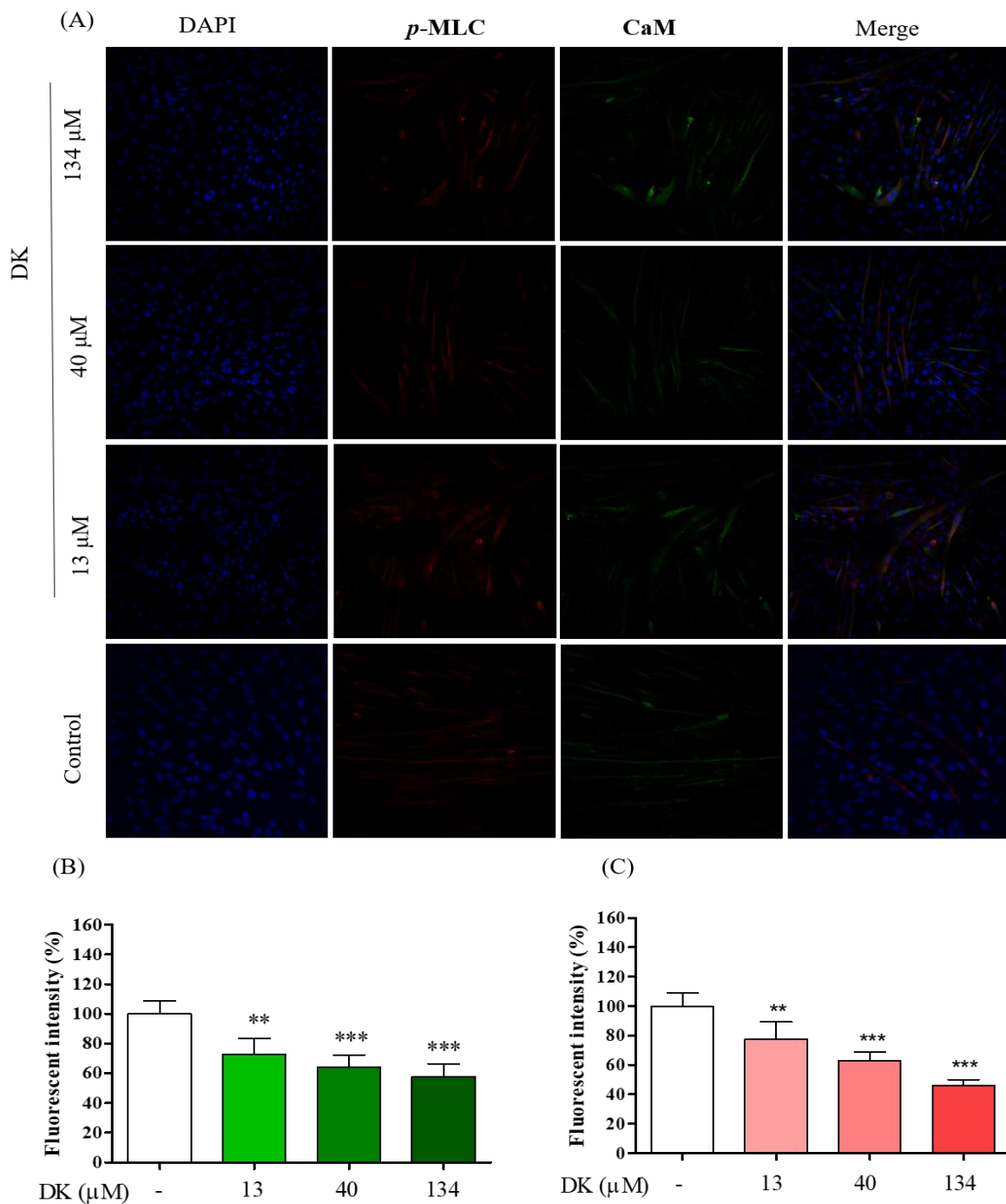


Figure 2- 15 Double-label immunofluorescence analysis of HCASMC under the DK treatments. (A) The images were represented the CaM and *p*-MLC expression (B) The analysis of fluorescence intensity under the treatment of different concentrations of DK. Experiments were performed in triplicates. Each column and bar represent the mean  $\pm$  standard deviation (S.D.). \*  $p < 0.05$ , \*\*\*  $p < 0.001$  significant difference compared to the control group. n.s: non-significant different; CaM: Calmodulin.

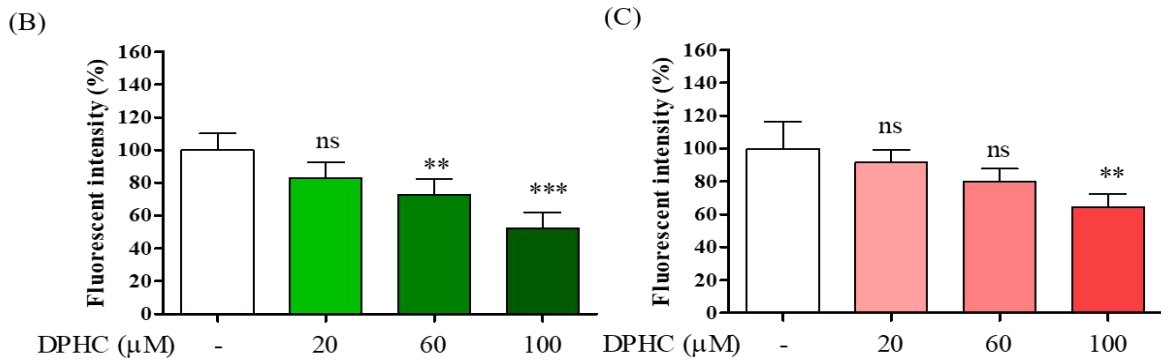
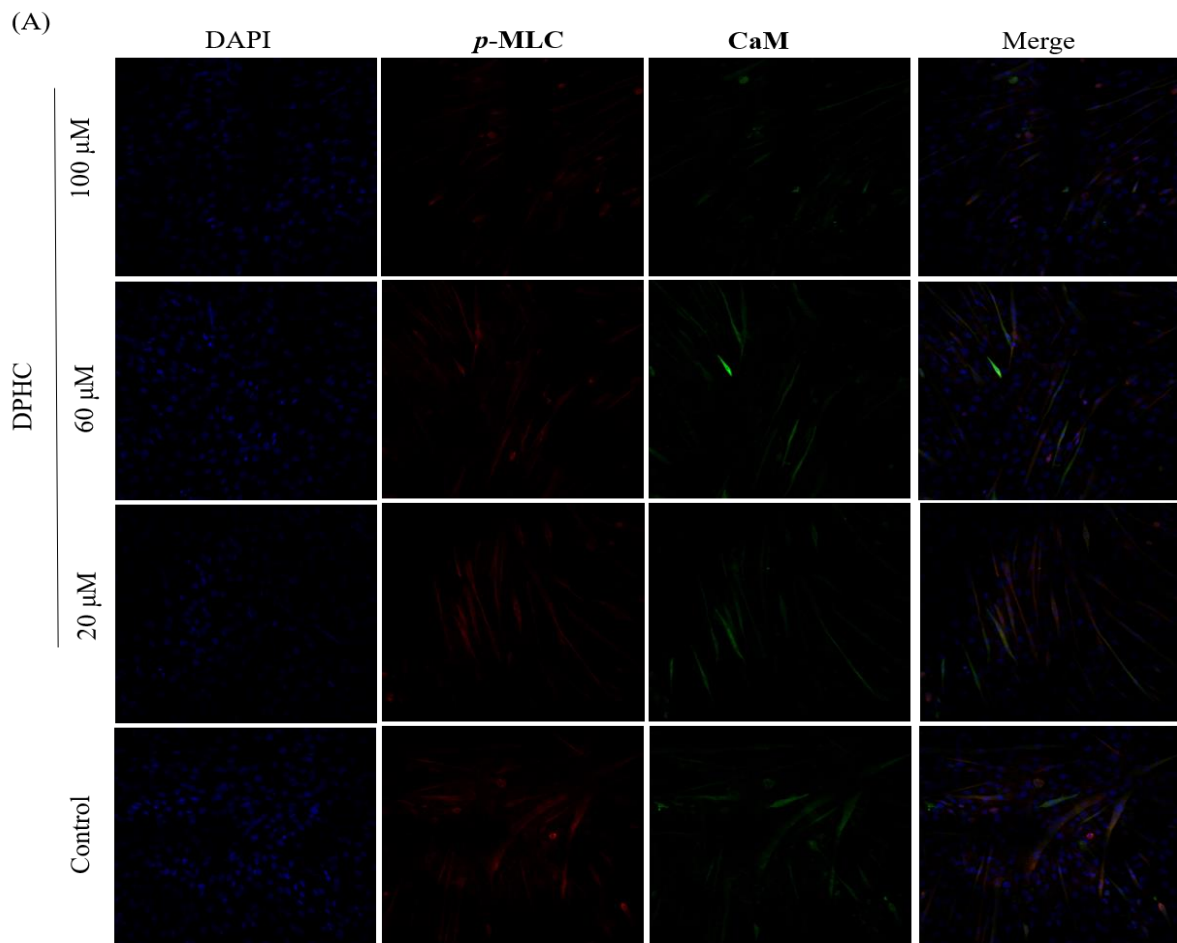


Figure 2- 16 Immunofluorescence analysis of HCASMC under the DPHC treatments. (A) The images were represented the CaM and *p*-MLC expression (B) The analysis of fluorescence intensity under the treatment of different concentrations of DPHC. Experiments were performed in triplicates. Each column and bar represent the mean  $\pm$  standard deviation (S.D.). \*  $p < 0.05$ , \*\*\*  $p < 0.001$  significant difference compared to the control group. n.s: non-significant different; CaM: Calmodulin.

### ***2.3.8. DK and DPHC down-regulated the expression of CaM and p-MLC in the co-culture system***

As shown in Figure 2-17B, a significant decrease was noticed at DK treatments (except 4  $\mu\text{M}$ ), and the dose-dependent down-regulation of CaM was observed in the DK treatments compared to control (Figure 2-17B). Furthermore, the phosphorylation of MLC was remarkably suppressed by DK treatments (Figure 2-17C).

On the other hand, a similar dose-dependent decreasing pattern was demonstrated in the CaM expression, which was affected by different concentrations of DPHC (Figure 2-18B). Unexpectedly, in Figure 2-18C, DPHC treatments gradually reduced the expression of p-MLC. However, the 100  $\mu\text{M}$  of DPHC suddenly enhanced the protein expression. We need to do a further experiment to investigate whether other factors influenced the pathway under this concentration.

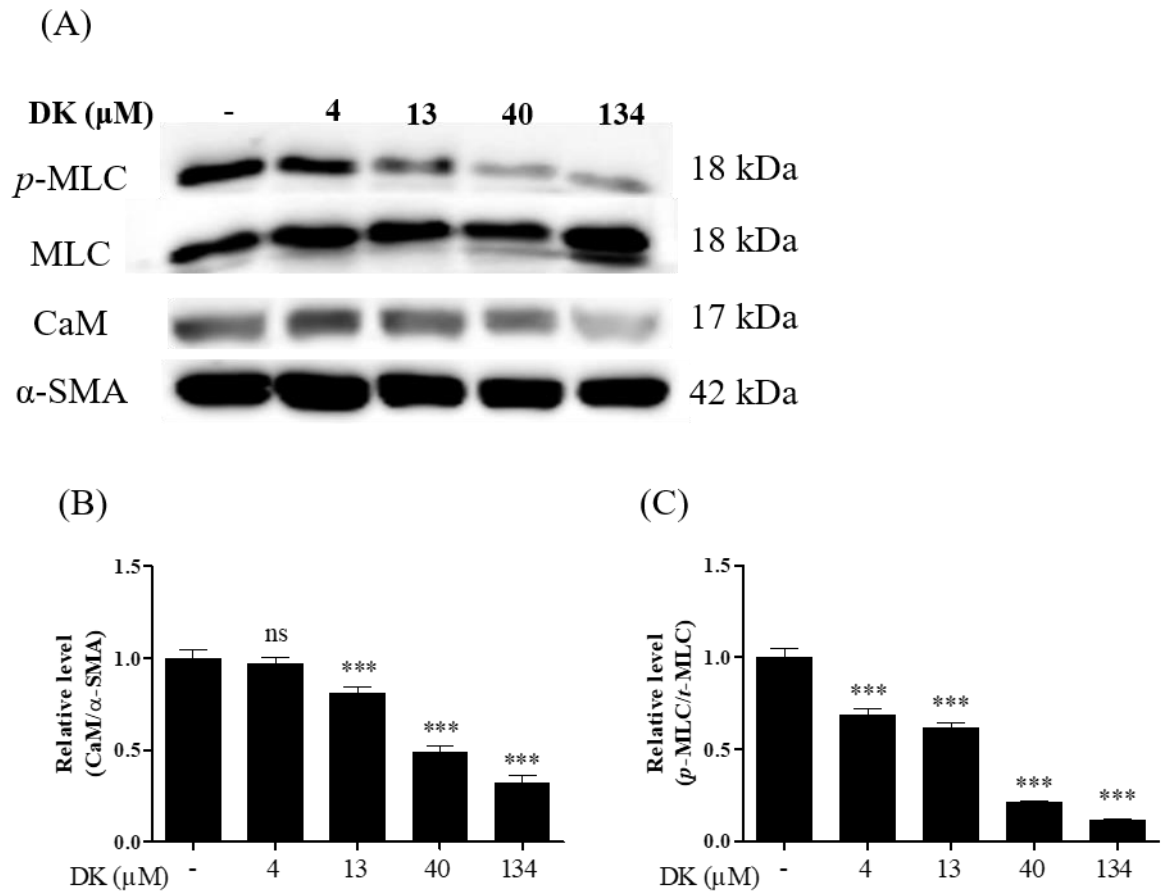


Figure 2- 17 Expression of CaM and phosphorylated myosin light chain (*p*-MLC) in HCASMC treated under different concentrations of DK. (A) The examples of the western blot (B) The relative level of CaM/ $\alpha$ -SMA (C) The relative level of *p*-MLC/MLC. Experiments were performed in triplicates. Each column and bar represent the mean  $\pm$  standard deviation (S.D.). \*  $p < 0.05$ , \*\*\*  $p < 0.001$  significant difference compared to the control group. n.s: non-significant different; CaM: Calmodulin.

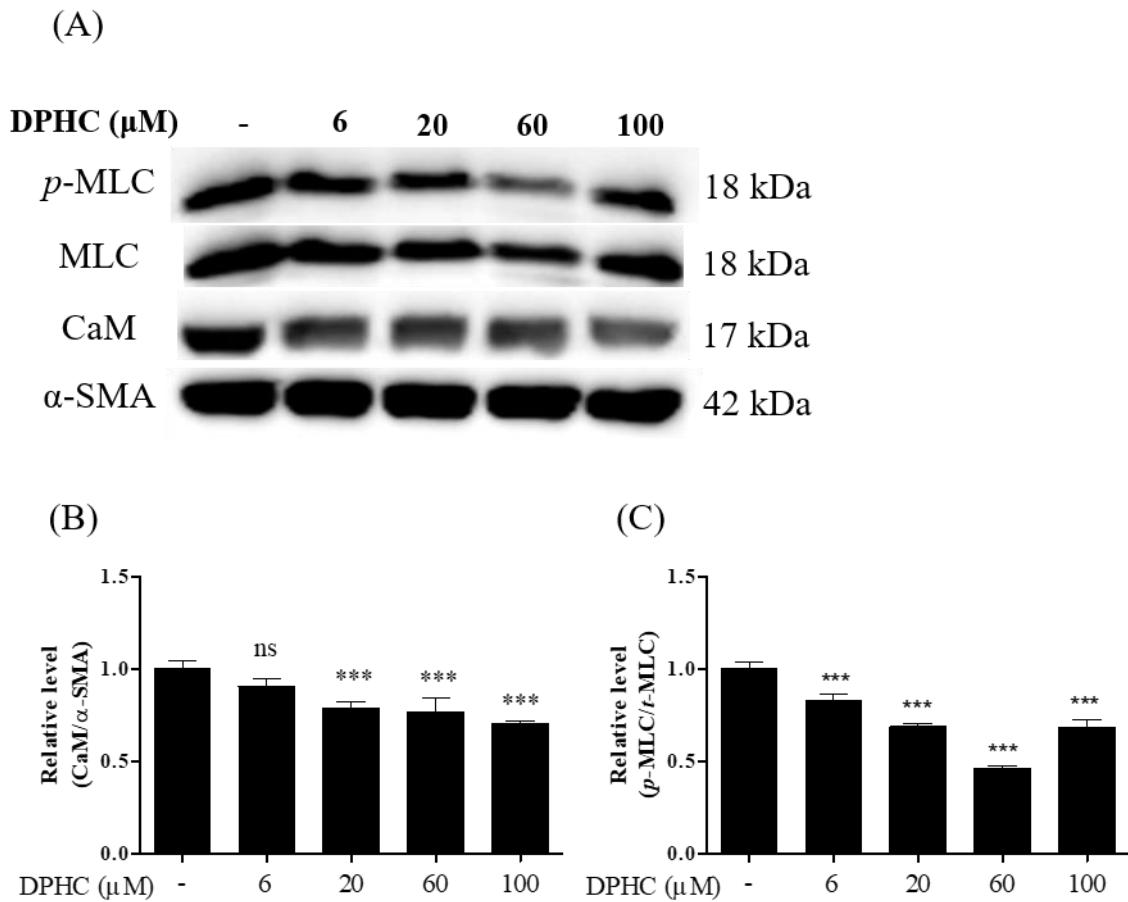


Figure 2- 18 Expression of CaM and phosphorylated myosin light chain (*p*-MLC) in HCASMC treated under different concentrations of DPHC. (A) The examples of the western blot (B) The relative level of CaM/ $\alpha$ -SMA (C) The relative level of *p*-MLC/*t*-MLC. Experiments were performed in triplicates. Each column and bar represent the mean  $\pm$  standard deviation (S.D.). \*  $p < 0.05$ , \*\*\*  $p < 0.001$  significant difference compared to the control group. n.s: non-significant different; CaM: Calmodulin.

## 2.4. Discussion

Well communication between EC and VSMC is an essential component of vascular functions. The vascular tone is closely maintained by an appropriate balance of vasodilation and vasoconstriction. It is well recognized that NO and H<sub>2</sub>S, the effective EDRF, would lead to VSMC relaxation [53]. Recently, many potential therapies for cardiovascular disorders (especially in hypertension) are designed to activate the endothelium relaxing factor in the EC [21, 54] and inhibit the specific signaling pathway in the VSMC [55, 56]. Our previous studies showed that DK and DPHC could promote the vasodilatory effect via calcium-dependent and calcium-independent pathways [14, 52]. However, the well-regulation of vessel tone also depends on the contribution of the VSMC. Thus, the mechanisms of the relaxation in VSMC are the next aim to investigate.

The cyclic guanine monophosphate (cGMP)-protein kinase G (PKG) pathway is the primary mechanism responsible for a broad range of the biological actions of endothelial-dependent NO (EDNO) [57]. EDNO may cause vasculature to relax by decreasing the [Ca<sup>2+</sup>]<sub>cytol</sub> level resulting from PKG-dependent stimulation of [Ca<sup>2+</sup>]-activated potassium channels, which leads to membrane hyperpolarization and [Ca<sup>2+</sup>] influx suppression [58]. EDNO may also cause vasodilatation by reducing the sensitivity of myofilaments to [Ca<sup>2+</sup>] via the PKG-dependent phosphorylation of the regulatory subunit of myosin light chain phosphatase at threonine-695 and -852 (Thr-695 and Thr-852, respectively, human sequence), which leads to increased dephosphorylation of the myosin light chain and reduced contractility [59]. In contrast, while the [Ca<sup>2+</sup>] binds to CaM ([Ca<sup>2+</sup>]-CaM) complex), causing conformational changes, which allow the interaction of the [Ca<sup>2+</sup>]-CaM complex with the MLC. These events subsequently lead to activation of MLC kinase and phosphorylation of the regulatory MLC. Protein kinase C (PKC) phosphorylates specific target proteins (e.g., contractile proteins, regulatory proteins, channels, pumps, etc.) and has contraction-promoting

effects [60]. It has been reported that dysfunctional EDNO- (soluble guanylyl cyclase) sGC-cGMP-PKG signaling pathway constitutes one of the most fundamental and initial changes in the development of hypertension [61], resulting from aberrant expression of eNOS, reduced NO production caused by eNOS uncoupling [62, 63], diminished NO bioavailability caused by oxidative stress [64], diminished activities of sGC and PKG, and augmented activity of phosphodiesterase type 5 [65]. Based on this evidence, we first focused on how the EDRF (NO and H<sub>2</sub>S) induced by DK and DPHC in endothelial cells influences the VSMC.

To examine it, we have used the co-culture system to demonstrate our experiments. Briefly, there are direct-contact and indirect-contact co-culture models, and there are several types of the model included in the indirect-contact methods [66-68]. The media transferred and inserted the trans-well used in the present study also belongs to indirect contact methods. Especially, advantages of using inserted trans-well are that first, the membrane separating the cells is transparent and allows continued observation of both cell layers throughout an experiment. Second, the separating membrane is very thin and contained a tiny pore (0.4 $\mu$ m), potentially allows for a physical interaction between the two cellular layers. Thus, we can mimic the vessel environment and observe the EC-VSMC model's interaction under the treatment of samples. According to our hypothesis, we assumed that EC would produce plenty amount of NO, H<sub>2</sub>S, and other EDRFs and further affected VSMC by diffusion, transportation, or other specific mechanisms. To better understand the mechanisms, we first used the media transfer methods to investigate whether the DK and DPHC and successfully induced the NO and H<sub>2</sub>S levels in HCAECs, further transferring this conditional media to HCASMC

Before starting the media transfer experiment, to ensure the conditional media can successfully be prepared, we have confirmed the vasodilatory effect of DK and DPHC in HCAEC by checking the NO concentration, H<sub>2</sub>S, and [Ca<sup>2+</sup>]<sub>cytol</sub> levels. Interestingly, at the initial data, we found that after transferred the conditional media, the NO concentration did not

significantly increase within 24 h. Indeed, it has been indicated that VSMC tended to receive the NO from EC rather than produce by itself to activate the downstream pathways [69, 70]. Further, the levels of endogenous H<sub>2</sub>S and the [Ca<sup>2+</sup>]<sub>cytol</sub> were also effectively induced by sample treatments. Therefore, we confirmed that DK and DPHC could stable promote the EDRF in EC. Soon after the conditional media was added into the VSMC and incubated for 24 h, the CaM and *p*-MLK were significantly reduced by DK and DPHC treatments.

Moreover, DK showed a higher potential to regulate vasodilatory protein expression. Many reports have indicated that intact endothelium protects VSMC from the superoxide attack resulting in maintaining the NO bioactivity and NO bioavailability [71, 72]. Due to these concepts, we were interested that if we shorted the distance of EC-SMC via a co-culture system, whether the DK and DPHC could more highly potentially desensitize the VSMC contractile apparatus. In other words, if we can make the VSMC receive the NO or H<sub>2</sub>S diffused from the EC soon after the sample treatments, the results might have some differences. As expected, the levels of CaM and *p*-MLC evaluated by immunostaining and western blot in the co-culture model have demonstrated the more highly regulation effect under DK and DPHC treatment compared to media transfer experiments. The possible reasons might be considered as bellowed: first, NO reacts with soluble guanylate cyclase SMC to produce cGMP, which, in turn, activates myosin light chain phosphatase that then removes phosphates from myosin, causing relaxation. The EDRFs diffuse rapidly between the two types of cells.

Especially, NO is a highly reactive substance, and reactive oxygen species (ROS) can decrease its concentration. Thus, short diffusion distances between the endothelium and VSMC are needed for NO to affect SMC [73]. Second, the co-culture model showed a higher desensitize contractile effect due to the short distance of two cell lines. The trans-well provides a thin layer (10 μm thick) to let EC-SMC communicate well (i.e., Diffusion NO). Third, one of the most important points related to vascular tone regulation, the myoendothelial gap

junction (MEGJ) between EC and VSMC [74]. These junctional structures are described to derive from endothelial cells and transverse a break in the continuity of the basal lamina to make contact with the smooth muscle membrane [75]. The functional coordination of cells within the vascular wall is believed to be dependent on signal transduction through gap junctions, and it is dependent on calcium ions and other signaling molecules ( $IP_3$  and cAMP) exchanges [76]. This implies that MEGJ would serve as a feedback mechanism to limit vasoconstriction [77]. Pogoda K. *et al.* have indicated that Cx37 plays a critical role in the NO effect on calcium signal propagation in the MEGJ region. The signal would lead the VSMC contractile [78]. Therefore, based on these pieces of evidence, we can reasonably assume that DK and DPHC might promote the specific role of MEGJ in the EC-SMC co-culture system. However, the limitation of the present study is that we need further detailed experiments to prove these points.

## **2.5. Conclusions**

DK and DPHC promoted endothelium-dependent relaxation through enhancing the calcium transduction, which affected the EDRF releasing (NO and  $H_2S$ ) then diffused to VSMC to desensitize the contractile effect by down-regulating the expression of CaM and suppressed the phosphorylation of MLC.

**Part III**

**Bioactive compounds isolated from *Ecklonia cava* and *Ishige okamurae*  
promote vasodilation in the zebrafish model**

### 3.1. Introduction

It is well known that the imbalance between vasoconstriction and vasodilation is deeply related to cardiovascular diseases, especially hypertension (HTN)[1, 2]. Recently, the zebrafish was performed as a promising model for the study of metabolic disorders, such as obesity [79], diabetes [80], and high blood pressure [81]. Owing to their outstanding advantages, such as the optical clarity of zebrafish embryos, rapid development, and similar organ systems and gene functions as humans, the zebrafish was considered a superior investigational model [14]. The zebrafish model has previously revealed several essential insights into vascular structure development and helped verify underlying molecular mechanisms [22]. Therefore, take all the advantages of the zebrafish, we determined to use it as the *in vivo* model in the present study. Moreover, the dorsal aorta (DA), a critical trunk artery, has been used to evaluate different cardiovascular parameters, such as mean linear flow, arterial pulse, and vessel diameter [23]. The change of DA's diameter in transgenic zebrafish was considered direct evidence when assessing sample treatment due to its visibility [14]. Under these viewpoints, we have used the DA as the main vessel to evaluate all the blood parameters.

*Ecklonia cava* (E. cava) and *Ishige okamurae* (IO) are famous for the different biological activities, including antioxidant, anti-inflammatory, attenuation of endothelial cell dysfunction, and anti-hypertension, in numerous studies [8-11]. *Son et al.* have indicated that E. cava ethanol extract (ECE) significantly alleviates BP in a mouse model of HTN. Furthermore, dieckol (DK), a polyphenolic compound present in ECE, has been suggested as one of the bioactive components responsible for the potential ACE inhibitory activity [12, 13]. Notably, IO ethanol extract (IOE) and its bioactive substances, diphloretohydroxycarmalol (DPHC), have shown the remarkable ability to regulate endothelial-dependent vasodilation [14]. Indeed, the vasodilatory effect of the DK and DPHC has been performed in the endothelial - smooth muscle

cell co-culture system (second part). Therefore, in the third part, we aim to investigate the vasodilatory effect of DK and DPHC *in vivo* model.

## 3.2. Material and methods

### 3.2.1. Zebrafish husbandry and fish strains

The transgenic zebrafish *Tg(flk: EGFP)* was used to perform an *in vivo* investigation [82]. Fish were housed in 3L tanks (aquatic habitats). The zebrafish facility contained buffered water (pH 7.5) at 28.5°C. Fertilized eggs were collected from the bottom of the tank in an automatic circulation culture system (ESEN, Beijing, China), maintained at 28.5°C, pH 7.5, and dissolved oxygen 7.0, conductivity 800 µS, containing methylene blue. The eggs were placed in Petri dishes after thorough washing in the system water and then transferred to the incubator. For experiments, the larvae were first maintained in 12-well plates containing egg water (reverse osmosis water containing 60 mg sea salt per liter of water [pH 7.5]). After sample treatment, the number of larvae was checked daily. The zebrafish experiment received approval from the Animal Care and Use Committee of Jeju National University (Approval No. 2017-0001).

### 3.2.2. Toxicity of DK and DPHC in zebrafish embryos

For DK and DPHC, the *in vivo* toxicity test was performed using the zebrafish model as follows. The test was based on the exposure of newly fertilized zebrafish eggs to the test sample for up to 120 h; 10 eggs per treatment (three replicates) were selected and distributed in 12-well microplates. Before the study, the stock solution of the test compound was dissolved in an E3 zebrafish embryo medium and then diluted to appropriate concentrations using this medium. The test was initiated with newly fertilized eggs exposed to 4, 13, 40, and 134 µM of DK; 6, 20, 60, and 100 µM of DPHC then run for 120 h. Embryos were observed for up to 120 h under a stereomicroscope (magnification used in the stereomicroscope for observations was 4x).

### ***3.2.3. Toxicity of vasoconstriction drug - phenylephrine in zebrafish embryos***

The chemical used in this experiment were purchased from Sigma. The (R)-(-)-Phenylephrine hydrochloride (P6126) was dissolved in a fish medium. The toxicity of PE was started evaluated from 4-hour post-fertilization (hpf), 15 embryos per well (12 well). Based on the previous studies, 10  $\mu\text{M}$  of PE has been demonstrated nontoxic in zebrafish experiments and no significant heart rate effect [23, 83]. Thus, we have tested the PE concentrations from 10, 20, 30, 40, and 50  $\mu\text{M}$ , and optimize the best concentration for further studies. Before the study, the stock solution of the PE was dissolved in the E3 zebrafish embryo medium and then diluted to appropriate concentrations using this medium. Each well contained 950  $\mu\text{L}$  of embryo media and 50  $\mu\text{L}$  of PE. The survival rate was examined every 24 hours up to a total of 120 hpf (0, 24, 48, 72, 96, 120 hpf). The protocol was briefly represented as bellowed.

### 3.2.4. The vasoconstrictive zebrafish model set up

A dose-response curve was used to determine optimal drug concentrations. Heart rate values of zebrafish embryos were counted by visual observation in 1 min under the stereomicroscope and counted manually. Five zebrafish were exposed individually to either the E3 fish medium or the vasoactive agent for each concentration of a vasoactive agent (Figure 3-1).

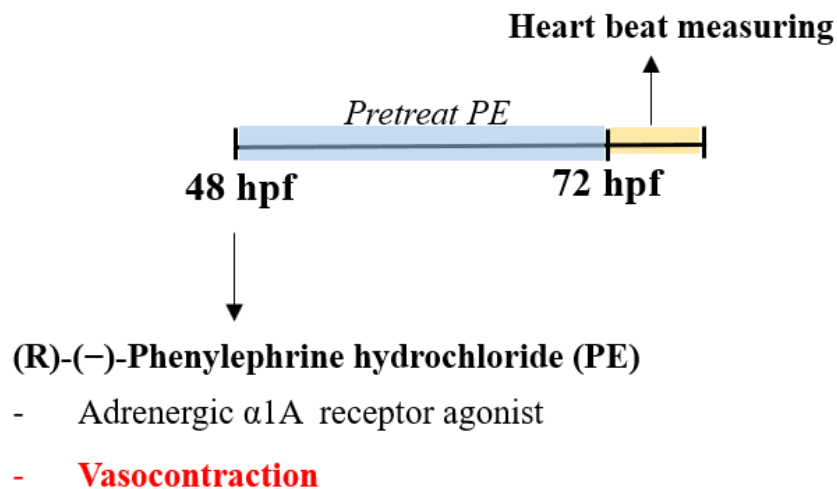


Figure 3- 1 The graphic represented the protocol of the vasoconstriction model in zebrafish

### 3.2.5. Assessment of whole-body fluorescence intensity in the *Tg(flk: EGFP)* transgenic zebrafish

The images were photographed using a fluorescence microscope at 4x magnification to capture blood vessels in the whole body. Fluorescence intensity signals of the whole body were measured using the Gen5 3.04 software (Biotek). Fluorescence images were imported into the Image J software to calculate the corrected total object fluorescence (CTOF), according to the following formula:

$$CTOF = Integrated\ density - (Area\ of\ selected\ object \times mean\ background\ fluorescence)$$

### ***3.2.6. Evaluation of associated cardiovascular parameters in the zebrafish model***

In the present study, the dorsal aorta (DA) was the main vessel to be evaluated. All the images of vessel diameter were captured using a fluorescence microscope (Gen5 3.04 software, BioTek Instruments), and the mean value was analyzed and calculated using Image J software. Three measurements were obtained from each region and averaged to obtain a vessel diameter. Moreover, the arterial pulse (beats per minute), mean blood flow velocity ( $\mu\text{m/s}$ ), and blood flow (nL/s) were determined using a pre-recorded video at 120 frames per second (fps) for 1 min using the Gen5 3.04 software (BioTek Instruments). Then, the MicoZebraLab application from ViewPoint (Version 3. 4. 4, Lyon, France) was used to evaluate and calculate the cardiovascular parameters mentioned above. We have evaluated the associated cardiovascular parameters showed as bellowed (Figure 3-2).

#### ***3.2.6.1. Diameter of DA ( $\mu\text{m}$ )***

The estimated diameter is determined from the region of pixel activity. Three measurements were obtained from each region and averaged to obtain a vessel diameter.

#### ***3.2.6.2. Arterial pulse (beat per min)***

Arterial pulse is the heartbeat per min (bpm), and it is calculated from the average of time durations between successive velocity peaks. The value is saved each second the user specifies in the vessel diameter time bin (s).

#### ***3.2.6.3. Mean blood velocity ( $\mu\text{m/s}$ )***

The area of the targeted blood vessel was carefully selected, avoiding any of the neighboring capillaries. Having multiple vessels and/or capillaries would interfere with the assessment of the DA. The software detected the movement of erythrocytes within the selected tracking area

to measure the blood flow parameter. This value refreshes every frame and is calculated by considering the displacement in pixel of the blood cells and the scale specified in the general settings.

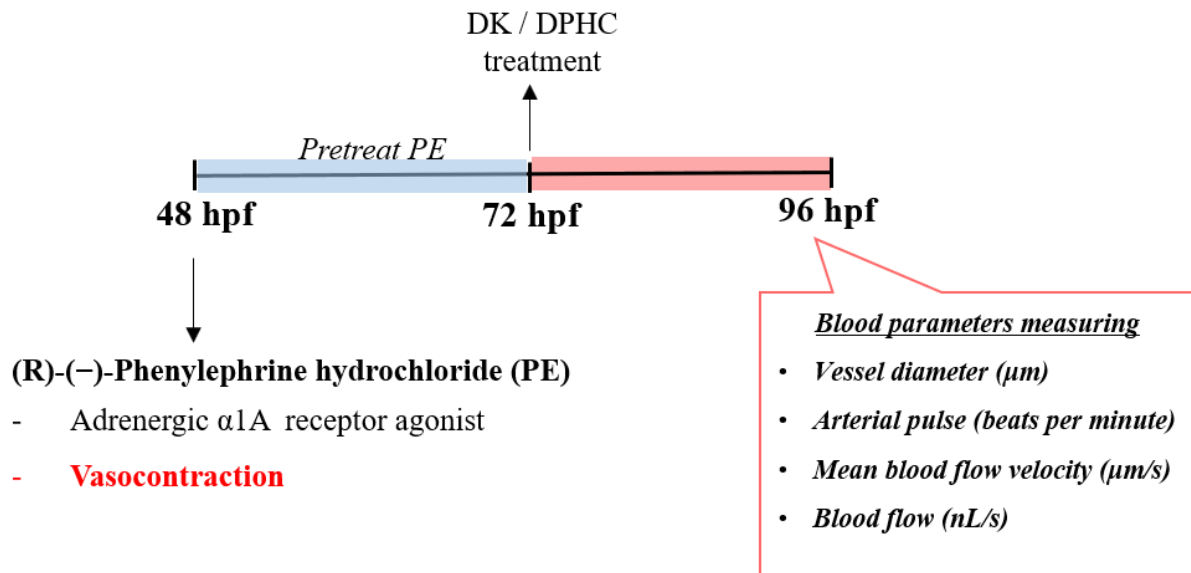


Figure 3- 2 The protocol of evaluation of associated cardiovascular parameters in the zebrafish model

### 3.2.7. Statistical analysis

All experiments were conducted in triplicates, and data are shown as mean  $\pm$  standard deviation. Statistical analysis was performed using the one-way analysis of variance (ANOVA) with Dunnett's post hoc test with the Prism 5.0 software (GraphPad Software, La Jolla, CA, USA). The following p-values were considered statistically significant, and they have been illustrated with asterisks in all figures: \*  $p < 0.05$ , \*\*  $p < 0.01$ , and \*\*\*  $p < 0.001$ .

### **3.3. Results**

#### ***3.3.1. Toxicity of DK and DPHC in zebrafish embryos***

The toxicity of different DK and DPHC concentrations was examined in zebrafish embryos. A survival rate exceeding 80% in the zebrafish experiment was considered nontoxic, which can be used for further investigations [84]. As shown in Figures 3-3A and 3B, the various DK and DPHC concentrations showed no toxicity in zebrafish embryos at 120 hpf.

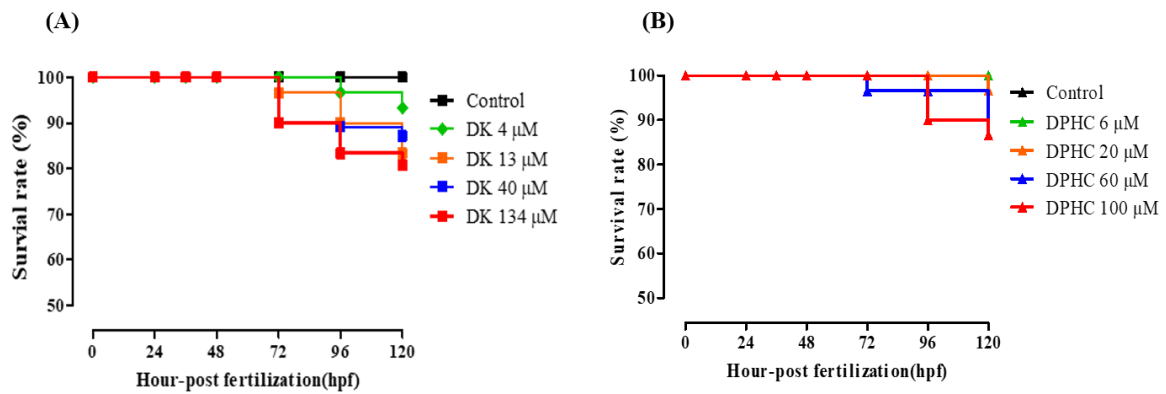


Figure 3- 3 The survival rate of the zebrafish embryos under-sample treatments. The test was based on the exposure of newly fertilized zebrafish eggs to different DK, DPHC, and PE concentrations for up to 120 h (n=15 per treatment, three replicates). Embryos were observed at each time point under the stereomicroscope (magnification used in the stereomicroscope for observations was 4x). (A) different concentrations of DK treatment (B) different concentrations of DPHC treatment. DK; diekol, DPHC: diphlorethohydroxycarmalol

### 3.3.2. *The vasoconstrictive zebrafish model set up by using vasoconstrictor*

In order to determine the vasodilatory effect of DK and DPHC, we first tested whether blood vessels constrict under the stimulator treatment and further optimized the best dosage for further experiments. The toxicity of PE was evaluated and showed in Figure 3-4A. The results indicated that except for the 50 $\mu$ M of PE, others' concentrations (10, 20, 30, and 40 $\mu$ M) were no toxic effects in the zebrafish model.

Moreover, Simple heart-rate measurement of zebrafish can provide predictive information regarding the interaction of chemicals with the components of the cardiac functional regulatory network [85]. According to the heartbeat results (Figure 3-4B), we observed that 10  $\mu$ M of PE would not affect the heartbeat rate; this is similar to the previous study [23]. Moreover, a significant increment was found from 20 to 50  $\mu$ M of PE treatments. However, heartbeat was considered as a cardiotoxicity factor. Thus, we have considered 20  $\mu$ M of PE maintained above 90% of survival rate after 120 hpf compared to 30  $\mu$ M (around 90%), 40, and 50  $\mu$ M (less than 80%). Based on these reasons, the 20  $\mu$ M of the  $\alpha$ 1-adrenoceptor agonists-PE was decided to be applied for further experiments.

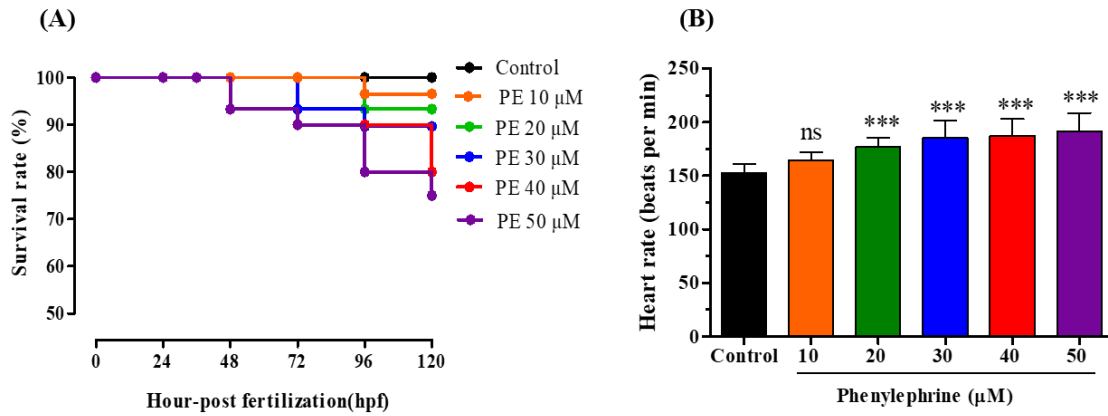
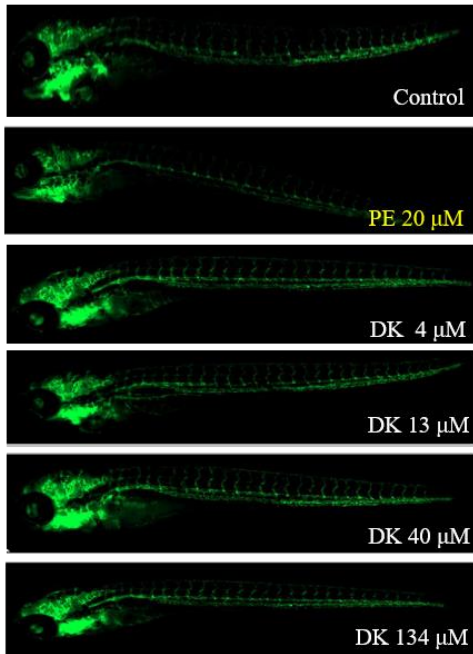


Figure 3- 4 The toxicity and heartbeat rate of the zebrafish larva under different concentrations of PE treatments. The test was based on the exposure of zebrafish larva to different concentrations of PE for 24 h (n=10 per treatment, three replicates). \*\*\*  $p < 0.001$  compared to the control group. Zebrafish larva was observed under the stereomicroscope (magnification used in the stereomicroscope for observations was 10 x). PE: Phenylephrine hydrochloride.

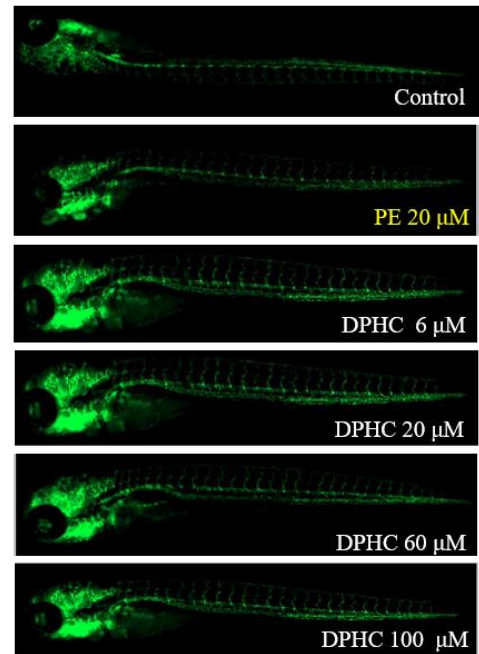
### 3.3.3. Assessment of whole-body fluorescence intensity in the *Tg(flk: EGFP)* transgenic zebrafish

To investigate whether DK and DPHC could exert a vasodilation effect *in vivo*, we used a *Tg(flk:eGFP)* transgenic zebrafish model. The vascular endothelial cells are fluorescently stained with the enhanced green fluorescent protein (eGFP). After the treatment of samples, changes in the vessel structure such as diameter and the fluorescence intensity can be observed easily using confocal microscopy (Figure 3-5A1 and 3-5B1). Zebrafish larvae were pre-treated with 20  $\mu\text{M}$  of PE at 48 dpf and incubated for 24 h. At the 72 dpf, different concentrations of DK (4, 13, 40, 134  $\mu\text{M}$ ) and DPHC (0, 6, 20, 60, and 100  $\mu\text{M}$ ) were treated and incubated for another 24 h. The whole-body fluorescence intensity was measured at 96 hpf (Figure 3-5A1 and 3-5B1). Treatment with 20  $\mu\text{M}$  of PE significantly decreased the fluorescence intensity in the whole body of zebrafish compared to control larvae. Moreover, we observed that the fluorescence intensity of DK treatment groups (4, 13, 40, and 134  $\mu\text{M}$ ) was significantly increased compared to the PE group, which is shown in Figure 3-5A2. However, the significant increment of fluorescence intensity compared to the PE group was only found under the treatment of 60 and 100  $\mu\text{M}$  of DPHC shown in Figure 3-5B2.

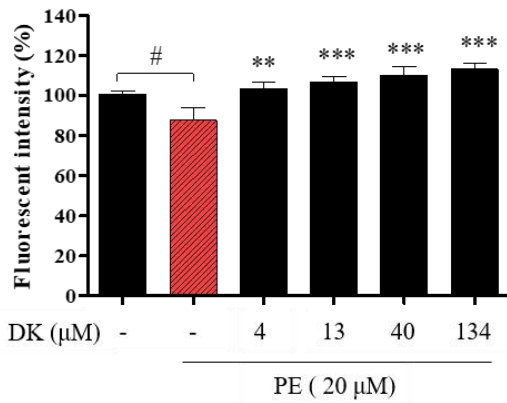
(A1)



(B1)



(A2)



(B2)

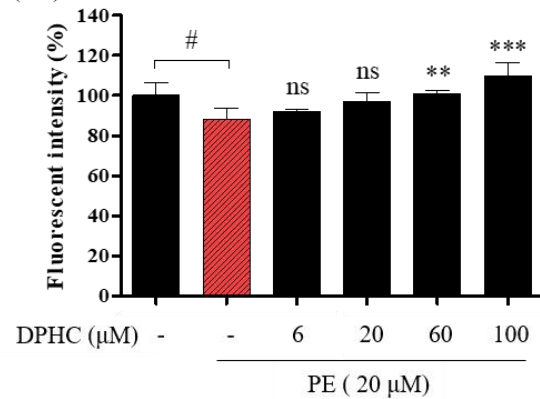


Figure 3- 5 DK and DPHC induce vasodilation in the whole-body vessel in a *Tg(flk: EGFP)* transgenic zebrafish model. (A1) and (B1) Representative images of the *Tg(flk: EGFP)* transgenic zebrafish larva's whole body under the DK and DPHC treatments; all images were captured using a fluorescence microscope (4 $\times$ ). (A2) and (B2) Quantification of the whole-body fluorescence intensity under the DK and DPHC treatments, respectively. Each column and bar represent the mean  $\pm$  standard deviation (S.D.),  $n = 8$  per group. #  $p < 0.05$ , ##  $p < 0.01$ , ###  $p < 0.001$ , significantly different between PE group and control group. \*  $p < 0.05$ , \*\*  $p < 0.01$ , \*\*\*  $p < 0.001$ , significantly different between the PE group and sample treatment groups; ns: not significant; DK; dikeol, DPHC: diphlorethohydroxycarmalol. PE: Phenylephrine hydrochloride.

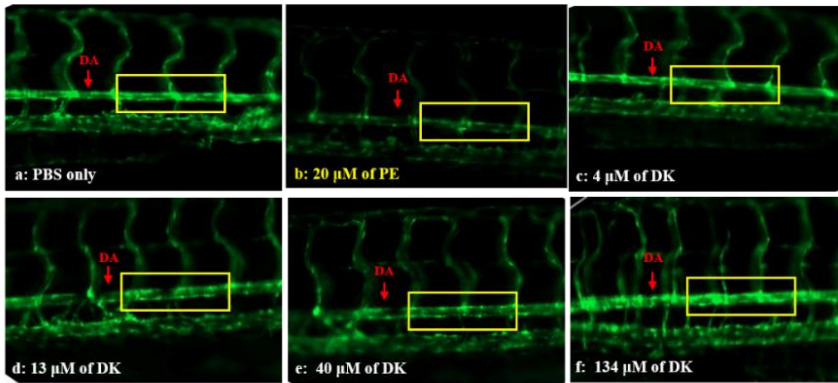
### ***3.3.4. Evaluation of associated cardiovascular parameters in the zebrafish model***

#### ***3.3.4.1. Dorsal aorta diameter ( $\mu\text{m}$ )***

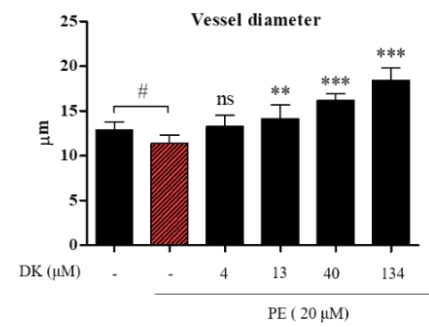
The dorsal aorta (DA) is the major trunk axial artery and is one of the first vessels to assemble in the early developmental stages in all vertebrates. A previous study demonstrated that the DA of the zebrafish acquires a vascular smooth muscle cell-containing vascular wall similar to that found in other vertebrates [86]. Therefore, evaluation of the DA diameter can be considered direct evidence for vasodilation.

The images of Figure 3-6 (A1) and 6 (B1) have represented the vessel activity of transgenic zebrafish under DK or DPHC treatments, respectively. The yellow box in each image has represented the area which used for evaluation. We provided direct evidence by measuring the DA diameter to confirm the transgenic model's vasodilatory effects induced by DK and DPHC treatments. As shown in Figure 3-6 (A2), the diameter of the PE treatment group showed a significantly decreased compared to the control group (\*  $p < 0.05$ ). Except for 4 and 13  $\mu\text{M}$  DK, the diameter of DA in DK treatment groups (40 and 134  $\mu\text{M}$ ) was significantly increased when compared with the PE group. On the other hand, the DA diameter significantly increased with DPHC treatment (60 and 100  $\mu\text{M}$ ) compared to the PE group, which showed in Figure 3-6 (B2). Thus, we confirmed that pre-treated with PE would decrease the diameter of DA, and the treatments of DK (40 and 134  $\mu\text{M}$ ) and DPHC (60 and 100  $\mu\text{M}$ ) were able to enlarge the vessel diameter.

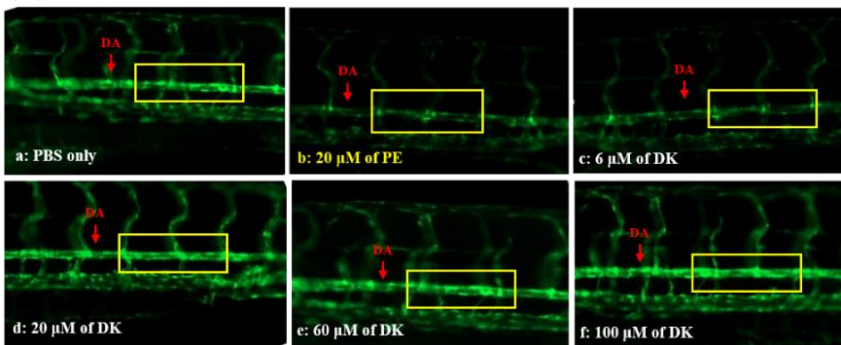
(A1)



(A2)



(B1)



(B2)

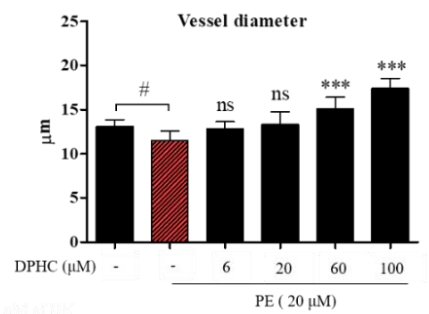


Figure 3- 6 DK and DPHC promote the vasodilation by enlarging the vessel diameter in a *Tg(flk: EGFP)* transgenic zebrafish model. (A1) and (B1) Images of the vessel were captured using a fluorescence microscope (20×). (a–f) were represented the change of diameter under sample treatments. (A2) and (B2) Measurement of the DA diameter. Each column and bar represent the mean  $\pm$  standard deviation (S.D.),  $n = 8$  per group #  $p < 0.05$ , ##  $p < 0.01$ , ###  $p < 0.001$ , significantly different between PE group and control group. \*  $p < 0.05$ , \*\*\*  $p < 0.001$ , significantly different between the PE group and sample treatment groups. DK; diekol, DPHC: diphlorethohydroxycarmalol. PE: Phenylephrine hydrochloride.

### 3.3.4.2. Arterial pulse

Other cardiovascular parameters were evaluated by ZebraLab software, as shown in Figure 3-7. The arterial pulse results were shown in Figures 3-8A and 8B. According to our results, the 20  $\mu\text{M}$  of PE successfully induced the vasoconstrictive behaviors in the DA of zebrafish via increasing the arterial pulse, blood flow, and mean blood flow velocity the 4 dpf. Gradually decreased were observed under DK and DPHC treatments.

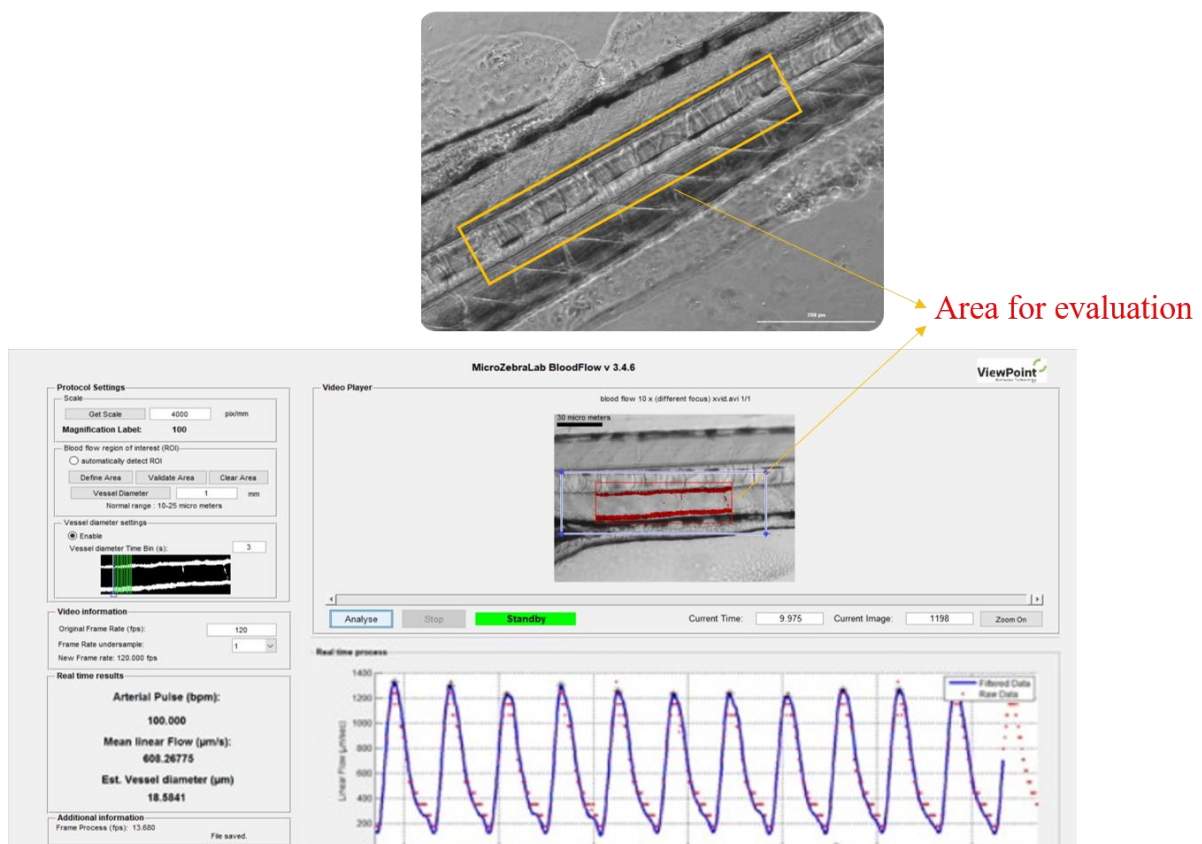


Figure 3- 7 The image was demonstrated by the MicoZebraLab software. The MicoZebraLab application from ViewPoint (Version 3. 4. 4, Lyon, France) was used to evaluate and calculate the cardiovascular parameters.

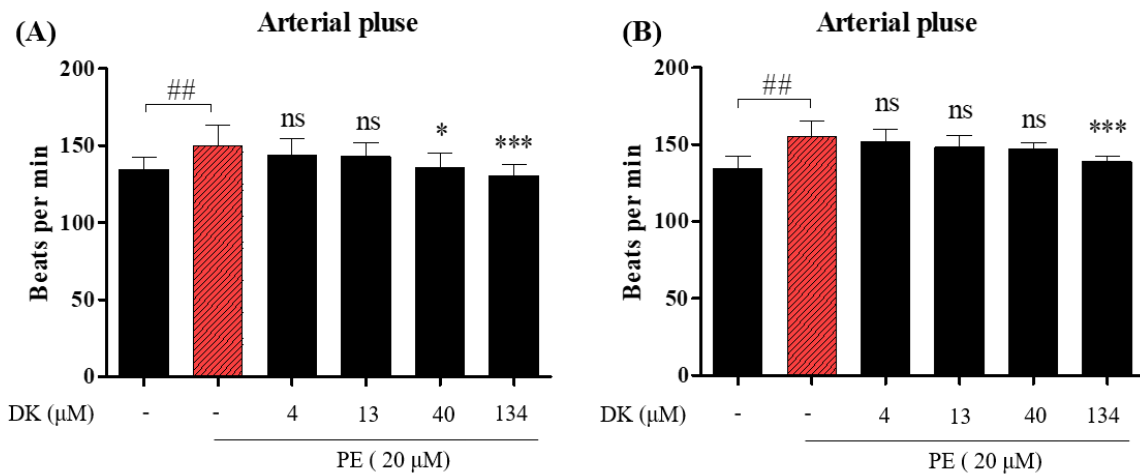


Figure 3- 8 Measurements of arterial pulse under the treatments of different concentrations of DK and DPHC. The change of arterial pulse (bear per min) under DK (A) and DPHC (B) treatments. Each column and bar represent the mean  $\pm$  standard deviation (S.D.),  $n = 8$  per group. \*  $p < 0.05$ , \*\*\*  $p < 0.001$ , significant difference compared to the control group; #  $p < 0.05$ , ##  $p < 0.01$ , ###  $p < 0.001$ , significant different compared to the PE group. DK; diekol, DPHC: diphlorethohydroxycarmalol. PE: Phenylephrine hydrochloride.

#### ***3.3.4.3. Blood flow and mean blood flow velocity***

The results of blood flow were shown in Figures 3-9A and 9B. Also, the results of mean blood flow velocity were demonstrated in Figures 3-9C and 9D. According to our results, the 20  $\mu\text{M}$  of PE successfully induced the vasoconstrictive behaviors in the DA of zebrafish via increasing the blood flow, and mean blood flow velocity the 4 dpf. A significantly decreasing trend were noticed at 13, 40, and 134  $\mu\text{M}$  of DK treatments. On the other hand, the effective dosages to regulate the blood flow and mean flow velocity were found at 20, 60, and 100  $\mu\text{M}$  of DPHC treatments.

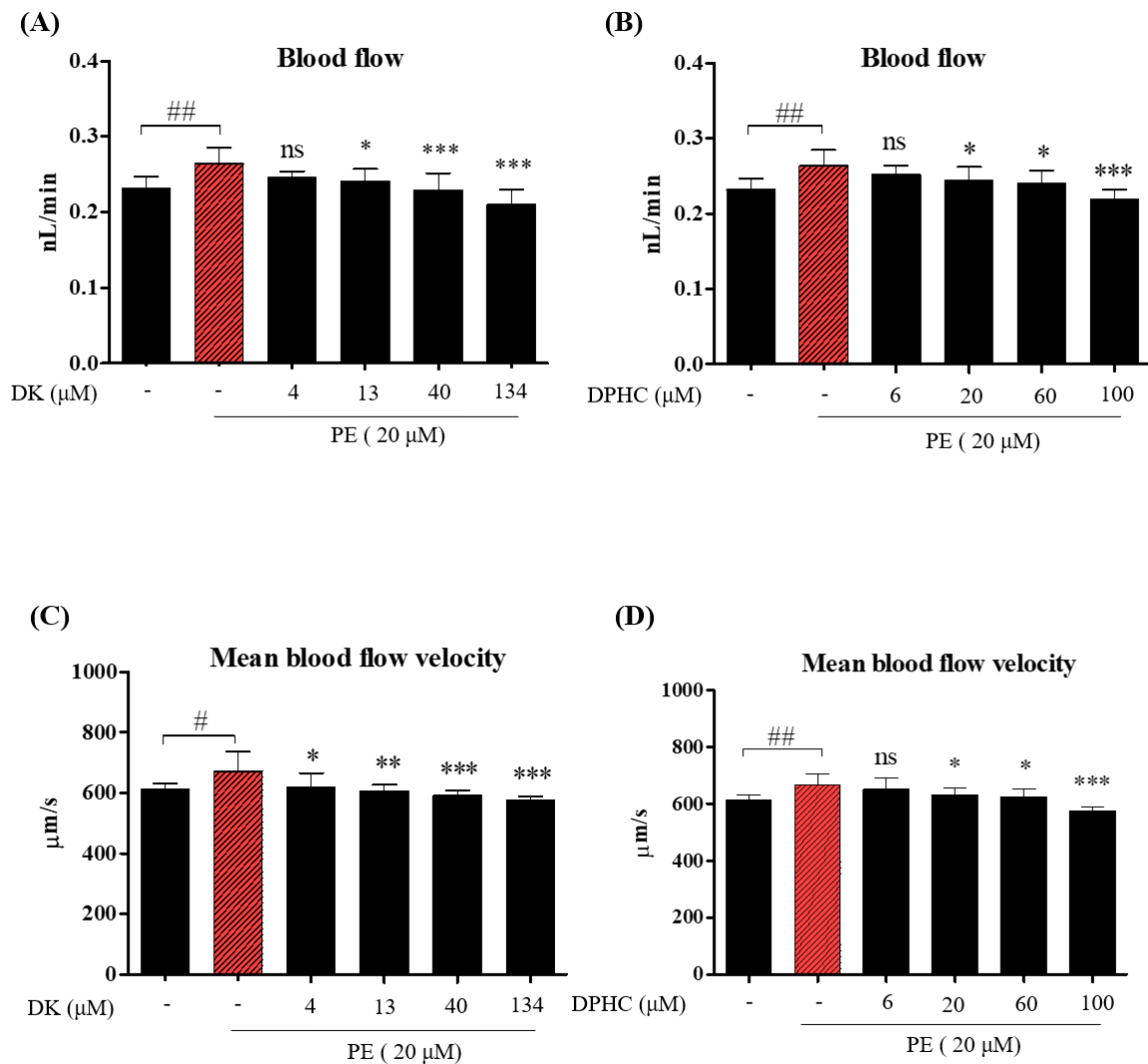


Figure 3- 9 Measurements of blood flow and mean blood velocity under the treatments of different concentrations of DK and DPHC. The change of blood flow (nL/min) under (A) DK and (B) DPHC treatments. The change of mean blood velocity ( $\mu\text{M/s}$ ) under (C) DK and (D) DPHC treatments. Each column and bar represent the mean  $\pm$  standard deviation (S.D.),  $n = 8$  per group. #  $p < 0.05$ , ##  $p < 0.01$ , ###  $p < 0.001$ , significantly different between PE group and control group. \*  $p < 0.05$ , \*\*\*  $p < 0.001$ , significantly different between the PE group and sample treatment groups. DK; diekol, DPHC: diphloretohydroxycarmalol. PE: Phenylephrine hydrochloride.

### 3.4. Discussion

Over the last decade, the zebrafish (*Danio rerio*) has emerged as a model organism for cardiovascular research. Embryos and larvae of zebrafish are transparent during a large portion of the development. This characteristic makes them excellent models for studies of early embryonic functions of the cardiovascular system [87]. For instance, the heart and vasculature can easily be observed with a microscope without any physical disruption to the animal [88]. Many of the regulatory peptides involved in cardiovascular regulation in adult animals are found in endocrine cells in embryonic tissue, which is interesting [89]. As a result, these peptides are likely to play a role in controlling processes. Several vasoactive products produced by endothelial cells, including prostacyclin, NO, ATP, hydrogen sulfate, and endothelin, contribute significantly to vascular tone in adult animals [90]. These influences may play an important role in vascular regulation in embryos and larvae since the endothelium is present in all vessels as soon as they mature. It has been reported that interactions between endothelial cells (EC) and vascular smooth muscle cells (VSMC) are thought to strengthen the maturing vascular wall to increases flow and shear stress while helping to regulate vessel contractility and tone in zebrafish [91]. The endothelium plays a recognized role in regulating vascular resistance and blood flow distribution by producing vasoactive mediators and diffusion between the vascular cavity and surrounding tissues [92].

In the G protein-coupled receptors (GPCR), adrenergic receptors (ARs) mediate the functional effects of catecholamine, like epinephrine and norepinephrine [93]. There are nine different subtypes of ARs were found, such as three  $\beta$  ( $\beta_1$ ,  $\beta_2$ ,  $\beta_3$ ), three  $\alpha_1$  ( $\alpha_{1a}$ ,  $\alpha_{1b}$ , and  $\alpha_{1d}$ ), and three  $\alpha_2$  ( $\alpha_{2A}$ ,  $\alpha_{2B}$ , and  $\alpha_{2C}$ ) receptor subtypes [94]. Among them, the  $\alpha_{1A}$ -adrenoceptor was most closely related to the blood vessel and vessel contraction. It has become increasingly evident that the variety of functional effects mediated by the  $\alpha_1$ -ARs in different organs must imply the activation of multiple signaling pathways beyond the activation of PLC

via Gq/11, and further releases  $[Ca^{2+}]$  from intracellular stores and activates protein kinase C (PKC) [95]. The release  $[Ca^{2+}]$  from intracellular stores and activates PKC resulted in stimulating SMC contraction [96]. Additionally, it has been indicated that PE predominates in resistance arteries, where its overexpression results in an increased sensitivity to vasoconstriction [97]. The overexpression of PE was particularly relevant in the pathogenesis of hypertension [98]. Thus, take the “vasocontraction property” of PE, we have used the PE, a classic  $\alpha 1A$ -adrenoceptors, to set up a vasocontraction model. *Beekhuijzen et al.* have indicated that drug exposure usually begins around 5 hpf, corresponding to late blastula/early gastrula stages, and ends at 96 hpf, where most organs are fully developed [99]. Therefore. We have measured all the parameters at 96 dpf to exclude the unstable factors (ie. immature vessel development). Our results indicated that the heart beat rate would significantly increase and follow a dose-dependent manner under the treatments of different concentrations of PE. However, at 10  $\mu M$  of PE are unable to raise the heartbeat rate, which is the same as the study performed by *Nabila Bahrami and Sarah J. Childs* [23]. The significant increments were observed at 20 to 50  $\mu M$  of PE.

Nevertheless, the heartbeat rate was considered as the cardiotoxicity factor in other studies [100]. Thus, we considered the survival rate at the same time, as the results, only 20 and 30  $\mu M$  of PE showed above 80% survival rate at 120 hpf. Based on these results, we decided to use 20  $\mu M$  of PE as the main concentration. Furthermore, this concentration can effectively induce the change of the cardiovascular parameters in the present study. Further, the vasodilation effect of DK and DPHC was confirmed via measuring the associated cardiovascular parameters such as vessel diameter ( $\mu M$ ), arterial pulse (beats per min), blood flow (nL/s), and linear velocity ( $\mu M/s$ ). As expected, compared with the PE group, the treatment of DK (13, 40, and 134  $\mu M$ ) and DPHC (60 and 100  $\mu M$ ) significantly increased the DA diameter. Determination of cell speed is important for evaluating flow rate for the vessels

and estimating the shear stress levels acting on the endothelial cells lining the vessel wall (i.e., shear stress is the frictional force of the endothelial cells from the flowing blood). Levels of red blood cell (RBC) velocities are about 300  $\mu\text{m}/\text{sec}$  to 750  $\mu\text{m}/\text{sec}$  for 2-5 dpf embryos [101]. Indeed, the average mean blood flow velocity was approximately 600  $\mu\text{m}/\text{sec}$  in the control group at 4 dpf. Moreover, the PE treatment stimulated the higher mean blood flow velocity (about 700  $\mu\text{m}/\text{sec}$ ).

On the other hand, we observed that blood flow was significantly decreased in DK (13, 40, and 134  $\mu\text{M}$ ) and DPHC (20, 60, and 100  $\mu\text{M}$ ). Reportedly, the velocity of blood flow is inversely proportional to the total cross-sectional area of blood vessels. As the total cross-sectional area of the vessel increases, the flow velocity decreases [102]. Sum up the *in vivo* data. We suggested that the appropriate DK and DPHC have a vasodilation effect via increasing the diameter and decreasing the blood flow rate in the zebrafish model.

### **3.5. Conclusions**

Our results demonstrated that DK and DPHC treatment could promote vasodilation by increasing the DA diameter, further regulating blood flow velocity in the zebrafish model. The results strongly suggest that the DK and DPHC possess superior vasodilatory effects and can be developed as suitable therapeutic agents.

## **Acknolegements**

I want to express my gratitude to my supervisor Professor Jeon You-Jin, Head, Marine Bio-Resource Technology Lab, Department of Marine Life Science, Jeju National University. His expertise was vital in forming the research, and his consistent guidance steered me in the right direction. I am grateful to Professor Jeon for allowing me to conduct my work and the opportunity created for me at his laboratory.

Many thanks to Dr. BoMi Ryu for guiding me to arrange my experiments and helping me to be successful in my research throughout the whole period.

Then, I would like to thank all of our lab members who helped me perform many different types of experiments in my research studies and complete my thesis works.

Also, I must express my profound gratitude to my family for providing me with unfailing support throughout my years of study. This would not have been accomplished without them.

At last, I would like to thank all those I have not mentioned above but who helped me during my study period to succeed in my studies at Jeju National University.

## References

1. Mordi, I., et al., *Endothelial dysfunction in human essential hypertension*. Journal of Hypertension, 2016. **34**(8): p. 1464-1472.
2. Konukoglu, D. and H. Uzun, *Endothelial Dysfunction and Hypertension*, in *Hypertension: from basic research to clinical practice*, M.S. Islam, Editor. 2017, Springer International Publishing: Cham. p. 511-540.
3. Saucedo, A.E.Q., et al., *Biological Actions of Phenolic Compounds*. Fruit and Vegetable Phytochemicals: Chemistry and Human Health, 2 Volumes, 2017: p. 125.
4. Daiber, A., et al., *New therapeutic implications of endothelial nitric oxide synthase (eNOS) function/dysfunction in cardiovascular disease*. International journal of molecular sciences, 2019. **20**(1): p. 187.
5. Gutierrez, J., et al., *Cardiovascular disease risk factors: Hypertension, diabetes mellitus and obesity among Tabuk Citizens in Saudi Arabia*. The open cardiovascular medicine journal, 2018. **12**: p. 41.
6. Touyz, R.M., et al., *Vascular smooth muscle contraction in hypertension*. Cardiovascular Research, 2018. **114**(4): p. 529-539.
7. Giles, T.D., et al., *Impaired Vasodilation in the Pathogenesis of Hypertension: Focus on Nitric Oxide, Endothelial-Derived Hyperpolarizing Factors, and Prostaglandins*. The Journal of Clinical Hypertension, 2012. **14**(4): p. 198-205.
8. Son, M., et al., *Ecklonia Cava Extract Attenuates Endothelial Cell Dysfunction by Modulation of Inflammation and Brown Adipocyte Function in Perivascular Fat Tissue*. Nutrients, 2019. **11**(11): p. 2795.
9. Choi, Y.-J., et al., *Antioxidant Activity of Brown Seaweed, Ecklonia maxima, Collected from South Africa*. Journal of Marine Bioscience and Biotechnology, 2019. **11**(1): p. 29-35.
10. Kang, N., et al., *Structural Evidence for Antihypertensive Effect of an Antioxidant Peptide Purified from the Edible Marine Animal Styela clava*. Journal of Medicinal Food, 2020. **23**(2): p. 132-138.
11. Son, M., et al., *Pyrogallol-Phloroglucinol-6,6'-Bieckol from Ecklonia cava Improved Blood Circulation in Diet-Induced Obese and Diet-Induced Hypertension Mouse Models*. Mar Drugs, 2019. **17**(5).
12. Oh, S., et al., *Protective effect of pyrogallol-phloroglucinol-6, 6-bieckol from Ecklonia cava on monocyte-associated vascular dysfunction*. Marine drugs, 2018. **16**(11): p. 441.
13. Wijesinghe, W.A.J.P., S.-C. Ko, and Y.-J. Jeon, *Effect of phlorotannins isolated from Ecklonia cava on angiotensin I-converting enzyme (ACE) inhibitory activity*. Nutr Res Pract, 2011. **5**(2): p. 93-100.
14. Lu, Y.A., et al., *Diphlorethohydroxycarmalol Isolated from Ishige okamurae Exerts Vasodilatory Effects via Calcium Signaling and PI3K/Akt/eNOS Pathway*. International Journal of Molecular Sciences, 2021. **22**(4): p. 1610.
15. Szabo, C., *Hydrogen sulfide, an enhancer of vascular nitric oxide signaling: mechanisms and implications*. Am J Physiol Cell Physiol, 2017. **312**(1): p. C3-C15.
16. Gheibi, S., et al., *Regulation of vascular tone homeostasis by NO and H2S: Implications in hypertension*. Biochemical Pharmacology, 2018. **149**: p. 42-59.
17. Lin, Q., et al., *Inositol 1, 4, 5-Trisphosphate Receptors in Endothelial Cells Play an Essential Role in Vasodilation and Blood Pressure Regulation*. Journal of the American Heart Association, 2019. **8**(4): p. e011704.
18. de Oliveira, T.S., et al., *Activation of PI3K/Akt pathway mediated by estrogen receptors accounts for estrone-induced vascular activation of cGMP signaling*. Vascul Pharmacol, 2018. **110**: p. 42-48.

19. Zhao, Y., P.M. Vanhoutte, and S.W.S. Leung, *Vascular nitric oxide: Beyond eNOS*. Journal of Pharmacological Sciences, 2015. **129**(2): p. 83-94.
20. Fulton, D., et al., *Regulation of endothelium-derived nitric oxide production by the protein kinase Akt*. Nature, 1999. **399**(6736): p. 597-601.
21. Younis, W., et al., *Endothelium-independent vasorelaxant effect of Asphodelus tenuifolius Cav. via inhibition of myosin light chain kinase activity in the porcine coronary artery*. Journal of Ethnopharmacology, 2021. **269**: p. 113693.
22. Huang, H., et al., *High-throughput screening for bioactive molecules using primary cell culture of transgenic zebrafish embryos*. Cell Rep, 2012. **2**(3): p. 695-704.
23. Bahrami, N. and S.J. Childs, *Development of vascular regulation in the zebrafish embryo*. Development, 2020. **147**(10): p. dev183061.
24. Dalal, P.J., W.A. Muller, and D.P. Sullivan, *Endothelial Cell Calcium Signaling during Barrier Function and Inflammation*. The American Journal of Pathology, 2020. **190**(3): p. 535-542.
25. Wijesinghe, W., S.-C. Ko, and Y.-J. Jeon, *Effect of phlorotannins isolated from Ecklonia cava on angiotensin I-converting enzyme (ACE) inhibitory activity*. Nutrition research and practice, 2011. **5**(2): p. 93-100.
26. Kim, E.-A., et al., *A marine algal polyphenol, dieckol, attenuates blood glucose levels by Akt pathway in alloxan induced hyperglycemia zebrafish model*. RSC advances, 2016. **6**(82): p. 78570-78575.
27. Xia, H., et al., *Endothelial Cell Cystathionine  $\beta$ -Lyase Expression Level Modulates Exercise Capacity, Vascular Function, and Myocardial Ischemia Reperfusion Injury*. 2020. **9**(19): p. e017544.
28. Hgel, H.M., et al., *Polyphenol protection and treatment of hypertension*. Phytomedicine, 2016. **23**(2): p. 220-231.
29. Khurana, S., et al., *Polyphenols: benefits to the cardiovascular system in health and in aging*. Nutrients, 2013. **5**(10): p. 3779-3827.
30. Dudzinski, D.M. and T. Michel, *Life history of eNOS: Partners and pathways*. Cardiovascular Research, 2007. **75**(2): p. 247-260.
31. Long, Y., et al., *ATP2B1 gene Silencing Increases Insulin Sensitivity through Facilitating Akt Activation via the Ca(2+)/calmodulin Signaling Pathway and Ca(2+)-associated eNOS Activation in Endothelial Cells*. International journal of biological sciences, 2017. **13**(9): p. 1203-1212.
32. Guizoni, D.M., et al., *Modulation of endothelium-derived nitric oxide production and activity by taurine and taurine-conjugated bile acids*. Nitric Oxide, 2020. **94**: p. 48-53.
33. Kida, T., et al., *Bile Acid Receptor TGR5 Agonism Induces NO Production and Reduces Monocyte Adhesion in Vascular Endothelial Cells*. Arteriosclerosis, Thrombosis, and Vascular Biology, 2013. **33**(7): p. 1663-1669.
34. Nakajima, T., et al., *Bile acids increase intracellular Ca<sup>2+</sup> concentration and nitric oxide production in vascular endothelial cells*. British Journal of Pharmacology, 2000. **130**(7): p. 1457-1467.
35. Martinotti, S., et al., *Endothelial Response Boosted by Platelet Lysate: The Involvement of Calcium Toolkit*. International Journal of Molecular Sciences, 2020. **21**(3): p. 808.
36. Bagur, R. and G. Hajnczyk, *Intracellular Ca<sup>2+</sup> Sensing: Its Role in Calcium Homeostasis and Signaling*. Molecular Cell, 2017. **66**(6): p. 780-788.
37. Martinez-Archundia, M., et al., *Molecular modeling of the M3 acetylcholine muscarinic receptor and its binding site*. J Biomed Biotechnol, 2012. **2012**: p. 789741.
38. Touyz, R.M., et al., *Vascular smooth muscle contraction in hypertension*. Cardiovasc Res, 2018. **114**(4): p. 529-539.
39. Ren, L.M., T. Nakane, and S. Chiba, *Muscarinic receptor subtypes mediating vasodilation and vasoconstriction in isolated, perfused simian coronary arteries*. Journal of cardiovascular pharmacology, 1993. **22**(6): p. 841-846.

40. Brown, P.T., P. Herbert, and R.I. Woodruff, *Vitellogenesis in Oncopeltus fasciatus: PLC/IP3, DAG/PK-C pathway triggered by CaM*. Journal of insect physiology, 2010. **56**(9): p. 1300-1305.
41. Zhang, W., et al., *CaSR participates in the regulation of vascular tension in the mesentery of hypertensive rats via the PLC-IP3/AC-V/cAMP/RAS pathway*. Molecular Medicine Reports, 2019. **20**(5): p. 4433-4448.
42. Pandey, A.K., et al., *Mechanisms of VEGF (vascular endothelial growth factor) inhibitor-associated hypertension and vascular disease*. Hypertension, 2018. **71**(2): p. e1-e8.
43. Tao, B.B., et al., *VEGFR2 functions as an H2S-targeting receptor protein kinase with its novel Cys1045-Cys1024 disulfide bond serving as a specific molecular switch for hydrogen sulfide actions in vascular endothelial cells*. Antioxid Redox Signal, 2013. **19**(5): p. 448-64.
44. Bencze, M., *The role of calcium influx and calcium sensitization in contraction of isolated arteries of normotensive and hypertensive rat*. 2017.
45. Greif, D.M., D.B. Sacks, and T. Michel, *Calmodulin phosphorylation and modulation of endothelial nitric oxide synthase catalysis*. Proceedings of the National Academy of Sciences of the United States of America, 2004. **101**(5): p. 1165-1170.
46. Takahashi, S. and M.E. Mendelsohn, *Calmodulin-dependent and -independent Activation of Endothelial Nitric-oxide Synthase by Heat Shock Protein 90 \**. Journal of Biological Chemistry, 2003. **278**(11): p. 9339-9344.
47. Leloup, A.J., et al., *Basal activity of voltage-gated Ca<sup>2+</sup> channels controls the IP3-mediated contraction by  $\alpha$ 1-adrenoceptor stimulation of mouse aorta segments*. European Journal of Pharmacology, 2015. **760**: p. 163-171.
48. Brozovich, F.V., et al., *Mechanisms of Vascular Smooth Muscle Contraction and the Basis for Pharmacologic Treatment of Smooth Muscle Disorders*. Pharmacol Rev, 2016. **68**(2): p. 476-532.
49. Garland, C.J., et al., *Voltage-dependent Ca<sup>2+</sup> entry into smooth muscle during contraction promotes endothelium-mediated feedback vasodilation in arterioles*. Science Signaling, 2017. **10**(486): p. eaal3806.
50. Wang, M.-J., W.-J. Cai, and Y.-C. Zhu, *Hydrogen sulphide in cardiovascular system: a cascade from interaction between sulphur atoms and signalling molecules*. Life sciences, 2016. **153**: p. 188-197.
51. Kimura, H., *Hydrogen sulfide and polysulfides as biological mediators*. Molecules, 2014. **19**(10): p. 16146-16157.
52. Lu, Y.-A., et al., *Ecklonia cava Extract and Its Derivative Dieckol Promote Vasodilation by Modulating Calcium Signaling and PI3K/AKT/eNOS Pathway in In Vitro and In Vivo Models*. Biomedicines, 2021. **9**(4): p. 438.
53. Nava, E. and S. Llorens, *The paracrine control of vascular motion. A historical perspective*. Pharmacological Research, 2016. **113**: p. 125-145.
54. Son, M., et al., *Pyrogallol-Phloroglucinol-6 6-Bieckol on Attenuates High-Fat Diet-Induced Hypertension by Modulating Endothelial-to-Mesenchymal Transition in the Aorta of Mice*. Oxid Med Cell Longev, 2021. **2021**: p. 8869085.
55. Wang, Y., et al., *NO-induced vasodilation correlates directly with BP in smooth muscle-Na/Ca exchanger-1-engineered mice: elevated BP does not attenuate endothelial function*. American Journal of Physiology-Heart and Circulatory Physiology. **0**(0): p. null.
56. Xiang, R., et al., *VSMC-Specific Deletion of FAM3A Attenuated Ang II-Promoted Hypertension and Cardiovascular Hypertrophy*. Circulation Research, 2020. **126**(12): p. 1746-1759.
57. Gao, Y., T. Chen, and J.U. Raj, *Endothelial and Smooth Muscle Cell Interactions in the Pathobiology of Pulmonary Hypertension*. Am J Respir Cell Mol Biol, 2016. **54**(4): p. 451-60.
58. Gao, Y., et al., *Role of Rho kinases in PKG-mediated relaxation of pulmonary arteries of fetal lambs exposed to chronic high altitude hypoxia*. American Journal of Physiology-Lung Cellular and Molecular Physiology, 2007. **292**(3): p. L678-L684.

59. Gao, Y., et al., *Preservation of cGMP-induced relaxation of pulmonary veins of fetal lambs exposed to chronic high altitude hypoxia: role of PKG and Rho kinase*. American Journal of Physiology-Lung Cellular and Molecular Physiology, 2008. **295**(5): p. L889-L896.
60. Gouloupoulou, S. and R.C. Webb, *Symphony of vascular contraction: how smooth muscle cells lose harmony to signal increased vascular resistance in hypertension*. Hypertension, 2014. **63**(3): p. e33-9.
61. Crosswhite, P. and Z. Sun, *Molecular mechanisms of pulmonary arterial remodeling*. Molecular medicine, 2014. **20**(1): p. 191-201.
62. Loomis, E.D., et al., *Endothelin mediates superoxide production and vasoconstriction through activation of NADPH oxidase and uncoupled nitric-oxide synthase in the rat aorta*. Journal of Pharmacology and Experimental Therapeutics, 2005. **315**(3): p. 1058-1064.
63. Crabtree, M.J., et al., *Ratio of 5, 6, 7, 8-tetrahydrobiopterin to 7, 8-dihydrobiopterin in endothelial cells determines glucose-elicited changes in NO vs. superoxide production by eNOS*. American Journal of Physiology-Heart and Circulatory Physiology, 2008. **294**(4): p. H1530-H1540.
64. Bailey, D.M., et al., *High-altitude pulmonary hypertension is associated with a free radical-mediated reduction in pulmonary nitric oxide bioavailability*. The Journal of physiology, 2010. **588**(23): p. 4837-4847.
65. Murthy, K.S., *Contractile agonists attenuate cGMP levels by stimulating phosphorylation of cGMP-specific PDE5; an effect mediated by RhoA/PKC-dependent inhibition of protein phosphatase 1*. British journal of pharmacology, 2008. **153**(6): p. 1214-1224.
66. Levorson, E.J., et al., *Direct and indirect co-culture of chondrocytes and mesenchymal stem cells for the generation of polymer/extracellular matrix hybrid constructs*. Acta biomaterialia, 2014. **10**(5): p. 1824-1835.
67. Venter, C. and C. Niesler, *A triple co-culture method to investigate the effect of macrophages and fibroblasts on myoblast proliferation and migration*. BioTechniques, 2018. **64**(2): p. 52-58.
68. Herzog, D.P.E., et al., *Cell Communication in a Coculture System Consisting of Outgrowth Endothelial Cells and Primary Osteoblasts*. BioMed Research International, 2014. **2014**: p. 320123.
69. Buchwalow, I.B., et al., *An in situ evidence for autocrine function of NO in the vasculature*. Nitric Oxide, 2004. **10**(4): p. 203-12.
70. Buchwalow, I.B., et al., *Vascular smooth muscle and nitric oxide synthase*. Faseb j, 2002. **16**(6): p. 500-8.
71. Walia, M., et al., *Effects of hydrogen peroxide on pig coronary artery endothelium*. European journal of pharmacology, 2000. **400**(2-3): p. 249-253.
72. Linas, S.L. and J.E. Repine, *Endothelial cells protect vascular smooth muscle cells from H<sub>2</sub>O<sub>2</sub> attack*. American Journal of Physiology-Renal Physiology, 1997. **272**(6): p. F767-F773.
73. Truskey, G.A., *Endothelial Cell Vascular Smooth Muscle Cell Co-Culture Assay For High Throughput Screening Assays For Discovery of Anti-Angiogenesis Agents and Other Therapeutic Molecules*. Int J High Throughput Screen, 2010. **2010**(1): p. 171-181.
74. Pogoda, K. and P. Kameritsch, *Molecular regulation of myoendothelial gap junctions*. Current Opinion in Pharmacology, 2019. **45**: p. 16-22.
75. Fleming, I., *Myoendothelial Gap Junctions*. Circulation Research, 2000. **86**(3): p. 249-250.
76. Isakson, B.E., *Localized expression of an Ins (1, 4, 5) P<sub>3</sub> receptor at the myoendothelial junction selectively regulates heterocellular Ca<sup>2+</sup> communication*. Journal of cell science, 2008. **121**(21): p. 3664-3673.
77. Wei, R., et al., *Vasoconstrictor stimulus determines the functional contribution of myoendothelial feedback to mesenteric arterial tone*. The Journal of physiology, 2018. **596**(7): p. 1181-1197.
78. Pogoda, K., et al., *NO, via its target Cx37, modulates calcium signal propagation selectively at myoendothelial gap junctions*. Cell communication and signaling : CCS, 2014. **12**: p. 33-33.

79. Oka, T., et al., *Diet-induced obesity in zebrafish shares common pathophysiological pathways with mammalian obesity*. BMC physiology, 2010. **10**(1): p. 1-13.
80. Heckler, K. and J. Kroll, *Zebrafish as a model for the study of microvascular complications of diabetes and their mechanisms*. International journal of molecular sciences, 2017. **18**(9): p. 2002.
81. Benchoula, K., et al., *The promise of zebrafish as a model of metabolic syndrome*. Experimental animals, 2019. **68**(4): p. 407-416.
82. Zhao, H., et al., *Lanthanide Hydroxide Nanoparticles Induce Angiogenesis via ROS-Sensitive Signaling*. Small, 2016. **12**(32): p. 4404-4411.
83. Zhang, D.X., K.M. Gauthier, and W.B. Campbell, *Characterization of Vasoconstrictor Responses in Small Bovine Adrenal Cortical Arteries in Vitro*. Endocrinology, 2004. **145**(4): p. 1571-1578.
84. Fernando, K.H.N., et al., *Diphlorethohydroxycarmalol Isolated from *Ishige okamurae* Represses High Glucose-Induced Angiogenesis In Vitro and In Vivo*. Mar Drugs, 2018. **16**(10).
85. Sarmah, S. and J.A. Marrs, *Zebrafish as a Vertebrate Model System to Evaluate Effects of Environmental Toxicants on Cardiac Development and Function*. International journal of molecular sciences, 2016. **17**(12): p. 2123.
86. Stratman, A.N., et al., *Interactions between mural cells and endothelial cells stabilize the developing zebrafish dorsal aorta*. Development, 2017. **144**(1): p. 115-127.
87. Zakaria, Z.Z., et al., *Using Zebrafish for Investigating the Molecular Mechanisms of Drug-Induced Cardiotoxicity*. BioMed Research International, 2018. **2018**: p. NA.
88. Fritsche, R., T. Schwerte, and B. Pelster, *Nitric oxide and vascular reactivity in developing zebrafish, *Danio rerio**. American Journal of Physiology-Regulatory, Integrative and Comparative Physiology, 2000. **279**(6): p. R2200-R2207.
89. Ortega Mateo, A. and A.A. de Artiñano, *Highlights on endothelins: a review*. Pharmacol Res, 1997. **36**(5): p. 339-51.
90. Brenner, B.M., J.L. Troy, and B.J. Ballermann, *Endothelium-dependent vascular responses. Mediators and mechanisms*. The Journal of clinical investigation, 1989. **84**(5): p. 1373-1378.
91. Stratman, A.N., et al., *Interactions between mural cells and endothelial cells stabilize the developing zebrafish dorsal aorta*. Development (Cambridge, England), 2017. **144**(1): p. 115-127.
92. Aird, W.C., *Endothelial cell heterogeneity and atherosclerosis*. Curr Atheroscler Rep, 2006. **8**(1): p. 69-75.
93. Cotecchia, S., *The  $\alpha$ 1-adrenergic receptors: diversity of signaling networks and regulation*. Journal of receptor and signal transduction research, 2010. **30**(6): p. 410-419.
94. Ciccarelli, M., et al., *Chapter 11 - Adrenergic Receptors*, in *Endocrinology of the Heart in Health and Disease*, J.C. Schisler, C.H. Lang, and M.S. Willis, Editors. 2017, Academic Press. p. 285-315.
95. Kaykı-Mutlu, G., et al., *Cardiac and Vascular  $\alpha$ 1-Adrenoceptors in Congestive Heart Failure: A Systematic Review*. Cells, 2020. **9**(11): p. 2412.
96. Stassen, F.R., et al., *Reduced responsiveness of rat mesenteric resistance artery smooth muscle to phenylephrine and calcium following myocardial infarction*. British journal of pharmacology, 1997. **120**(8): p. 1505-1512.
97. Ruan, Y., et al., *The Role of Adrenoceptors in the Retina*. Cells, 2020. **9**(12): p. 2594.
98. Villalobos-Molina, R., et al., *Vascular  $\alpha$ 1D-adrenoceptors are overexpressed in aorta of the aryl hydrocarbon receptor null mouse: role of increased angiotensin II*. Autonomic and Autacoid Pharmacology, 2008. **28**(2-3): p. 61-67.
99. Beekhuijzen, M., et al., *From cutting edge to guideline: A first step in harmonization of the zebrafish embryotoxicity test (ZET) by describing the most optimal test conditions and morphology scoring system*. Reproductive toxicology (Elmsford, N.Y.), 2015. **56**: p. 64-76.
100. Miklosz, J., et al., *Cardiovascular and Respiratory Toxicity of Protamine Sulfate in Zebrafish and Rodent Models*. Pharmaceutics, 2021. **13**(3): p. 359.

101. Brian Bagatto and Warren Burggren, *A Three-Dimensional Functional Assessment of Heart and Vessel Development in the Larva of the Zebrafish (Danio rerio)*. *Physiological and Biochemical Zoology*, 2006. **79**(1): p. 194-201.
102. Margiotta-Casaluci, L., et al., *Testing the Translational Power of the Zebrafish: An Interspecies Analysis of Responses to Cardiovascular Drugs*. *Frontiers in pharmacology*, 2019. **10**: p. 893-893.